University of Belgrade
Faculty of Chemistry

Jelena B. Ostojić

Development of voltammetric methods for the detection and quantification of xanthine alkaloids using disposable printed sensors

Doctoral Dissertation

Belgrade, 2026.

Универзитет у Београду
Хемијски факултет

Jelena B. Ostojić

Развој волтаметријских метода за детекцију и квантификацију ксантинских алкалоида применом једнократних штампаних сензора

Докторска дисертација

Београд, 2026.

Supervisors:

Dr Dalibor Stanković
Assistant professor,
University of Belgrade - Faculty of Chemistry

_____

Dr Radovan Metelka
Assistant professor,
University of Pardubice - Faculty of Analytical Chemistry

_____

Committee members:

Dr Jelena Mutić
Full Professor,
University of Belgrade - Faculty of Chemistry

_____

Dr Slađana Đurđić
Docent,
University of Belgrade - Faculty of Chemistry

_____

Dr Vesna Stanković
Senior Research Associate,
Institute of Chemistry, Technology and Metallurgy

_____

Date: _____

Acknowledgments

I would like to express my deepest gratitude to my supervisor, Dr. Dalibor Stanković, for his expertise, professionalism, patience, and valuable advice, and for the knowledge he generously shared. I am grateful to have had the opportunity to collaborate with such an outstanding expert throughout the entire process of this work.

I also extend my special thanks to my co-supervisor, Dr. Radovan Metelka from the Faculty of Chemical Technology, University of Pardubice, who generously shared his knowledge and provided exceptional guidance during the preparation and writing of this dissertation. I am also thankful for his hospitality during my visits to the University of Pardubice, Czech Republic.

I am grateful to the committee members, Dr. Jelena Mutić, Dr. Vesna Stanković, and Dr. Slađana Đurđić.

I would also like to thank Dr. Dragan Manojlović. His lectures during my undergraduate studies sparked my interest in this field and he was the one who recommended Dr. Dalibor Stanković as my supervisor, allowing me to complete my bachelor's, master's, and doctoral studies within the same research group.

I am thankful to Dr. Kurt Kalcher and Dr. Astrid Ortner from the University of Graz (Karl-Franzens-Universität Graz) for their generous advice, guidance during my studies and dissertation, for their moral support and encouragement during the finalization of this work and for their hospitality during my stay.

I am thankful to Dr. Marian Vojs and his research group from the Institute of Electronics and Photonics at the Slovak University of Technology in Bratislava, with whom I had the opportunity to work and learn a great deal. I am grateful for their willingness to share their knowledge, experience, and for their hospitality during my stay.

I would like to acknowledge my colleague Slađana Savić Jovanović for her cooperation, dedication, and effort, which contributed to parts of the results presented in this research.

I am thankful to my colleagues Đurđa Ivković and Aleksandra Kovačević, as well as Rajo Petrić, for their patience, constructive advice, and careful review of this work.

I am thankful to my colleague and friend Milica Miljković for her support and encouragement throughout all levels of my studies, and for making this period unforgettable together with Rajo.

I am deeply grateful to my family-my mother Snežana, my father Branko, and my brother Nikola-for their constant support. I also thank my aunt Svetlana, uncle Arpad, and my grandmothers Ljubica and Agata.

Finally, I am thankful to my chosen family, Pavle and William, for their immense understanding, patience, and support, which have been the foundation of my work, perseverance, and determination. I also wish to thank “dear mom” Slavica, and Uroš.

Захвалница

Највећу захвалност дугујем свом ментору, др Далибору Станковићу, за стручност, професионалност, стрпљење и корисне савете, као и за знање које је несебично делио. Захвална сам што сам имала прилику да са тако врсним стручњаком сарађујем током целог процеса израде овог рада.

Посебну захвалност упућујем и ментору др Радовану Метелки (Radovan Metelka) са Факултета за хемијске технологије Универзитета у Пардубицама, који је такође несебично делио своја знања и пружао изузетне савете током израде и писања овог рада. Захвална сам му и на гостопримству током мојих боравака на Универзитету у Пардубицама, Чешка.

Захваљујем се члановима комисије, др Јелени Мутић, др Весни Станковић и др Слађани Ђурђић. Захваљујем се и др Драгану Манојловићу, чија су предавања на основним студијама пробудила моје интересовање за ову област и који је предложио др Далибора Станковића као мог ментора, омогућивши ми да завршим завршни рад, мастер и докторске студије у истој истраживачкој групи.

Захвална сам др Курту Калхеру (Kurt Kalcher) и др Астрид Ортнер (Astrid Ortner) са Универзитета у Грацу (Карл Франц Универзитет, Грац) на несебичним саветима, смерницама током студија и израде дисертације, на моралној подршци и бодрењу током финализације рада и гостопримству током мојих боравака.

Захвална сам др Мариану Војсу (Marian Vojs) и његовој истраживачкој групи са Института за електронику и фотонику, Словачког техничког Универзитета у Братислави, са којима сам имала прилику да радим и научим много тога. Хвала им на дељењу знања, искустава и гостопримству током мог боравка.

Захвалност дугујем колегиници Слађани Савић Јовановић на сарадњи, преданости и труду који су допринели деловима резултата овог истраживања.

Захвална сам и колегиницама Ђурђи Ивковић и Александри Ковачевић, као и колеги Рају Петрићу, на стрпљивом прегледању рада и конструктивним саветима.

Захваљујем се својој колегиници и другарици Милици Миљковић на подршци и бодрењу током свих нивоа студија, и што је заједно са Рајом учинила овај период незаборавним.

Искрено захваљујем својој породици-мајци Снежани, оцу Бранку и брату Николи-на константној подршци. Захвална сам и тетки Светлани, течку Арпаду и бакама Љубици и Агати.

На крају, захвалност дугујем својој изабраној породици, Павлу и William-у, на неизмерном разумевању, стрпљењу и подршци, која је била темељ мог рада, упорности и истрајности. Такође, захваљујем се „драгој мами" Славици, и Урошу.

List of abbreviations

AMP - Adenosine monophosphate
BDD - Boron-doped diamond
BRB - Britton-Robinson buffer
CA - Chronoamperometry
CAF - Caffeine
CCD - Charge-coupled device
CE - Counter electrode
CNS – Central nervous system
CV - Cyclic voltammetry
CVD - Chemical vapor deposition
DME - Dropping mercury electrode
DPV - Differential pulse voltammetry
DWCNTs - Double-walled carbon nanotubes
FE-SEM - Field emission scanning electron microscope
FET - Field-effect transistor
HFCVD - Hot filament chemical vapor deposition
HPHT - High-pressure-high-temperature
I - Current intensity
Ipa - Intensities of anodic peak
Ipc - Intensities of cathodic peak
IUPAC - International Union of Pure and Applied Chemistry
LA-MWCVD - Large-area linear antenna microwave chemical vapor deposition
LOD - Limit of detection
LOQ - Limit of quantification
MWCNTs - Multi-walled carbon nanotubes
MW-PECVD - Microwave plasma-enhanced chemical vapor deposition
NPV - Normal pulse voltammetry
PB - Phosphate buffer
PET - Polyethylene terephthalate
RE - Reference electrode
SP - Screen-printed
SPCE - Screen-printed carbon electrode
SWCNTs - Single-walled carbon nanotubes
SWV - Square wave voltammetry
TB - Theobromine
TMB - Trimethyl borate
TP - Theophylline
WE - Working electrode

List of symbols

Symbol	Meaning
A	Electrode area (cm^2)
c	Concentration (mol L^{-1})
D	Diffusion coefficient (cm^2 s^{-1})
Eo	Standard electrode potential
E_{pa}	Anodic peak potential (V)
E_{pc}	Cathodic peak potential (V)
F	Faraday's constant (96485.33 C mol^{-1})
I	Peak current (A)
k_s	Heterogeneous electron transfer rate constant (cm s^{-1})
α	Charge transfer coefficient
n	Number of electrons
R	Gas constant (8.314 J mol K^{-1})
T	Temperature (K)
v	Scan rate (V s^{-1})

ABSTRACT

The present doctoral dissertation describes the development of voltammetric methods for the determination of xanthine alkaloids using two types of compact, disposable electrochemical sensors. The innovative aspect of this research lies in the use of screen-printed platforms with advanced electrode materials, boron-doped diamond and multi-walled carbon nanotubes, integrated into ready-to-use sensor formats. This approach enables simplified, cost-effective, and sensitive on-site analysis of xanthine alkaloids, with minimal sample preparation.

Cyclic voltammetry, differential pulse, and square wave voltammetry were employed to evaluate the electrochemical performance of the sensors in the detection and quantification of xanthine alkaloids.

The SP/BDD sensor was successfully applied for the quantification of caffeine in coffee, energy drink, and soft drink samples; theobromine in chocolate samples; and theophylline in pharmaceutical tablet samples. The SP/MWCNT sensor was effectively used for the quantification of caffeine in coffee and energy drink samples.

The results demonstrate the potential of using screen-printed sensors with boron-doped diamond and multi-walled carbon nanotube working electrodes for the development of fast, reliable, and miniaturized analytical tools suitable for real-world applications in food and pharmaceutical analysis.

Keywords: sensors, electrochemistry, BDD, MWCNT, screen-printing technologies, disposable sensors, caffeine, theobromine, theophylline, xanthine alkaloids

Scientific field: Chemistry

Scientific subfield: Analytical Chemistry

РЕЗИМЕ

У оквиру ове докторске дисертације је описан развој волтаметријских метода за одређивање ксантинских алкалоида коришћењем два типа компактних, једнократних електрохемијских сензора. Иновативни аспект овог истраживања лежи у употреби једнократних штампаних платформи са напредним електродним материјалима, дијамантом допираним бором и вишезидним угљеничним наноцевчицама, интегрисаним у формате сензора спремне за употребу. Овај приступ омогућава поједностављену, исплативу и осетљиву анализу ксантинских алкалоида на лицу места, уз минималну припрему узорка.

Циклична волтаметрија, диференцијални импулсни и волтаметрија квадратног таласа коришћене су за процену електрохемијских перформанси сензора у детекцији и квантификацији ксантинских алкалоида.

SP/BDD сензор је успешно примењен за квантификацију кофеина у узорцима кафе, енергетских пића и безалкохолних пића; теобромина у узорцима чоколаде; и теофилина у узорцима фармацеутских таблета. SP/MWCNT сензор је ефикасно коришћен за квантификацију кофеина у узорцима кафе и енергетских пића.

Резултати показују потенцијал коришћења штампаних сензора са дијамантом допираним бором и вишезидним радним електродама од угљеничних наноцеви за развој брзих, поузданих и минијатуризованих аналитичких алата погодних за примену у стварном свету у анализи хране и фармацеутских производа.

Кључне речи: сензори, електрохемија, бором допован дијамант, вишезидне угљеничнне наноцеви, штампани сензори, сензори за једнократну примену, кофеин, теобромин, теофилин, ксантински алкалоиди

Научна област: Хемија

Ужа научна област: Аналитичка хемија

Table of contents

1. Introduction

The development of fast, reliable, and cost-effective analytical methods has led to the rapid development of electrochemical sensors in various scientific and industrial fields. Since the first official electrochemical sensor (for monitoring of oxygen concentration) was introduced not so long ago in 1956, the field of electroanalysis has evolved significantly, with applications expanding to environmental monitoring, food safety, pharmaceutical analysis, and clinical diagnostics.

Among the compounds of great interest in analytical chemistry are xanthine alkaloids, a group of naturally occurring purine derivatives that include caffeine, theobromine, and theophylline. These compounds are widely present in food and beverages such as coffee, tea, chocolate, and energy drinks, as well as in pharmaceutical formulations. Due to their physiological effects on the central nervous and cardiovascular systems, the accurate determination of xanthine alkaloid content in various samples is of significant importance for both health monitoring and quality control.

Traditional methods for the determination of xanthine alkaloids include chromatographic and spectrophotometric techniques, which, although sensitive and accurate, often require complex instrumentation, long analysis times, and time-consuming sample preparation. In contrast, electrochemical methods, especially voltammetric techniques, have emerged as attractive alternatives due to their simplicity, low cost, high sensitivity, and compatibility with miniaturized and portable systems.

A crucial aspect of developing electrochemical methods lies in the choice of the working electrode. Screen-printed electrodes (SPEs) have gained considerable attention as disposable sensing platforms due to their low production cost, ease of mass fabrication, and flexibility in surface modification. In particular, BDD and MWCNT have shown excellent properties for electrochemical applications. BDD offers a wide potential window, low background current, and remarkable chemical and mechanical stability, while MWCNTs contribute high electrical conductivity and large surface area, as well as enhanced electrocatalytic activity.

This doctoral dissertation is focused on the development and validation of electrochemical methods for the quantification of xanthine alkaloids using screen-printed sensors. Two types of working electrodes were investigated. The first one has a chemically deposited boron-doped diamond working electrode. Another one is based on a multi-walled carbon nanotube working electrode.

The research aimed to characterize the physical and electrochemical properties of these electrodes, develop sensitive voltammetric methods for alkaloid determination, and validate their application on real samples such as coffee, soft drinks, energy drinks, chocolate, and pharmaceutical products.

Although various studies have explored the use of boron-doped diamond and carbon nanotube materials in electrochemical sensing, most rely on conventional bulk electrodes or require complex electrode modification procedures. In contrast, this research focuses on the application of compact, disposable sensor platforms with integrated BDD or MWCNT working electrodes,

offering practical advantages such as ease of use, low cost, and minimal pre-treatment. The innovative contribution lies in adapting these materials into screen-printed miniaturized sensor formats and validating their performance for real-sample analysis of xanthine alkaloids, an approach not extensively covered in the existing literature.

The dissertation is structured into four main chapters:

1. General Part,
2. Experimental Part,
3. Results and Discussion, and
4. Conclusion.

The General Part provides an overview of the physicochemical and electrochemical properties of boron-doped diamond and multi-walled carbon nanotubes, with emphasis on their role in electroanalysis. It also includes a literature review of electrochemical methods for xanthine alkaloid determination, as well as a theoretical background on voltammetric techniques and characterization methods such as Raman spectroscopy, FE-SEM, and voltammetry techniques.

The Experimental Part describes the materials, reagents, instrumentation, and procedures used for electrode characterization, method development, and real sample preparation and analysis.

The Results and Discussion chapter presents the findings of electrode surface characterization, optimization of voltammetric parameters and conditions, electroanalytical performance of the developed methods, and their comparison with literature data. The successful application of the methods to real samples and their validation parameters are also discussed.

Finally, the Conclusion summarizes the scientific contributions of this work in the field of electrochemical sensing using disposable sensors, highlighting the potential of BDD and MWCNT materials for future development of portable and efficient sensing platforms.

2. General part

2.1 Boron-doped diamond

2.1.1 Brief history of boron-doped diamond

Diamond is one of the oldest known engineering materials, popular for its exceptional hardness and chemical inertness. Historically, it was used primarily as an abrasive, with evidence of its use dating back several thousand years. A significant turning point came in the early 1950s, when a high-pressure-high-temperature (HPHT) method was discovered to synthesize diamond artificially. This breakthrough led to massive growth in industrial diamond applications. Over the following decades, synthetic diamond became a cornerstone material in engineering, cutting tools, and optics (*Prelas, Mark Antonio, 1998*).

Despite its widespread use in mechanical applications, diamond remained limited in electronics and electrochemistry due to its wide band gap (~5.5 eV), which made it a strong electrical insulator under standard conditions. This changed in the late 20th century when a new technique was developed. Chemical vapor deposition (CVD) technique enabled the growth of high-purity diamond films under controlled conditions. CVD made it possible to modify the material's electronic properties by introducing dopants during growth, a process known as doping *(Prelas, Mark Antonio, 1998)*.

Researchers explored various dopants to create a conductive diamond. The idea was to alter the electronic structure of diamond to create either n-type (electron-donating) or p-type (hole-conducting) semiconductors, depending on the type of dopant used. Two main types of dopants were investigated. Nitrogen for n-type behavior, and boron for p-type conductivity. While nitrogen is more easily incorporated during growth, it leads to deep donor levels that do not contribute significantly to conductivity at room temperature. In contrast, boron introduces shallow acceptor states, and when added in sufficiently high concentrations (typically above ~10^{20} atoms/cm^3), it can induce metallic-like conductivity in diamond (*Einaga, 2022)*.

In the late 1980s and early 1990s, researchers observed that heavily boron-doped diamond (BDD) exhibited exceptional electrochemical properties if used as an electrode material. These included a wide potential window in aqueous media, low background current, and chemical and physical stability of the surface even in harsh conditions. These characteristics made BDD highly attractive for use as a new electrode material. As a result, interest rapidly grew in developing these types of electrodes for electroanalytical applications. Improvements in CVD growth methods and better control of boron concentration led to reproducible, high-quality BDD thin film electrodes capable of operating in extreme chemical environments and detecting trace-level analytes with precision. What began as an effort to tune the semiconductor properties of diamond evolved into one of the most significant innovations in modern electrochemistry *(Einaga, 2022)*.

2.1.2 Structure of boron-doped diamond

The boron-doped diamond (BDD) has the fundamental crystal structure of pure diamond: a face-centered cubic lattice where each carbon atom is covalently bonded to four neighbouring carbon atoms in a tetrahedral geometry. This robust sp^3-bonded network gives diamond its well-known mechanical strength, thermal conductivity, and chemical inertness. In BDD, boron atoms substitute for carbon atoms within this lattice without significantly disturbing its overall crystalline structure (*Watanabe et al., 2018*).

Figure 1 illustrates the atomic arrangement in BDD. In this scheme, the boron dopants are shown occupying substitutional sites within the carbon lattice. Each boron atom has three valence electrons, compared to carbon's four, which creates an electron deficiency or "hole" in the structure, and holes act as positive charge carriers, which enables p-type conductivity when the boron concentration reaches a sufficient level. The dopant atoms are distributed throughout the bulk material rather than simply on the surface, which ensures uniform electrochemical behavior across the material (*Crawford et al., 2021*).

At low levels of boron doping (typically below 10^{18} atoms/cm^3), the material shows mostly insulating properties. As the boron content increases, the conductivity improves, eventually reaching a metallic-like regime at concentrations exceeding ~10^{20} atoms/cm^3. This high level of doping is necessary for most electrochemical applications and is achieved during the chemical vapor deposition (CVD) growth process by introducing a boron-containing precursor gas (*Watanabe et al., 2018*).

Despite the incorporation of boron, the structural integrity of the diamond lattice is preserved. However, the presence of dopants can introduce localized distortions and affect the electronic band structure. These changes are critical to the electrochemical properties of BDD, influencing factors such as the width of the potential window, background current, and surface reactivity. The combination of structural rigidity and tunable electric properties makes boron-doped diamond a unique and valuable material for advanced applications (*Watanabe et al., 2018*).

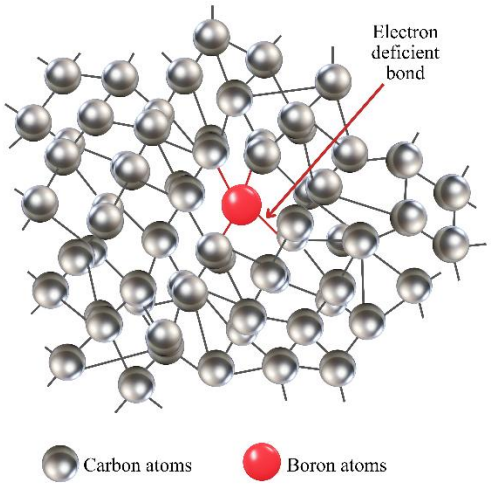

Figure 1. Atomic arrangement in boron-doped diamond.

2.1.3 Fabrication

2.1.3.1 High-pressure-high-temperature (HPHT) method

The High-pressure-high-temperature (HPHT) method was the first technique that artificially synthesized diamond. This technique reproduces the environmental conditions of the Earth's mantle that give rise to diamond formation. Carbon is exposed to pressures above 5 GPa and temperatures exceeding 1500 °C in the presence of a catalyst, usually metals like iron, nickel, or cobalt. For the fabrication of boron-doped diamond (BDD), boron-containing compounds such as boron carbide (B_4C) are introduced into the growth system as dopant sources (*Lin et al., 2024*).

Despite its historical importance, the HPHT method has notable limitations during the production of the BDD materials intended for electrochemical applications. The main drawback is the difficulty in achieving a uniform boron distribution throughout the bulk material. Moreover, HPHT diamonds are typically produced as single crystals or polycrystalline blocks, which are challenging to process into thin films or large-area electrodes *(T. Luong et al., 2009)*. Additionally, the presence of metal catalysts in the growth environment can introduce impurities that degrade electrochemical performance (*Wang et al., 2024*). While HPHT-grown BDD remains of academic interest, especially for fundamental studies of doping mechanisms and defect structures, it is rarely used in practical electrode material fabrication.

Due to these limitations, the HPHT method has been replaced by chemical vapor deposition (CVD) techniques, which allow for better control over boron incorporation, film thickness, and surface morphology.

2.1.3.2 Chemical vapor deposition (CVD) method

2.1.3.2.1 Hot filament chemical vapor deposition (HFCVD)

HFCVD is one of the earliest and most accessible CVD-based methods used for fabricating boron-doped diamond (BDD) films. In this process, a resistant, heated tungsten or tantalum filament, which typically operates at temperatures between 2000 and 2500 °C, serves to thermally dissociate a gas mixture containing hydrogen and a carbon source, most commonly methane (CH_4), into reactive species (*Fang et al., 2025; Liu and Dandy, 1995*). To introduce boron into the growing diamond film, a boron precursor such as diborane (B_2H_6) is added to the gas phase.

The activated hydrogen atoms generated by the hot filament play a critical role in selectively removing non-diamond carbon phases and stabilizing the growth of the sp^3-bonded diamond lattice. Concurrently, boron atoms from the dopant gas are incorporated substitutionally into the diamond structure, producing p-type semiconducting films. The boron concentration in the deposited film can be adjusted by varying the B/C ratio in the feed gas mixture, which allows some degree of tunability in the electrical and electrochemical properties of the material (*Song et al., 2020*).

One of the main advantages of HFCVD is its simplicity and relatively low cost compared to plasma-based CVD systems. The setup does not require high-frequency power supplies or vacuum plasma chambers. Additionally, it enables the growth of BDD films over large surface areas and complex geometries (*Liu and Dandy, 1995*).

However, HFCVD has significant limitations. The hot filament degrades over time due to carburization and oxidation, potentially introducing metallic contaminants into the film and reducing process stability. Uniform temperature control across the substrate can be challenging, leading to non-uniform film thickness or dopant distribution (*Fang et al., 2025*). Moreover, the technique generally results in relatively rough and polycrystalline diamond surfaces, which may require post-deposition polishing for certain applications. Despite these challenges, HFCVD remains a viable and widely used method for producing functional BDD electrodes.

2.1.3.2.2 Microwave plasma-enhanced chemical vapor deposition (MW-PECVD)

MW-PECVD is the most advanced and widely used method for fabricating high-quality boron-doped diamond thin films. The technique utilizes microwave energy (typically at 2.45 GHz) to generate a dense and stable plasma from a gas mixture of hydrogen and a carbon source, such

as methane. A boron precursor, commonly diborane (B_2H_6) or trimethyl borate (TMB), is introduced into the gas phase to achieve boron doping during the growth process (*Taylor et al., 2022*).

The plasma is generated within the reaction chamber, where the substrate (which is often silicon, quartz, or metals) is positioned directly beneath the plasma ball and heated to temperatures around 900 °C. In this environment, carbon-containing radicals and atomic hydrogen are formed and interact at the substrate surface. Atomic hydrogen suppresses graphitic carbon and promotes the growth of sp^3-bonded diamond (*Das and Banerjee, 2015*). Boron atoms are simultaneously incorporated into the diamond lattice at substitutional sites, leading to p-type conductivity if the doping level is sufficiently high.

MW-PECVD offers several advantages over other methods mentioned. It allows precise control over process parameters such as gas composition, pressure, temperature, and plasma power, which translates into excellent control over film quality, thickness, and dopant concentration. This method can produce BDD films with exceptional purity, uniformity, and smooth surface morphology (*Taylor et al., 2022*). Moreover, the absence of a physical filament eliminates contaminations associated with filament degradation.

The main flaws of the MW-PECVD method are complexity and cost. The equipment is expensive and requires advanced plasma control systems and vacuum infrastructure. Additionally, the quality of the deposited films is high, and the growth rate is generally slower than in hot filament CVD, making it less efficient for thick film deposition or large-scale industrial applications (*Neralla, 2016*).

Despite these drawbacks, this method remains the standard for applications requiring high-performance BDD electrodes, such as advanced electroanalytical sensors, biosensors (*Meškinis et al., 2023*), and microelectronic devices (*Neralla, 2016*), due to its ability to produce highly uniform and electrochemically stable BDD films.

2.1.3.2.3 Large-area linear antenna microwave chemical vapor deposition (LA-MWCVD)

The LA-MWCVD method is a specialized variant of the standard microwave plasma-enhanced CVD technique, designed to enable uniform diamond film growth over extended surface areas (*Behul et al., 2025*). Unlike traditional microwave plasma systems that use resonant cavities or single-point plasma sources, LA-MWCVD employs a linear antenna configuration that distributes microwave energy more evenly across the substrate. This configuration generates a large, stable plasma zone, allowing for controlled and homogeneous deposition over large surfaces, which is useful for sensor material fabrication.

In this technique, a mixture of hydrogen and methane gas is activated by the linear microwave antenna under low-pressure conditions, producing the necessary reactive carbon species for diamond film growth. Boron is introduced into the gas phase, typically TMB, to achieve p-type doping *(Marton et al., 2022)*. The boron atoms are incorporated into the diamond lattice during growth, producing a conductive diamond layer suitable for electrochemical applications.

The main advantage of LA-MWCVD is its scalability and precision. It allows for the deposition of boron-doped diamond films with excellent uniformity, high purity, and reproducible electrochemical properties. Compared to conventional microwave CVD systems, LA-MWCVD offers better control over film thickness and doping level across larger substrates *(O. Matvieiev et al., 2022)*.

2.1.3.3 Ion implantation

Ion implantation is a technique used in semiconductor fabrication, where ions of a dopant element are accelerated and directed into a solid substrate. In the context of boron-doped diamond, this method involves bombarding pure diamond, typically single-crystal or polycrystalline, with high-energy boron ions to introduce the dopant into the lattice. Unlike the CVD technique, which incorporates boron during the growth phase, ion implantation is a post-growth doping method (*Ivandini et al., 2005; Ziegler, 1992*).

In this process, the depth and concentration profile of boron in the diamond lattice can be partially controlled by adjusting the energy and dosage of the implanted ions. After implantation, an annealing step at high temperatures is typically required to repair lattice damage caused by ion bombardment and to activate the dopant atoms, i.e., allow them to occupy substitutional positions in the diamond lattice and contribute to electrical conductivity (*Williams, 1998*).

Despite its precision in theory, ion implantation presents several challenges in BDD material fabrication. One of the major limitations is that the high-energy ion bombardment often creates significant damage to the diamond lattice, which can degrade the material's desirable physical and electrochemical properties. Although annealing helps to restore the crystalline structure, complete recovery is difficult, and residual defects can reduce conductivity and chemical stability. Additionally, the doping depth is usually shallow (limited to a few hundred nanometers), which restricts its application for thick or bulk BDD thin films used in electrochemistry (*Ziegler, 1992*).

2.1.4 Application of boron-doped diamond

Boron-doped diamond is recognized as a broadly adaptable electrode material suitable for numerous scientific and industrial uses. Its special properties, such as mechanical strength, resistance to fouling, chemical inertness, and excellent thermal conductivity, make this material suitable for use in challenging environments and demanding applications. BDD is also biocompatible (*Garrett et al., 2016*), which further broadens its range of potential uses.

BDD is utilized in microelectronics, sensors, biosensors (*Svítková et al., 2016*), wastewater treatment (*Oturan, 2021*), quantum technologies (*Alkahtani et al., 2022; Das et al., 2022*), thermal management systems (*Liu et al., 2024*), and specialized coatings to enhance durability and performance (*Zhang et al., 2023*). In the semiconductor industry, it is valued for its high breakdown voltage and thermal stability (*Zhao et al., 2024*). In optics, transparent BDD films are being investigated for protective coatings on high-power laser windows and infrared optics (*Bogdanowicz, 2014; Sobaszek et al., 2015*). Its durability and chemical resistance also make BDD a suitable material for cutting tools and biomedical implants (*Alcaide et al., 2016; Garrett et al., 2016*). However, among all its uses, one of the most studied and impactful applications is as an electrochemical material.

2.1.4.1 Boron-doped diamond in electrochemistry

In electrochemistry, BDD has proven to be a revolutionary electrode material. Compared to traditional electrodes, BDD offers several distinct advantages. These include an exceptionally wide potential window (from -3 V to +3 V in aqueous solutions), very low background (capacitive) current, excellent chemical and mechanical stability, and a low tendency to adsorb interfering species. These features make BDD especially attractive for applications that require

long-term stability, high sensitivity, and operation in aggressive media *(T. Luong et al., 2009; Yasuaki Einaga, 2022*).

BDD electrodes are widely used for the detection of trace-level analytes in environmental *(Costa et al., 2017; Kramplová et al., 2023; Mijajlović et al., 2025; Pratik Joshi et al., 2022)*, pharmaceutical *(Feier et al., 2018; Merve Yence et al., 2021; Sousa et al., 2019)*, and biomedical samples (*Ishii et al., 2022; Moriyama et al., 2022*). Their robustness enables operation in harsh conditions, such as strongly acidic or alkaline environments, as well as in the presence of organic solvents or oxidizing agents. Furthermore, BDD is resistant to electrode fouling, which is a major limitation of conventional carbon-based materials when analyzing complex biological samples or organic molecules (*Fortin et al., 2005; Švorc and Kalcher, 2014*). BDD is also used in electrosynthesis (*Ganiyu et al., 2022; Griesbach et al., 2005; Mora et al., 2022*) and wastewater treatment (*Feier et al., 2018; Lin et al., 2024; Mordačíková et al., 2020)*.

In analytical chemistry, BDD is frequently employed in voltammetric techniques due to its ability to provide sharp, well-defined peaks with low noise. This enables accurate quantification of target analytes, even at very low concentrations (*Moriyama et al., 2022*). It also performs well in miniaturized sensor platforms, including screen-printed electrodes *(O. Matvieiev et al., 2022)* and microelectrodes (*Suzuki et al., 2007*), further supporting its role in point-of-care diagnostics and portable sensing devices.

2.1.5 Boron-doped diamond films

Boron-doped diamond films are synthetic diamond layers in which boron atoms are incorporated into the diamond lattice during growth, altering the electrical properties of the insulating diamond material. These films can be grown on a variety of substrates and are typically categorized based on their grain size and morphology, ranging from microcrystalline to nanocrystalline and ultrananocrystalline forms. Among these, microcrystalline BDD films are the most commonly used in electrochemistry due to their favorable combination of structural properties and electrochemical performance *(Knittel et al., 2019; Marton et al., 2022)*.

Structurally, BDD films retain the exceptional mechanical hardness and chemical stability of pure diamond. Boron atoms, when present in sufficient concentrations (typically $\geq 10^{20}$ cm^3), introduce acceptor levels into the diamond band structure, leading to p-type semiconducting or even quasi-metallic behavior. The microcrystalline form consists of diamond grains with well-defined crystalline boundaries, which contribute to mechanical strength but also influence electrochemical properties such as active surface area and double-layer capacitance *(Granger et al., 2000; Srikanth et al., 2012)*.

In electrochemical applications, BDD films are prized for their wide potential window in aqueous and non-aqueous media, extremely low background current (capacitive current), high resistance to chemical fouling, and long-term operational stability, even in harsh or corrosive environments. These properties make BDD an ideal material for sensor development *(Granger et al., 2000; Jishou Xu et al., 1997)*, especially in the detection of trace-level analytes, long-term environmental monitoring *(Czupryniak et al., 2012; Ganiyu and Martínez-Huitle, 2019)*, biomedical diagnostics *(Pippione et al., 2017), and electrocatalysis (Zhao et al., 2010)*.

Additionally, BDD films are highly resistant to surface mechanical degradation *(Tully et al., 2024)*, which makes them suitable for integration into robust, miniaturized devices like screen-printed electrodes or lab-on-a-chip systems *(O. Matvieiev et al., 2022; Šelešovská et al., 2022)*.

2.2 Carbon nanotubes

Carbon nanotubes (CNTs) are cylindrical nanostructures composed entirely of carbon atoms arranged in a hexagonal lattice, similar to a rolled-up sheet of graphene. They are part of the family of carbon-based nanomaterials and are renowned for their exceptional mechanical strength, thermal conductivity, chemical stability, and unique electronic properties (*Dai, 2002)*. Since their discovery, CNTs have generated significant interest across various scientific and engineering fields, from materials science to energy storage and biosensing (*Ajayan and Zhou, 2001*).

CNTs are classified into two basic types, depending on the number of concentric graphene layers in them. Single-walled carbon nanotubes (SWCNTs) consist of a single cylindrical graphene layer, and multi-walled carbon nanotubes (MWCNTs) are made up of multiple concentric graphene cylinders, resembling a series of tubes (*Figure 2*). (*Dresselhaus et al., 2000*).

The properties of CNTs depend significantly on their structure, including diameter, length, number of walls, and the way the graphene sheet is rolled. These structural variations influence their electrical behavior. Some CNTs behave like metals, while others act as semiconductors, and this versatility makes CNTs attractive for a wide range of applications, such as electronics, sensors, and electrochemical devices (*Popov, 2004*).

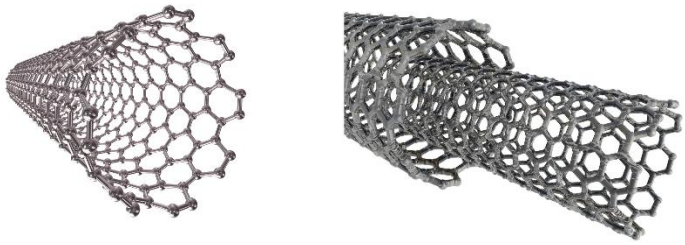

Figure 2. Single-walled carbon nanotube (left) and multi-walled carbon nanotube (right) with the diameter range written below.

2.2.1 Single-walled carbon nanotubes

Single-walled carbon nanotubes represent the simplest form of carbon nanotube structures. They consist of a single sheet of graphene rolled into a cylindrical tube, typically about 1 nanometer in diameter, with lengths that can span several micrometers. Due to this unique morphology, SWCNTs exhibit extraordinary aspect ratios and distinct electronic, mechanical, and chemical properties *(Nanot et al., 2013; Niyogi et al., 2002)*.

The idea of SWCNTs emerged in the early 1990s, following the discovery of fullerenes. When SWCNT was successfully synthesized, it sparked a global interest in these novel nanomaterials. Since then, SWCNTs have been extensively studied for their unique characteristics and potential applications across different technologies *(Jin, 2016)*. SWCNT production typically requires catalysts of defined size and optimal reaction environments, making bulk synthesis more challenging, less economical, and prone to defects.

The properties of SWCNTs are closely tied to their atomic arrangement. The way in which the graphene sheet is rolled into a cylinder, described mathematically by a so-called chiral vector,

determines the nanotube's chirality and thus its electronic properties. Specifically, if the chiral vector yields an "armchair" structure, the nanotube behaves as a metal; "zigzag" and other chiral configurations generally produce semiconducting nanotubes. Therefore, the seemingly simple act of rolling a graphene sheet can actually produce a range of electronic behaviors depending on the exact direction and angle in which the rolling occurs, making SWCNTs exceptional for applications in nanoelectronics and sensors *(Ouyang et al., 2002; Zhou et al., 2009)*.

2.2.2 Multi-walled carbon nanotubes

Multi-walled carbon nanotubes are composed of multiple concentric graphene cylinders placed within one another. Each cylinder, or "wall", is a rolled-up graphene sheet, with the spacing between layers roughly 0.34 nm. The overall diameter of MWCNTs typically ranges from 2 to 100 nm, with lengths that can extend to several micrometers *(Kukovecz et al., 2013)*.

MWCNTs were discovered earlier than SWCNTs, and they sparked interest in carbon nanomaterials. Despite their seemingly more complex morphology, MWCNTs are generally easier to synthesize than SWCNTs due to their less stringent growth requirements. Their formation tolerates a wider range of synthesis conditions, including higher temperatures, varied gas compositions, and less precise catalyst control. They are typically synthesized by methods such as arc discharge, laser ablation, or CVD, which enable the simultaneous formation of several graphene layers without the need for highly precise control of conditions like catalyst particle. Also, and are more stable under mechanical and chemical stress than SWCNTs *(Haldar et al., 2021; Ismail et al., 2020; Mostafa et al., 2021; Sahar Tabrizi et al., 2013; Yumura, 1999).*

MWCNTs tend to exhibit metallic behavior due to the presence of multiple concentric layers with varying chiralities. This gives them a broad range of electronic properties, although it also makes their behavior more complex to predict.

MWCNTs possess several remarkable properties, including extremely high mechanical strength, excellent electrical conductivity, high surface area, and strong resistance to chemical degradation. These features make them suitable for reinforcing materials, fabricating conductive films, and enhancing the sensitivity of sensors *(Ando et al., 1999; Andrews et al., 2002)*.

Additionally, their hollow, layered structure allows for functionalization, i.e, chemical modification of the surface, which improves their compatibility with other materials and extends their application in areas such as drug delivery *(Dineshkumar et al., 2015; Levi-Polyachenko et al., 2009)*, catalysis *(Gonçalves et al., 2010; Yang et al., 2008)*, and as nanocomposite material in electrochemical sensing *(Abdulla et al., 2015; Aleksanyan et al., 2022; Dalmas et al., 2005; Kiamahalleh et al., 2012; Ye et al., 2004)*.

Despite their advantages, MWCNTs face challenges related to their potential toxicity *(Jain et al., 2011; Muller et al., 2005; Tan et al., 2009)*. Nevertheless, due to their robustness and relatively easier synthesis compared to SWCNTs, MWCNTs have become a widely used and studied nanomaterial across various scientific disciplines.

2.2.3 Application of carbon nanotubes

Carbon nanotubes, with their exceptional properties including mechanical strength, thermal conductivity, and electrical properties, have found applications across various scientific and

technological fields. These cylindrical structures, whether single-walled or multi-walled, offer unique advantages coming from their nanometer-scale size and graphitic structure *(Popov, 2004)*.

In materials science, CNTs are often used as reinforcing agents in polymer composites *(Mohd Nurazzi et al., 2021)*. Their high strength allows them to significantly improve the mechanical properties of plastics, rubbers, and metals. This makes them valuable in the aerospace, automotive *(Abbasi et al., 2020, p. 25)*, and sports equipment industries *(da Costa, 2020)*. Their thermal conductivity also enhances thermal regulation in electronic devices and coatings *(Cao and Rogers, 2008; Peng et al., 2019)*. In electronics, CNTs are applied in the development of field-effect transistors (Abdalla et al., 2015), supercapacitors, batteries *(de las Casas and Li, 2012; Wu et al., 2014)*, and conductive inks *(Kordás et al., 2006)*.

Their unique structure also enables CNTs to be used in biotechnology and medicine *(Bekyarova et al., 2005; Negri et al., 2020)*. Functionalized CNTs can deliver drugs *(Bianco et al., 2005; Kaur et al., 2019)*, genes *(Mohajeri et al., 2019; Pantarotto et al., 2004; Zare et al., 2021)*, or imaging agents directly to cells *(Gong et al., 2013; Hernández-Rivera et al., 2016)*. Their high surface area allows efficient interaction with biological molecules, and their hollow cores can be used for encapsulation. However, concerns about toxicity and biocompatibility issues are still under investigation.

In environmental science, CNTs have proven useful for pollutant detection and removal. Their large surface area and ability to be chemically modified make them effective in water filtration systems and in sensors designed to detect gases, heavy metals, and organic contaminants *(Chung et al., 2022; Peng et al., 2021)*.

One of the most impactful areas for CNTs has been in sensing technologies. Due to their exceptional electron transport properties and large surface area available for analyte interaction, both SWCNTs and MWCNTs are utilized in chemical and biosensors. When combined with other materials or incorporated into structured platforms, they can detect analytes with high sensitivity and selectivity *(Ajayan and Zhou, 2001; De Volder et al., 2013)*.

As synthesis methods improve and cost barriers decrease, CNTs are expected to play an increasingly significant role in advanced technology.

2.2.3.1 MWCNT in electrochemistry

Carbon nanotubes, due to their high electrical conductivity, large surface area, and chemical stability, have found wide application in the field of electrochemistry. Their unique cylindrical nanostructure, composed of rolled graphene sheets, enables efficient electron transfer processes at the electrode surface, making them highly suitable for sensing and analytical applications.

In electrochemical systems, CNTs can act as both active electrode materials and conductive modifiers in electrochemical systems. Their high aspect ratio and π-π interaction capabilities enable strong adsorption of various organic molecules, particularly those with planar aromatic structures *(Umadevi et al., 2014)*, enhancing sensitivity in electrochemical detection. CNTs also exhibit excellent electrochemical stability over a broad potential window, which makes them ideal for use in complex matrices such as biological fluids or environmental samples.

Moreover, the surface of CNTs can be easily functionalized with various chemical groups, nanoparticles *(Hu and Dong, 2008; Zhang et al., 2006)*, or biomolecules *(Katz and Willner, 2004; Vardharajula et al., 2012)*, further expanding their utility in designing selective and

robust sensors. This versatility allows tailoring electrode surfaces to detect a wide range of analytes, usually metal ions *(Liu et al., 2005; Morton et al., 2009)*, small organic molecules *(Hafaiedh et al., 2013; Zima et al., 2009)*, and large biomolecules *(Ferrier and Honeychurch, 2021; Kim et al., 2007)*.

CNT-modified electrodes often display improved signal-to-noise ratios due to the high surface area and enhanced electron transfer kinetics, which is particularly valuable in trace analysis *(Helbling et al., 2010)*. Additionally, their mechanical strength and resistance to fouling contribute to the longevity and repeatability of measurements, which is critical for both disposable *(Chen et al., 2016; Killard, 2017; Laschi et al., 2008)* and reusable sensor platforms *(Ouyang and Li, 2009; Sobhan et al., 2020)*.

Multi-walled carbon nanotubes exhibit a unique multilayer graphitic structure that provides abundant electroactive sites and a high specific surface area *(Redkin et al., 2021)*. Structural features, combined with the presence of numerous defects and edge sites, significantly enhance the electrocatalytic activity and facilitate rapid electron transfer kinetics *(Flores-Lasluisa et al., 2024)*. Consequently, MWCNT sensors and MWCNT-modified electrodes exhibit superior sensitivity and improved electrochemical response in electrochemical measurements.

Additionally, because of their robustness and adaptability, MWCNTs are frequently integrated into screen-printed electrodes *(Favero et al., 2015; Viswanathan et al., 2012, 2009)*, thin films *(Jiang and Gerhardt, 2021; Raut and Sankapa*l, 2016), and composite materials *(Kumar et al., 2021; Luo et al., 2018; Wang et al., 2008)*. They are particularly valuable in the development of point-of-care diagnostic devices *(Jin et al., 2024; Li et al., 2021; Supraja et al., 2023)* and environmental sensors *(Manasa et al., 2023)*, where reproducibility, stability, and fast response times are essential. Moreover, their surface can be chemically or physically modified *(Khan and Alamry, 2022; Liu, 2016; Xu and Yang, 2012)* to improve selectivity, allowing for targeted detection of specific biomolecules *(Alam et al., 2018; Kumar et al., 2023)*, pharmaceuticals *(Abdel-Haleem et al., 2021; Sagar et al., 2025)*, or pollutants *(Wang and Hu, 2016; Zhou, 2024)*.

MWCNTs also demonstrate excellent compatibility with other nanomaterials such as metal nanoparticles *(Wildgoose et al., 2006)*, polymers *(Liu, 2016)*, and enzymes *(Diaconu et al., 2011)*, enabling the design of hybrid sensors that combine high sensitivity with molecular recognition. This multifunctionality expands their application beyond simple detection to include electrocatalysis *(Valenzuela-Muñiz et al., 2013)*, biosensing, and even energy storage *(Al-Ahmed et al., 2020; Baral et al., 2023; Roy et al., 2018)*.

Cost-effectiveness, scalability, and robust performance are key for MWCNTs to be an essential material in electroanalytical chemistry, applying nanostructured materials in the design of effective sensing platforms.

2.3 Methods

2.3.1 Electrochemical methods

Electrochemistry is the field of chemistry that studies the relationship between electrical phenomena and chemical reactions occurring at electrode-electrolyte interfaces. Electrochemical techniques are widely used in analytical chemistry to investigate the identity, concentration, and reactivity of chemical species through the measurement of electrical signals such as potential, current, or charge. The central component of every electrochemical system is the electrode, which enables the transfer of electrons between the analyte and the electrode surface *(Allen J. Bard and Larry R. Faulkner, 2000)*.

Depending on the type of interaction involved, electrochemical techniques can be divided into non-faradaic and faradaic methods. Non-faradaic methods, such as conductometry and potentiometry, do not involve electron transfer reactions and are based on changes in solution conductivity or equilibrium potential. Faradaic methods, including voltammetry and amperometry, rely on redox reactions in which electrons are directly transferred between the analyte and the electrode surface. Electrodes that take part in these reactions are referred to as working electrodes. For redox processes to occur, the analyte must reach the electrode surface, which happens through diffusion, migration, or convection. Diffusion results from a concentration gradient, migration from the influence of an electric field, and convection from the physical movement of the solution, such as stirring or bubbling. When a specific potential is applied to the electrode, redox reactions occur at the electrode surface, resulting in the generation of a measurable current. The main components of total measured current are the faradaic current and the capacitive current, shown in *Figure 3*. The faradaic current arises from the actual redox process and provides valuable information about the analyte, while the capacitive current originates from the charging of the electrical double layer at the electrode surface and contributes background noise. In most applications, the aim is to enhance the faradaic signal while minimizing the capacitive contribution to achieve better sensitivity and accuracy. Electrochemical methods offer numerous practical advantages, including high sensitivity and selectivity, short analysis time, low reagent consumption, and simple sample preparation, making them competitive alternatives to more complex or expensive analytical techniques *(Dragan Manojlović et al., 2010)*.

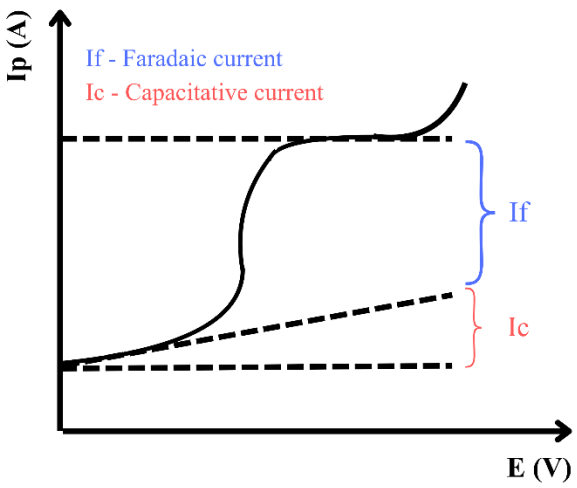

Figure 3. The main components of the total measured current and the relationship between Faradaic and capacitive current.

Voltammetry is one of the most widely used electrochemical methods and is based on the application of a varying potential to the working electrode while recording the resulting current. The output of this measurement is a voltammogram, a graph that shows how the current changes in response to the applied potential. From the voltammogram, important information can be obtained, such as the potential at which the analyte undergoes oxidation or reduction, as well as its concentration. This makes voltammetry especially useful for investigating electrochemical properties and determining the presence of specific compounds in solution *(Kissinger and Hieneman, 2018)*.

Voltammetric measurements are typically performed in a three-electrode setup, as shown in *Figure 4*. This system includes a working electrode (WE), where the redox reaction of interest occurs; a reference electrode (RE), which maintains a stable potential; and a counter electrode (CE), which completes the electrical circuit, carries the current, and protects the reference electrode from polarization and thus change of the potential. All three electrodes are immersed in a solution containing the analyte and a supporting electrolyte. During the experiment, the potential of the working electrode is precisely controlled relative to the reference electrode, and the current generated by the redox reaction flows between the WE and CE. To prevent interference from electroactive oxygen during the measurement of cathodic processes, the solution is often purged with an inert gas, usually nitrogen (N_2) or argon (Ar), before measurement. Oxygen practically does not interfere with measurements of anodic processes. The electrodes in the electrochemical cell are connected to an instrument known as a potentiostat, which regulates the applied voltage and records the resulting current with high accuracy *(Dragan Manojlović et al., 2010)*.

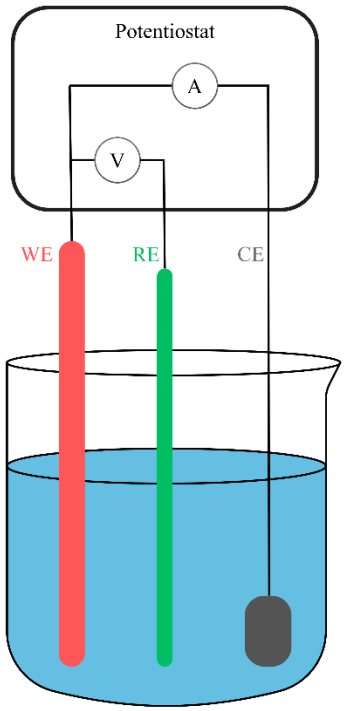

Figure 4. Three-electrode setup. WE - working electrode, RE - reference electrode, CE - counter electrode.

Cyclic voltammetry (CV) is commonly used for exploring the reversibility and mechanism of redox reactions. Square wave voltammetry (SWV) and differential pulse voltammetry (DPV) are particularly valued for their high sensitivity and ability to minimize capacitive background current. Techniques like polarography, which use a dropping mercury electrode (DME), are still applied in the analysis of certain metal ions and organic compounds due to the high potential of hydrogen evolution on the mercury and thus a large cathodic range. Voltammetric methods are capable of detecting extremely low concentrations of analytes, often in the nanomolar range. Additionally, they allow for the simultaneous detection of multiple components in a mixture, without requiring complex sample preparation or separation steps *(Dragan Manojlović et al., 2010)*.

In this doctoral dissertation, electroanalytical techniques such as cyclic voltammetry (CV), differential pulse voltammetry (DPV), and square wave voltammetry (CWV) were employed. The following section provides an overview of the fundamental principles and a concise explanation of each of these methods.

2.3.1.1 Cyclic voltammetry

Cyclic voltammetry is a widely used electrochemical technique in which the potential applied to the working electrode is linearly varied in one direction and then reversed, forming a triangular potential waveform (*Figure 5*). This reversal enables both oxidation and reduction processes to be observed within the same experiment, resulting in a cyclic voltammogram that provides detailed information about the redox behavior of the analyte. In a reversible system, the forward scan induces oxidation of the analyte at the electrode surface, while the reverse scan promotes the reduction of the oxidized species back to its original form. The resulting voltammogram typically displays two peaks: an anodic peak corresponding to oxidation and a cathodic peak corresponding to reduction *(Allen J. Bard and Larry R. Faulkner, 2000; Dragan Manojlović et al., 2010).*

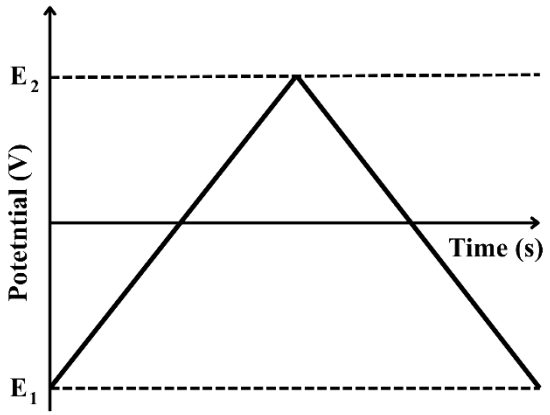

Figure 5. Potential change profile over time.

In general, a reversible cyclic voltammogram is observed when chemically stable species are present in the solution and the electron transfer between the redox species and the electrode is fast (*Figure 6*). Under these conditions, the surface concentrations of the electroactive species remain in equilibrium with the bulk solution throughout the potential sweep, regardless of the scan rate. This equilibrium allows both the forward and reverse redox processes to occur efficiently, resulting in symmetric and well-defined anodic and cathodic peaks. For electrochemically reversible reactions, the peak separation (ΔEp) between anodic and cathodic peaks is close to 0.059/n V at 25°C, where n is the number of electrons transferred, and both peak currents are nearly equal, as described with *Equation 1*. The relationship between peak current and scan rate depends on the mass transport mechanism. For diffusion-controlled processes, peak currents are proportional to the square root of the scan rate (Ip vs. $v^{1/2}$), whereas for adsorption-controlled processes, peak currents are directly proportional to the scan rate (Ip vs. v). The Randles-Ševčík equation (*Equation 2*), derived for diffusion-controlled reversible systems, quantitatively relates the peak current to the concentration of the analyte, number of electrons involved, electrode area, diffusion coefficient, and scan rate. These parameters, combined with the Nernst equation (*Equation 3*), enable researchers to model the interfacial electron transfer and understand the thermodynamic and kinetic behavior of redox couples. The behavior of the system at the phase boundary, i.e., the interface between electrode and electrolyte, must be considered, as it directly influences the observed response (Allen J. Bard and Larry R. Faulkner, 2000; Dragan Manojlović et al., 2010). The analysis of how the peak current scales with scan rate is a key diagnostic for determining the mass transport mechanism (diffusion vs. adsorption), while the peak separation ΔEp is used to assess the electrochemical reversibility of the electron transfer process *(Allen J. Bard and Larry R. Faulkner, 2000; David Harvey, 1999)*.

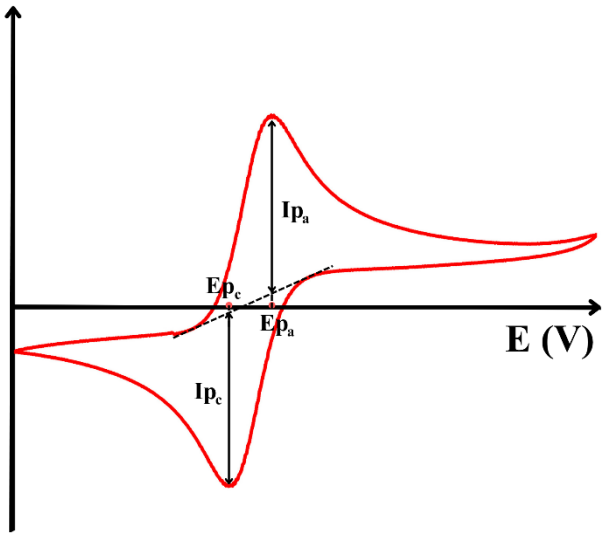

Figure 6. Representation of a CV for a reversible electrochemical process.

$$\Delta Ep = | E_{pa} - E_{pc} | = \frac{0.059}{n} \qquad \textit{Equation 1}$$

where ΔEp is the peak potential separation, Ep_a is the anodic peak potential, Ep_c is the cathodic peak potential, n is the number of electrons transferred, and 0.059 V represents the value of

RT/F at 25°C (298 K), with R being the universal gas constant, T the temperature, and F the Faraday constant.

$$\mathrm{Ip} = 0.4463\ (F^3/\ RT)^{1/2}\ \mathrm{n}^{3/2}\mathrm{A}D^{1/2}\ c_0 v^{1/2} \qquad \textit{Equation 2}$$

where Ip is the peak current, n is the number of electrons transferred in the redox reaction, A is the electrode surface area, D is the diffusion coefficient of the electroactive species, C_o is the bulk concentration of the electroactive species, *v* is the scan rate, F is the Faraday constant, R is the universal gas constant, and T is the temperature.

$$E = \mathrm{E^o} + \left(\frac{RT}{nF}\right) ln \frac{[Ox]}{[Red]} \qquad \textit{Equation 3}$$

where E is the electrode potential, E^o is the standard redox potential, R is the universal gas constant, T is the temperature, n is the number of electrons transferred, F is the Faraday constant, and [Ox] and [Red] are the concentrations of the oxidized and reduced species, respectively.

In contrast, irreversible systems exhibit voltammograms where one of the peaks is absent or extremely diminished (*Figure 7*). This occurs because the backward reaction is kinetically hindered, meaning that the electron transfer is too slow to maintain equilibrium between the electrode surface and the bulk solution, or the redox product rapidly undergoes a follow-up chemical reaction. As a result, only a single peak is observed, and no meaningful reverse process is visible. The peak potential shifts noticeably with the scan rate, and the current response becomes dominated by electron transfer kinetics rather than thermodynamic equilibrium, diffusion, and concentration *(Allen J. Bard and Larry R. Faulkner, 2000; David Harvey, 1999)*.

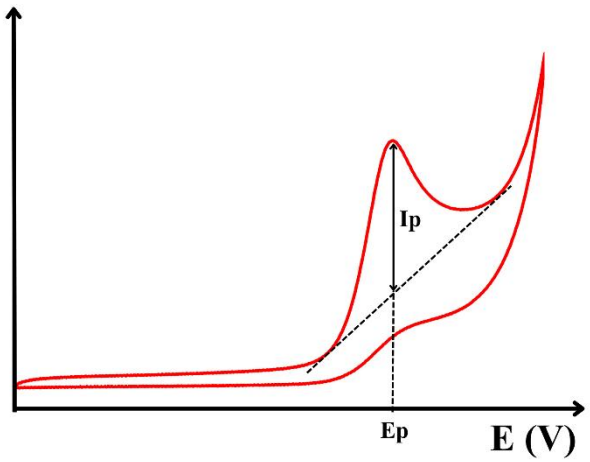

Figure 7. Representation of a cyclic voltammogram of an irreversible process, where only one peak appears.

Quasi-reversible systems represent an intermediate case, where both oxidation and reduction peaks are present, but their separation increases with scan rate, and the anodic and cathodic peak currents become unequal. The distinction between quasi-reversible and irreversible

systems is largely based on the kinetic parameters governing electron transfer and their influence on the shape and position of the voltammetric peaks *(Joseph Wang, 2023)*.

Scan rate plays a critical role in diagnosing reversibility. In irreversible systems, increasing the scan rate often results in increased peak currents but without the appearance of a reverse peak, or with minimal improvement in peak symmetry. Additionally, the peak potential (Ep) shifts significantly with scan rate in irreversible systems, cathodic peaks shift to more negative potentials and anodic peaks to more positive potentials as scan rate increases. This shift in Ep is a key diagnostic for irreversibility, whereas in reversible systems, Ep remains independent of scan rate. For irreversible reactions, the peak current depends on both the rate constant of electron transfer and the applied scan rate. Mathematical models and equations describing the peak potential and current in irreversible systems can be used to estimate kinetic parameters such as the charge transfer coefficient (α) and the heterogeneous electron transfer rate constant (k°). The relationship between peak current and scan rate is independent of whether the system is reversible or irreversible. It reflects the mass transport mechanism. Reversibility is assessed primarily through peak separation (ΔEp), peak potential shift with scan rate, and the ratio of anodic to cathodic peak currents (Ipa/Ipc). By analyzing these characteristics (peak separation, potential shifts, current ratios, and the presence or absence of reverse peaks), it categorizes the system as reversible, quasi-reversible, or irreversible *(David Harvey, 1999; Joseph Wang, 2023)*.

CV is useful for studying reaction mechanisms, determining redox potentials, and evaluating the reversibility of electron transfer processes. However, it is not ideal for precise quantitative analysis due to the capacitive background current and limitations in sensitivity at low analyte concentrations.

In this doctoral thesis, while establishing procedures for the determination of xanthine alkaloids, cyclic voltammetry was employed to electrochemically characterize the working electrodes, to examine the reversibility of the electrochemical system, and to select and optimize the pH of the most suitable supporting electrolyte.

2.3.1.2 Pulse techniques in voltammetry

Pulse techniques in voltammetry are a group of electrochemical methods in which the potential applied to the working electrode is changed in the form of short, discrete pulses rather than being varied continuously *(Dragan Manojlović et al., 2010)*. These techniques are designed to improve the quality of the measured signal, especially in cases where the analyte is present at very low concentrations or where the background (non-faradaic) current interferes with accurate detection *(Joseph Wang, 2023)*.

In traditional voltammetric methods, the applied potential is usually swept linearly over time, and the current is recorded continuously. However, this approach often leads to high background signals due to the charging of the electrical double layer at the electrode surface *(Kissinger and Hieneman, 2018).* Pulse techniques address this issue by measuring the current at specific time points, typically at the end of each pulse, when the capacitive (non-faradaic) current has largely decayed. This allows the signal resulting from the actual redox process (faradaic current) to be more easily distinguished from background noise *(Joseph Wang, 2023; Molina and González, 2016)*.

The principal pulse voltammetry techniques are pulse voltammetry include normal pulse voltammetry (NPV), differential pulse voltammetry (DPV), and square wave voltammetry (SWV) (*Figure 8*). Each technique applies potential pulses in a defined pattern and records the current response at specific intervals. Despite operational differences, all pulse techniques rely on precise timing of potential application and current measurement to optimize faradaic processes detection *(Dragan Manojlović et al., 2010)*.

All pulse techniques operate by applying a sequence of precisely controlled potential pulses and monitoring the system's response. Because the current is sampled only at selected moments, after the non-faradaic interference has subsided, these methods offer greater sensitivity and selectivity than many traditional techniques. This makes pulse voltammetry particularly valuable for detecting trace levels of electroactive species in complex matrices *(Joseph Wang, 2023; Molina and González, 2016; Osteryoung and Schreiner, 1988)*.

In this work, pulse voltammetric techniques were employed due to their ability to minimize background current and enhance analytical sensitivity. Specifically, Differential Pulse Voltammetry and Square Wave Voltammetry were used and will be discussed in detail in the following chapters.

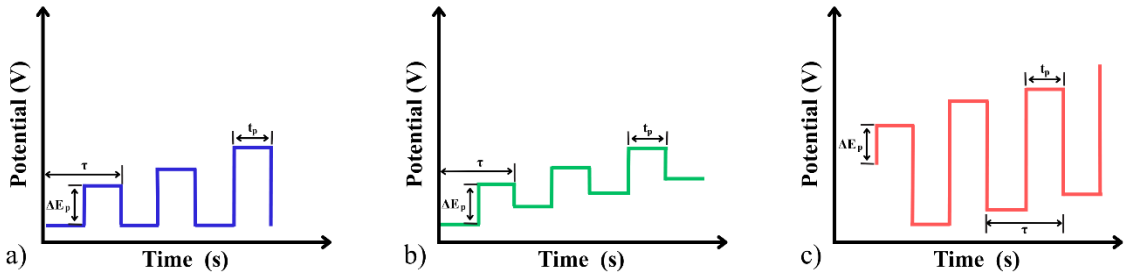

Figure 8. The potential waveform of a) normal pulse voltammetry, b) differential pulse voltammetry, and c) square wave voltammetry. ΔE_p is the pulse amplitude, t_p is the pulse width (pulse duration), and τ is the step time/period.

2.3.1.2.1 Differential pulse voltammetry

In differential pulse voltammetry (*Figure 8b*), a sequence of small potential pulses is superimposed onto a slowly increasing staircase potential. For each step, the current is measured twice: once just before the pulse and once at the end of the pulse. The difference between these two current values is plotted against the corresponding potential, resulting in a differential voltammogram *(Dragan Manojlović et al., 2010; Joseph Wang, 2023; Osteryoung and Schreiner, 1988)*.

This approach effectively suppresses capacitive (non-faradaic) current, which decays rapidly and contributes equally to both measurements, while preserving the faradaic current that decays more slowly in response to the redox reaction. As a result, the signal is sharper and more distinct, allowing improved detection of electroactive species even at low concentrations *(Joseph Wang, 2023; Kissinger and Hieneman, 2018; Molina and González, 2016)*.

The typical output of a DPV experiment is a voltammogram consisting of narrow, symmetric peaks. The peak potential is shifted from the formal redox potential of the analyte by half the pulse amplitude, while the peak current for electrochemical redox process is directly

proportional to analyte concentration. DPV is known for its excellent sensitivity and high resolution, making it especially valuable in analytical applications involving complex mixtures or in cases where redox processes occur at similar potentials, resulting in overlapping signals *(Joseph Wang, 2023; Molina and González, 2016)*.

The shape and intensity of the peaks depend on several experimental parameters, including modulation amplitude and modulation time. The modulation amplitude refers to the height of the small pulse superimposed on the linear potential sweep. It determines the extent of the potential jump applied at each step and directly influences the sensitivity of the measurement. Higher amplitudes can enhance the current response but may also broaden peaks or reduce resolution. The modulation time is the duration for which each pulse is applied before the current is measured. It must be long enough to allow the redox process to occur, but short enough to minimize capacitive currents. Together, these parameters affect both the shape and intensity of the voltammetric peaks, and the proper optimization of these parameters is essential to improve sensitivity *(Joseph Wang, 2023)*.

2.3.1.2.2 Square wave voltammetry

Square wave voltammetry (*Figure 8c*) is a highly advanced and sensitive pulse voltammetric technique. It integrates differential measurement with high-speed potential modulation, enabling efficient, rapid analysis, low-concentration detection, and suitability for systems exhibiting fast electron transfer kinetics *(Dragan Manojlović et al., 2010; Mirceski et al., 2018)*.

In SWV, a symmetrical square wave is superimposed onto a staircase baseline potential. For each potential step, two current measurements are taken, one at the end of the forward pulse and one at the end of the reverse pulse. The difference between these two current values is plotted as a function of the staircase potential. Because both measurements occur after the capacitive current has decayed, and their difference further reduces background contributions, the resulting signal represents almost purely the faradaic response of the redox-active species *(Joseph Wang, 2023)*.

SWV voltammograms typically display sharp, symmetrical peaks with high intensity. The peak potential reflects the formal potential of the redox couple, and the peak height is proportional to the analyte concentration. Due to its differential measurement and fast scanning, SWV achieves excellent sensitivity, rapid data acquisition, and effective suppression of non-faradaic current, often allowing detection in the nanomolar range with minimal sample preparation *(Mirceski et al., 2018)*.

A main advantage of SWV is its speed. Measuring both forward and reverse processes at each potential step enables scanning of the entire potential range in a short time, which is ideal for time-sensitive applications. Additionally, the technique is particularly suitable for systems where the redox reaction is chemically reversible or quasi-reversible, although it can also be applied in studies of irreversibility through analysis of peak shape and position *(Joseph Wang, 2023; Kissinger and Hieneman, 2018)*.

The analytical performance of SWV depends on parameters such as modulation amplitude and frequency. The modulation amplitude is the height of the square-shaped pulses applied on top of the staircase waveform. It controls how far the potential shifts during each forward and reverse pulse and affects the magnitude of the measured current. The frequency defines how fast the pulses are applied and is inversely related to the duration of each pulse. Higher frequencies allow for faster scans and can improve sensitivity for reversible systems, but may

distort the signal in slower, quasi-reversible, or irreversible systems. The choice of amplitude and frequency must balance sensitivity, resolution, and kinetic compatibility with the studied electrochemical process while avoiding signal distortion *(Joseph Wang, 2023)*.

2.3.1.3 Chronoamperometry

Chronoamperometry is an electrochemical method where a fixed potential is imposed on the working electrode while the time-dependent current response is monitored (*Figure 9*). It is classified as a time-dependent method and is commonly used to investigate charge transfer processes, mass transport phenomena, and reaction kinetics. It is also applied in material science for controlled electrochemical modification or deposition of species onto electrode surfaces *(Gueshi et al., 1978; Joseph Wang, 2023; Rafiee et al., 2024)*.

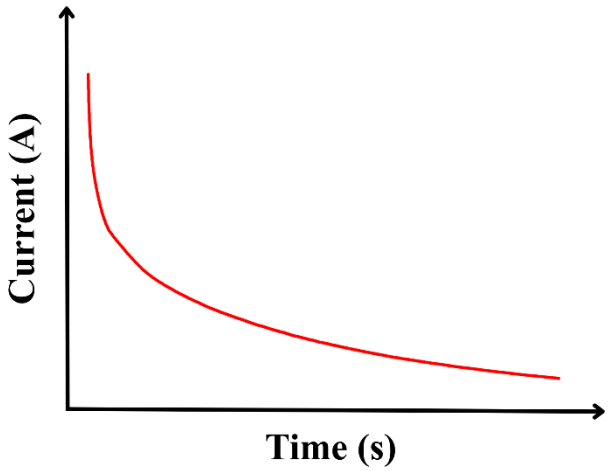

Figure 9. Typical current-time plot of a chronoamperometry measurement.

When the potential is stepped from a value where no faradaic reactions occur to one where the redox process of interest takes place, the current initially increases sharply due to the sudden onset of the electrochemical reaction. Over time, the current decays as the electroactive species near the electrode surface are depleted, and the system becomes diffusion-controlled *(Brian R. Eggins, 2002; Joseph Wang, 2023)*.

This technique is typically performed using a three-electrode configuration: a working electrode, a reference electrode with a stable and known potential, and a counter (auxiliary) electrode to complete the circuit. Measurements are usually conducted in quiescent (unstirred) solutions to preserve the diffusion layer, although hydrodynamic variants of CA can also be applied for different analytical purposes *(Brian R. Eggins, 2002)*.

CA provides valuable information about the diffusion coefficient of the analyte, the number of electrons involved in the redox process, and the overall reversibility of the system. It can also be used to study adsorption processes, catalytic effects, or the formation of reaction intermediates on the electrode surface *(Joseph Wang, 2023)*.

In this research, CA was employed for the electrochemical formation of Ag/AgCl reference electrodes by depositing chloride ions onto a silver working electrode. When a positive potential is applied to a silver surface in the presence of chloride ions, silver is oxidized to Ag^+, which immediately reacts with Cl^- to form a layer of silver chloride (AgCl) *(O. Matvieiev et*

al., 2022). This layer serves as a stable and reproducible reference system, commonly used in electrochemical measurements. The current-time response observed during chronoamperometric deposition reflects the kinetics of silver oxidation and the formation of the AgCl layer. Initially, a high current is recorded due to the rapid electrochemical reaction at the electrode surface. As the AgCl layer forms and grows, it acts as a barrier to ion transfer, causing the current to gradually decay *(Cho et al., 2022; Torres-González et al., 2022)*.

Chronoamperometric deposition offers several advantages for the fabrication of reference electrodes. It allows precise control over the thickness and uniformity of the AgCl layer by adjusting the applied potential and deposition time. This method is particularly suitable for screen-printed electrodes. The technique is generally performed in a three-electrode setup, with the silver electrode serving as the working electrode, accompanied by a counter electrode and a reference electrode. The deposition is carried out in a chloride-containing electrolyte, usually 0.1 mol L-1 KCl, under quiescent conditions to ensure stable diffusion layers and consistent film growth *(Temsamani and Lu Cheng, 2001)*.

2.3.2. Methods for morphological investigation of electrode surfaces

2.3.2.1 Scanning electron microscopic method

Scanning Electron Microscopy (SEM) is a technique used to examine the surface and structure of solid materials. Instead of using visible light and glass lenses like optical microscopes, SEM uses a focused beam of high-energy electrons that scans the sample's surface. The signals produced by these electron-sample interactions enable SEM to achieve very high magnification and detail, sometimes as low as 1 nanometer. Due to this, SEM is widely utilized in materials science, nanotechnology, and electrochemistry *(Goldstein et al., 2003)*.

In a typical SEM system, the electron beam is generated by an electron gun, commonly a field-emission gun (FEG), which produces a stable and focused stream of electrons. These sources provide the brightness and narrow beam diameter, essential for achieving high-resolution surface imaging. The beam is accelerated by an electric potential and shaped using a series of electromagnetic lenses and scanning coils, which steer the beam systematically over the surface of the sample to build a high-resolution image *(Goldstein et al., 2003; Reimer, 1998)*.

When the electron beam hits the sample, it produces several signals, including secondary electrons, backscattered electrons, and characteristic X-rays. Secondary electrons, emitted from the top few nanometers of the surface due to inelastic scattering, are most commonly used for imaging and provide detailed information about surface texture and fine topography. Backscattered electrons, resulting from elastic scattering and penetrating deeper into the material, provide compositional contrast based on atomic number differences. Additionally, when electrons from the incident beam displace inner-shell electrons in the sample's atoms, the resulting electronic transitions generate X-rays. These characteristic X-rays can be detected and analyzed using energy-dispersive spectroscopy (EDS) for qualitative and quantitative elemental analysis *(Goldstein et al., 2003).*

The SEM chamber is maintained under high vacuum to prevent air molecules from scattering the electrons. This keeps the beam stable and the images clear (Goldstein et al., 2003; Reimer, 1998).

SEM can be used to study both conductive and non-conductive sample. Modern SEM instruments with low-energy beam settings also enable analysis of beam-sensitive materials. Furthermore, the integration of X-ray detection enables combined morphological and

compositional analysis, increasing the method's applicability across scientific disciplines *(Reimer, 1998)*.

In this dissertation, SEM was employed to evaluate the surface morphology of the working electrodes, to observe structural uniformity. These observations were essential for correlating electrode surface properties with their electrochemical behavior.

2.3.2.2 Raman spectroscopy

Raman spectroscopy is an analytical technique used to examine the vibrational and rotational modes of molecules in solid, liquid, or gaseous samples. It is a non-destructive method that provides detailed structural information about materials based on the interaction of light with matter. The technique relies on the inelastic scattering of monochromatic light, typically from a laser source. When this light is directed at a sample, most photons are scattered elastically (Rayleigh scattering), but a small portion is scattered inelastically. This inelastic scattering results in a shift in the energy of the photons, known as the Raman shift, which corresponds to the vibrational energy levels of the molecules in the material *(Kolesov, 2022; Singh et al., 2024)*.

A standard Raman spectroscopy setup includes a laser, usually in the visible range, and a sample illumination and collection system, often based on a microscope. It also features a notch or edge filter to remove intense Rayleigh-scattered light, a monochromator or spectrograph to disperse the scattered light, and a sensitive detector, such as a charge-coupled device (CCD) *(Singh et al., 2024)*. The sample is typically placed on a stage under the microscope, and the laser is focused onto a small spot, enabling spatially resolved spectral acquisition *(Singh et al., 2024)*.

This technique is particularly valuable for identifying molecular structures, detecting functional groups, and assessing crystallinity, phase transitions, and molecular orientation. It is widely used in the characterization of inorganic materials, polymers, ceramics, biological samples, and nanomaterials. The greatest advantages of Raman spectroscopy are that minimal sample preparation is required, and measurements can be performed in ambient conditions. Additionally, Raman spectroscopy allows for non-contact measurements, making it highly suitable for delicate or sensitive samples *(Ajayan and Zhou, 2001)*.

Despite its advantages, Raman spectroscopy has certain limitations. The technique can be affected by fluorescence interference, particularly when analyzing complex organic materials or samples with impurities. The Raman scattering cross-section is inherently low, meaning the signal can be weak unless enhanced methods, such as surface-enhanced Raman spectroscopy (SERS) or resonance Raman spectroscopy, are used. Nevertheless, the high specificity of Raman peaks and the ability to couple the system with microscopic imaging provide significant benefits for material characterization *(Ajayan and Zhou, 2001; Singh et al., 2024)*.

In this thesis, Raman spectroscopy was included among the standard surface characterization tools used to confirm structural properties of boron-doped diamond electrode material.

2.4 Sensors - general terms

A sensor is a device that detects or measures a physical or chemical property and produces a readable or observable response. It functions by converting a real-world parameter into a signal, which can be electrical, optical, thermal, or mechanical in nature and which is usually proportional to the magnitude of the property being measured. The main parts of a sensor are

a recognition element, which selectively interacts with the target substance or stimulus, a transducer that converts this interaction into a measurable signal, and a signal processing or display system that presents the output in a useful format (*Soloman, 2010*).

Sensors are broadly classified as physical sensors, chemical sensors, and biosensors. Physical sensors measure physical quantities such as temperature, pressure, or mass. Chemical sensors detect and quantify chemical substances through selective chemical interactions. Biosensors represent a specialized subgroup of chemical sensors distinguished by the use of biological recognition elements, such as enzymes, antibodies, nucleic acids, or receptors, which provide high specificity and selectivity towards biological analytes. These biosensors are widely employed in fields such as medical diagnostics and environmental monitoring due to their ability to detect biologically relevant molecules with precision (*Brian R. Eggins, 2002*).

The recognition element is crucial in imparting selectivity to the sensor and is responsible for binding or reacting with the analyte of interest, which generates a signal change. This change must be converted or transduced into a measurable signal by the transducer component. There are many types of transducers, depending on how the sensor works and what it is used for. Optical transducers measure changes in the properties of light, like absorption, fluorescence, or luminescence, often benefiting from advancements in fiber optics for greater flexibility and miniaturization. Piezoelectric transducers detect changes in mass or mechanical vibrations by measuring variations in the frequency of a vibrating crystal. Thermal transducers, such as thermistors and thermocouples, detect heat changes produced or consumed during reactions. Electrochemical transducers are among the most common and include potentiometric devices that measure electrode potential in response to analyte concentration; amperometric or voltammetric sensors that detect currents resulting from oxidation or reduction reactions; conductometric sensors that monitor changes in solution conductivity; and field-effect transistor (FET)-based sensors that offer miniaturization and enhanced sensitivity *(Brian R. Eggins, 2002; Soloman, 2010).*

The operation of a sensor can be schematically represented as the selective interaction between the recognition element and the analyte, which induces a physicochemical change transduced into an electrical or optical signal for measurement and interpretation. Biosensors, in particular, combine biological recognition with signal transduction, enabling the selective detection of analytes ranging from small molecules to complex biomolecules. Together, these components enable sensors to provide crucial quantitative or qualitative information in a wide variety of analytical, clinical, and industrial applications.

2.4.1 Electrochemical sensors

Electrochemical sensors are analytical devices that use electrochemical processes to detect and quantify chemical species. They work by converting chemical information from an analyte into an electrical signal, exploiting electron transfer reactions at electrode-solution interfaces. The primary measurable quantities include current (amperometry), potential difference (potentiometry), or charge (coulometry), which change in response to electrochemical interactions of the analyte *(Giuseppe Maruccio and Jagriti Narang, 2022)*. *Figure 10* shows a schematic representation of elements of an electrochemical sensor.

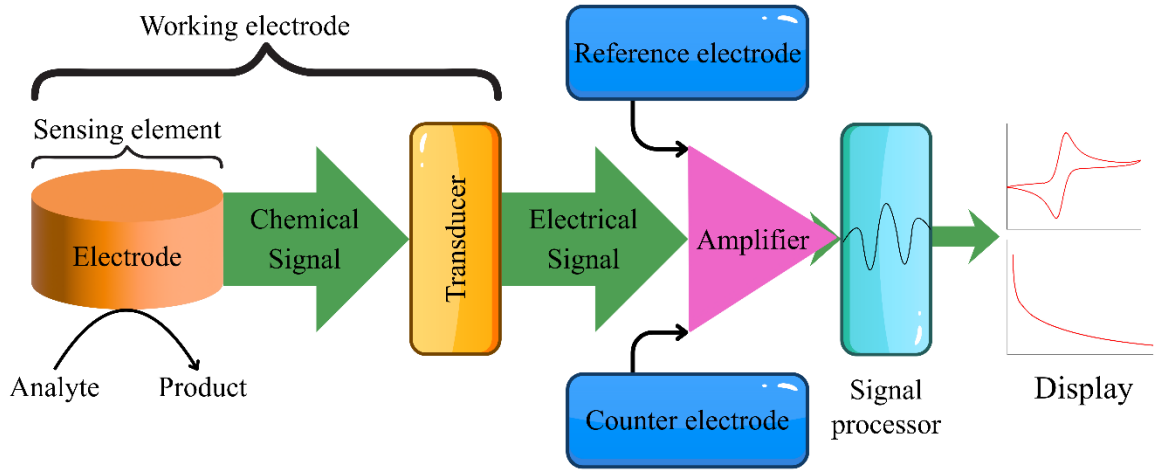

Figure 10. Schematic representation of the elements of an electrochemical sensor.

Electrochemical sensors rely fundamentally on the working electrode, where the key redox reactions involving the analyte occur. These electrodes can be made more selective towards specific analytes by modifications of their surface, which introduce functional groups that interact selectively with target molecules *(Soloman, 2010)*. Sensor efficiency largely depends on the properties of the electrode material used. Traditional materials include mercury, precious metals such as platinum and gold, and various forms of carbon. Mercury electrodes, DME, have been historically valuable due to their wide cathodic potential window and self-renewing surface, which enhances reproducibility. However, concerns over mercury's toxicity and limited anodic potential range have driven the search for alternatives *(Dragan Manojlović et al., 2010)*. Bismuth- and antimony-based electrodes, along with different amalgam electrodes, have emerged as promising substitutes. Precious metal electrodes act as catalysts in electron transfer reactions and are widely used in the anodic potential region, although their application in the cathodic range is limited because of high background current, which is caused by oxide layer formation *(Mikkelsen and Schrøder, 2003; Serrano et al., 2016; Švancara et al., 2010)*.

Carbon-based electrodes are widely used in electrochemical sensing due to their structural properties *(Uslu and Ozkan, 2007)*. Commonly used carbon electrodes include graphite, glassy carbon electrodes (GCE), and boron-doped diamond electrodes *(Pereira et al., 2012; Shi and Shiu, 2001)*. Recently, nanomaterials such as graphene derivatives and carbon nanotubes have gained attention due to their large surface area, enhanced electrocatalytic activity, broad potential windows, and cost-effectiveness *(Kim et al., 2007; Szunerits and Boukherroub, 2018)*. Advances in electrode design include the development of heterogeneous carbon electrodes like carbon paste electrodes (CPE) and screen-printed carbon electrodes (SPCE), which have expanded the applicability of electrochemical sensors, especially in medical diagnostics, where low detection limits are essential *(Okpara et al., 2021; Rejithamol and Beena, 2022)*.

In this dissertation, SP/BDD and SP/MWCNT were used as WEs. The basic principles of "screen-printing" technology and the characteristics of electrodes are given below.

2.4.1.1 Screen-printed sensors and screen-printing technique

Screen-printed electrochemical sensors (SPESs) have gained significant attention due to their adaptability, cost-efficiency, and ease of fabrication. These sensors are produced using the screen-printing technique, an industrial process that enables the rapid and reproducible fabrication of complex electrode structures directly on different substrates. The technique is based on a mesh stencil typically made of polyester or stainless steel, through which conductive or insulating inks are deposited layer by layer. The patterned inks define the geometry and functionality of the electrodes and insulation layers, forming compact and integrated three-electrode systems comprising a working electrode, a counter electrode, and a reference electrode *(Suresh et al., 2021)*.

The versatility of this method allows for the use of various ink formulations, including carbon-based, metallic, or composite inks, which can be tailored to specific analytical applications. Additionally, the technique is compatible with a wide range of substrates, including ceramics, polymers, glass, alumina, and paper, allowing for sensor development on both rigid and flexible platforms (*Paimard et al., 2023; Singh et al., 2022)*.

Screen-printed sensors are particularly attractive in applications that require miniaturized, portable, and disposable platforms. Their design enables the integration of all necessary electrode components into a single, compact unit, thereby significantly reducing the complexity of the experimental setup. This configuration is especially valuable for in situ, point-of-care diagnostics, environmental monitoring, and on-site analysis, where ease of use and rapid response are critical. The inherent disposability of these sensors minimizes the risk of contamination, while their ability to be mass-produced at a low cost makes them accessible for large-scale applications *(Suresh et al., 2021)*.

Despite their numerous advantages, screen-printed sensors also have certain limitations. Variability between production batches can occur due to minor inconsistencies in the printing process, which may affect sensor-to-sensor reproducibility. Additionally, some standard ink materials may offer a limited electrochemical window or insufficient long-term stability under aggressive conditions. These drawbacks, however, can be addressed through the incorporation of advanced materials such as boron-doped diamond, carbon nanotubes, or metal nanoparticles, which enhance the chemical stability, sensitivity, and selectivity of the sensors *(Singh et al., 2022)*.

A representative schematic of a typical screen-printed sensor configuration is provided in *Figure 11*. As illustrated, the integration of a three-electrode system and insulating layers within a single structure shows the simplicity and functionality of this sensor design.

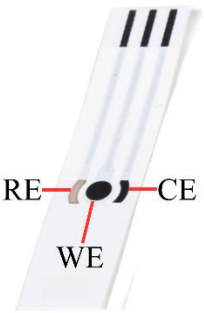

Figure 11. Schematic representation of screen-printed sensor; three-electrode platform (WE – Working electrode; RE – Reference electrode; CE – Counter electrode).

2.4.1.1.1 Screen-printed sensors with boron-doped diamond films as working electrode

In this work, a novel screen-printed sensor with a chemically deposited boron-doped diamond electrode (SP/BDD) was used. The sensor was produced by combining large-area linear antenna microwave chemical vapor deposition (LA-MWCVD) and screen-printing, two complementary techniques that enable the construction of advanced electrochemical platforms *(O. Matvieiev et al., 2022; Šelešovská et al., 2022)*.

The boron-doped diamond films were deposited on alumina (Al_2O_3) ceramic substrates using the LA-MWCVD method. This process enables the uniform, large-area growth of diamond films with controlled boron incorporation, resulting in stable and conductive diamond surfaces suitable for electrochemical applications. These films were used to form the working and counter electrodes.

Following the diamond deposition, the silver reference electrode and insulating layer were applied via screen-printing, a method well-suited for the prototyping and reproducible fabrication of sensor components *(O. Matvieiev et al., 2022)*.

This sensor configuration offers a robust, disposable, and chemically stable platform, making it ideal for sensitive electrochemical detection under harsh or variable conditions. Its design makes it especially promising for point-of-care diagnostics and environmental monitoring, including measurements in complex biological fluids.

2.4.1.1.2 Screen-printed sensor with multi-walled carbon nanotube working electrode

Screen-printed electrodes modified with multi-walled carbon nanotubes represent a practical and efficient solution for electrochemical sensing. SP/MWCNT electrodes are often fabricated as part of an all-in-one, three-electrode system, consisting of a MWCNT-modified carbon working electrode, a carbon counter electrode, and a silver or Ag/AgCl reference electrode. This configuration enables rapid and convenient measurements without the need for extensive setup or pre-treatment of the electrode. In addition, these sensors are compatible with both aqueous and non-aqueous media and support a broad range of voltammetric techniques.

Because of their robustness, affordability, and ease of mass production, SP/MWCNT sensors have found wide use in pharmaceutical, environmental, and biological applications. They are particularly useful for point-of-care analysis and on-site environmental testing, where disposable, low-maintenance, and reliable sensing platforms are required.

In this work, the SP/MWCNT sensor (Metrohm DropSens) was employed as one of the sensing platforms for voltammetric analysis. This commercial screen-printed electrode features a working electrode with carboxyl-functionalized (-COOH) multi-walled carbon nanotubes deposited on the carbon surface, typically by drop-casting a MWCNT suspension, offering enhanced electroactive surface area and improved electron transfer kinetics. The auxiliary electrode is made of carbon, while the reference electrode is composed of silver. Electrical contacts are silver-based. The entire system is printed on a ceramic substrate with dimensions of 3.38 cm × 1.02 cm and a thickness of 0.05 cm.

2.5 Xanthine alkaloids

Xanthine alkaloids represent a group of naturally occurring purine-based compounds widely distributed in plants, and to a lesser extent in microorganisms and animals. The most well-known members of this group are caffeine, theobromine, and theophylline, collectively referred to as methylxanthines, as they are methylated derivatives of the parent compound xanthine, with the general formula shown in *Figure 12*. Due to their pharmacological properties, primarily stimulation of the central nervous system, diuretic effects, and bronchodilation, these alkaloids are of great significance in both medicine and the food industry *(Ashihara et al., 2017; Kapri et al., 2022; Singh et al., 2018).*

These compounds are naturally present in many widely consumed plant species. Caffeine is predominantly found in coffee (Coffea arabica), tea (Camellia sinensis), guarana (Paullinia cupana), and energy drinks, while theobromine is present in cocoa (Theobroma cacao) and chocolate products. Theophylline occurs in trace amounts in tea but is more widely used as a therapeutic agent in respiratory medicine due to its ability to relax bronchial smooth muscle *(Scheindlin, 2007).*

Even with their structural similarity, the specific number and arrangement of methyl groups on the purine nitrogen atoms lead to divergent biological activities and pharmacokinetic profiles. Caffeine contains three methyl groups (1,3,7-trimethylxanthine), theobromine two (3,7-dimethylxanthine), and theophylline also two, but at different positions (1,3-dimethylxanthine). These differences influence their potency, metabolic rate, and specific therapeutic applications *(Ashihara et al., 2017).*

Given their frequent co-occurrence in plant-based and pharmaceutical matrices, and the potential for multiple methylxanthines to be present in a single sample, precise and selective analytical detection of these compounds is a significant challenge. As such, xanthine alkaloids are not only pharmacologically important but also analytically relevant, making them suitable targets for the development and validation of sensor-based and electrochemical detection methods.

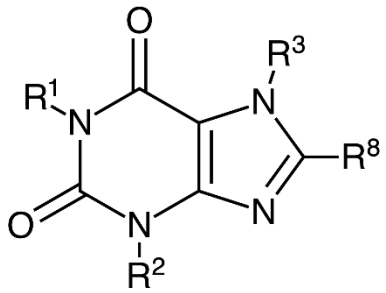

Figure 12. General formula of xanthine alkaloids.
For CAF and TP, $R^1 = CH_3$; for TB, $R^1 = H$; For all three compounds, $R^2 = CH_3$;
For CAF and TB, $R^3 = CH_3$; for TP, $R^3 = H$; $R^8 = H$ for all compounds.

2.5.1 Caffeine

Caffeine (1,3,7-trimethylxanthine; IUPAC name: 1,3,7-trimethylpurine-2,6-dione; *Figure 13*) is a naturally occurring methylxanthine alkaloid and the most widely consumed psychoactive substance worldwide. Found in over sixty plant species, including *Coffea arabica*, *Camellia*

sinensis, *Theobroma cacao*, and *Cola nitida*, caffeine is commonly ingested through beverages such as coffee, tea, energy drinks, and cocoa-based products *(Scheindlin, 2007)*. Its content in these sources varies depending on plant species, agricultural practices, and processing methods. Chemically, caffeine is a white, odorless, bitter-tasting compound, freely soluble in water, and structurally defined as 1,3,7-trimethylxanthine *(Juliana dePaula and Adriana Farah, 2019)*.

Beyond its well-known stimulant effects on the central nervous system, caffeine also exhibits diuretic, analgesic, and cardiostimulatory properties. These pharmacological effects result from its ability to act as a non-selective antagonist of adenosine receptors and an inhibitor of phosphodiesterases. While moderate intake is generally considered safe, excessive or chronic consumption has been associated with adverse effects such as anxiety, hypertension, gastrointestinal disturbances, and arrhythmias *(Robin Poole et al., 2017; R.P. Heaney, 2002)*. Regulatory authorities typically define a daily intake of up to 400 mg as safe for most healthy adults *(Antonio et al., 2024; Tomas Brodin et al., 2014).* The children under the of 12, the limit ranges from 45 to 85 mg per day, and children in adolescence are advised not to exceed 100 to 175 mg daily *(Mitchell et al., 2014)*. Individuals with preexisting conditions, such as cardiovascular disorders or hypertension, are usually advised to limit caffeine intake to less than 300 mg per day to reduce potential health risks *(Elvira Gonzalez de Mejia and Marco Vinicio Ramirez-Mares, 2014)*.

Due to its widespread use, caffeine has become a compound of analytical relevance in pharmaceutical, food safety, and environmental monitoring. It has even been proposed as a chemical marker of anthropogenic contamination in aquatic systems *(Hans-Rudolf Buser et al., 2003; Ivan Senta et al., 2015)*. Considering the broad range of concentrations in which it appears across complex sample matrices, the development of sensitive, selective, and rapid analytical methods for caffeine determination remains a key priority in applied analytical chemistry.

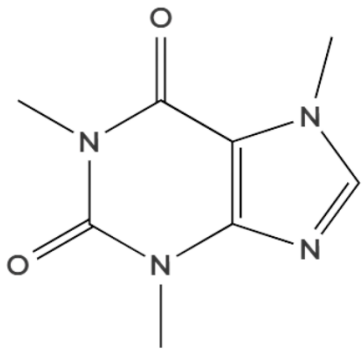

Figure 13. Caffeine structure.

2.5.2 Theobromine

Theobromine (3,7-dimethylxanthine; IUPAC name: 3,7-dimethyl-1*H*-purine-2,6-dione, *Figure 14*) is a naturally occurring methylxanthine alkaloid and a close structural analog of caffeine. It is most abundant in cocoa beans and their derivative products such as dark and milk chocolate, making it one of the principal bioactive compounds found in chocolate *(Hendrik J. Smit. and Rachel J. Blackburn, 2005)*. The concentration of TB in cocoa-derived products varies depending on the cacao content and processing method. Levels typically range from 1.2-

5 g/100 g in cocoa beans, ~1 g/100 g in dark chocolate, and 0.1-0.5 g/100 g in milk chocolate. Trace amounts are also present in tea, yerba mate, guarana, and cola nuts, while it is largely absent from coffee *(Ilaria Cova et al., 2019)*.

Theobromine appears as a white, crystalline powder, with limited water solubility (330 mg/L at room temperature) and greater solubility in hot water or alcohol *(Pulok K. Mukherjee, 2019)*. Its acidic dissociation constant (pKa ≈ 9.28) allows for greater oxidative activity in acidic media, which can be exploited in analytical electrochemical detection. Pharmacologically, TB acts as a mild central nervous system stimulant, markedly less potent than caffeine, but still capable of producing cortical stimulation, smooth muscle relaxation, bronchodilation, vasodilation, and diuretic effects. It has also been shown to exert antitussive activity, act as a myocardial stimulant, and contribute to enamel protection in dental applications (*Eva Martínez Pinilla et al., 2015; F. Estelle R Simons et al., n.d.; Hendrik Jan Smit, n.d.; L. J. Dorfman and M. E. Jarvik, n.d.; Mitsugu Yoneda et al., 2017)*.

Despite its relatively moderate CNS effects, theobromine has been the subject of growing interest due to its antioxidant potential, low toxicity in humans, and possible therapeutic applications. Notably, the compound is considered a banned stimulant in veterinary and equine sports, and its toxicity is well-documented in several animal species, particularly dogs, rabbits, and rodents, in which even small doses can be fatal due to slower metabolic clearance. In humans, however, no confirmed cases of acute theobromine toxicity have been reported under normal dietary intake *(E R Strachan and A Bennett, 1994; Soffietti et al., 1989, 1989; Y Wang and D P Waller, 1994; Ying Wang et al., 1992)*. However, given the increasing consumption of high-cocoa-content products and theobromine's presence in various plant-based matrices, monitoring its concentration in complex food and pharmaceutical samples remains relevant.

Taken together, theobromine's pharmacological, nutritional, and toxicological properties, as well as its structural similarity to caffeine, make it an analytically significant compound. Its relatively high natural abundance, moderate electrochemical activity, and variable concentration in real samples support the need for reliable detection techniques, particularly in the context of method validation through sensitivity and selectivity metrics.

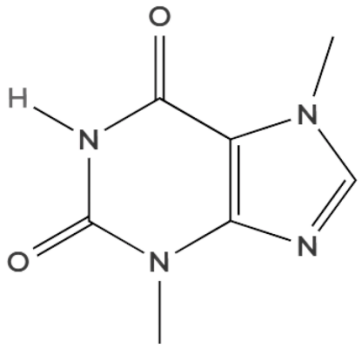

Figure 14. Theobromine structure.

2.5.3 Theophylline

Theophylline (3,7-dihydro-1,3-dimethyl-1H-purine-2,6-dione; IUPAC name: 1,3-dimethyl-7*H*-purine-2,6-dione; *Figure 15*) is a naturally occurring methylxanthine alkaloid and a

structural isomer of theobromine, traditionally found in low concentrations in tea leaves (*Camellia sinensis*) and certain other plant sources. Despite its natural origin, theophylline is primarily known and used as a synthetic therapeutic agent in the management of respiratory diseases, particularly asthma and chronic obstructive pulmonary disease (COPD) *(Boylan et al., 2023; Crapnell and Banks, 2021; Ma et al., 2016)*. It has been used clinically for over a century and remains part of treatment regimens either alone or in combination with other bronchodilators and corticosteroids *(Mahemuti et al., 2018)*.

Pharmacologically, TP acts as a non-selective phosphodiesterase inhibitor, leading to increased intracellular cyclic adenosine monophosphate (AMP) levels and resulting in bronchodilation, anti-inflammatory activity, and modulation of immune responses. Additionally, it functions as a non-selective adenosine receptor antagonist, contributing to both its desired therapeutic and undesired side effects *(Margay et al., 2015; Scurek and Brat, 2024)*. The therapeutic plasma concentration range of theophylline in adults is generally accepted to be between 10-20 μg/mL. Below this range, bronchodilatory effects are insufficient, while plasma levels above 20 μg/mL are associated with dose-dependent toxicity, including nausea, insomnia, irritability, tachycardia, cardiac arrhythmias, and seizures *(Althagafi, 2022; Crapnell and Banks, 2021; Gastel, 2022; Goh et al., 2023; Ichikawa et al., 2017; Mahemuti et al., 2018)*. Inter-individual variability in metabolism, primarily via cytochrome P450 1A2, makes theophylline particularly challenging to dose accurately, often requiring therapeutic drug monitoring in clinical settings *(Sohn et al., 2017)*.

Theophylline's narrow therapeutic index, coupled with its widespread use and physiological accumulation potential, underscores the importance of precise analytical determination in pharmaceutical formulations, biological fluids, and food or beverage products where methylxanthines may co-exist. Moreover, its physicochemical characteristics, including a relatively low molecular weight (180.2 g/mol), moderate water solubility, and electrochemical activity, make TP a relevant target for sensor-based and electrochemical detection techniques. From a toxicological perspective, although well tolerated within therapeutic limits, chronic or excessive intake can result in multisystem side effects ranging from gastrointestinal discomfort and CNS excitation to bronchial muscle flaccidity and cardiovascular dysfunction, particularly in individuals with impaired metabolism or in pediatric populations. Given the clinical relevance of theophylline, the development of sensitive, selective, and rapid detection methods is crucial, not only to support pharmaceutical quality control but also to ensure safe therapeutic monitoring and explore environmental and nutritional exposures *(A. Douglas Kinghorn et al., 2017)*.

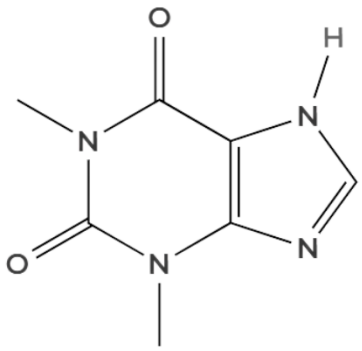

Figure 15. Theophylline structure.

2.5.4 Boron-doped diamond for xanthine alkaloids sensing - a literature review

Boron-doped diamond has proven to be a highly applicable material in electrochemistry. As previously discussed, its wide working potential window, low background current, and exceptional chemical and mechanical stability provide a unique set of advantages for the development of highly sensitive electrochemical sensors. These characteristics make BDD particularly suitable for the detection of a broad range of analytes in diverse types of real samples, including beverages, food products, environmental matrices, pharmaceuticals, and biological fluids.

Table 1 presents a literature overview of electrochemical sensors based on BDD working electrodes used for the determination of xanthine alkaloids. The table summarizes key electroanalytical parameters reported in these studies: the operating concentration range, sensitivity of the obtained methods, and the detection limit, as well as the specific xanthine alkaloid (e.g., caffeine, theobromine, theophylline) targeted in each case.

Following the development of electroanalytical methods for the determination of xanthine alkaloids using SP/BDD, the obtained parameters were compared with those reported in the selected literature studies. This comparison was carried out in order to evaluate the analytical performance and potential advantages of the proposed methods.

The literature review confirms the feasibility of developing highly sensitive and reliable methods for xanthine alkaloid detection using BDD as the working electrode.

Electrode	Xanthine alkaloid	Supporting solution	Techniq.	Peak potential [V vs. Ag/AgCl]	Linear range [µmol L^{-1}]	LOD [µmol L^{-1}]	Ref.
SP/BDD	caffeine	0.5 mol L^{-1} H_2SO_4	DPV	+1.28	20 - 500	2.80	This work
BDD	caffeine	0.4 mol L^{-1} $HClO_4$	DPV	+1.55	0.4 - 25	0.15	*(Švorc et al., 2012)*
BDD film	caffeine	Acetate buffer (pH 4.5)	DPV	+1.35	0.5 - 83	0.038	*(Lourenção et al., 2009)*
BDD	caffeine	PB (pH 2.5)	SW stripping voltammetry	+1.49	26-644	1.4	*(Yiğit et al., 2016)*
BDD	caffeine	Acetate buffer (pH 5)	SWV	+1.37	1.00 - 54.1	0.027	*(Júnior et al., 2020)*
BDD	caffeine	BRB pH 1	SWV	+1.50	3.09–28.32	0.51	*(Yardım et al., 2013)*
SP/BDD	theobromine	0.5 mol L^{-1} H_2SO_4	DPV	+0.90	1-7 7-60	0.51	This work
BDD thick-film	theobromine	1 mol L^{-1} H_2SO_4	DPV	+1.20	0.99 - 54.5	0.42	*(Ľubomír Švorc et al., 2018)*
BDD	theobromine	Acetate buffer (pH 5)	SWV	+1.39	1.00 - 54.1	0.025	*(Júnior et al., 2020)*
SP/BDD	theophylline	0.5 mol L^{-1} H_2SO_4	SWV	+1.04	3.8 – 27	0.24	This work

BDD film	theophylline	1 mol L^{-1} H_2SO_4	DPV	+1.63	2 - 380	0.91	*(Cinková et al., 2015)*

Table 1. Literature review of xanthine alkaloids determination with boron-doped diamond sensors.

2.5.5 Multi-walled carbon nanotubes for xanthine alkaloid sensing – a literature review

Multi-walled carbon nanotubes have attracted considerable attention in electrochemical sensing due to their large surface area and good electrical conductivity. Their ability to facilitate electron transfer reactions makes them particularly attractive for enhancing the sensitivity of sensors targeting small organic molecules such as xanthine alkaloids.

While numerous studies have investigated MWCNT-based detection of various xanthine derivatives, most analytical approaches have centered on caffeine because of its high prevalence in beverages, pharmaceuticals, and food items, and its physiological importance.

In recent years, numerous electroanalytical methods for the determination of caffeine have been developed using electrodes modified with MWCNTs. These include a variety of sensor platforms in which MWCNTs are combined with other materials such as polymers (e.g., Nafion) and metal nanoparticles. Such modifications are often aimed at improving the selectivity, signal stability, and detection limits of the method.

Table 2 presents an overview of selected literature reports on the electrochemical determination of caffeine using MWCNT-based modified electrodes. The table includes key electroanalytical parameters: operating range, LODs, along with the type of supporting electrolyte and technique used. A relevant studies were selected and reviewed based on its scientific contribution, methodological clarity, and use of MWCNTs as a core electrode component.

The study implemented a screen-printed MWCNT electrode for constructing an electroanalytical method aimed at caffeine detection. Analytical characteristics were subsequently evaluated in relation to previously reported methods to assess overall performance and applicability. The review highlights that MWCNT-based electrodes, including screen-printed configurations, represent a promising strategy for the sensitive, selective, and reproducible electrochemical detection of caffeine.

Electrode	**Supporting solution**	**Technique**	**Peak potential [V vs. Ag/AgCl]**	**Linear range [µmol L^{-1}]**	**LOD [µmol L^{-1}]**	**Ref.**
SP/MWCNT	BRB (pH 2)	DPV	+1.27	33 -500	9.40	This work
MWCNT-GCE	PB (pH 7.2)	SWV	+1.5	10 - 500	0.003	*(Gupta et al., 2013)*
f-MWCNTs	PB (pH 7)	DPV	+1.5	5.3 - 166	0.043	*(Chen et al., 2024)*
MWCNT-Nafion/GCE	0.04 mol L^{-1} BRB (pH 4.1)	DPASV	+1.3	2.945 - 377.0	0.513	*(Zhang et al., 2011)*

Table 2. Literature review of caffeine determination with multi-walled carbon nanotube sensors.

2.6 Subject and goals of research

The main idea of this work is to develop a novel electroanalytical methods for the determination of xanthine alkaloids in real world matrices using compact, disposable sensor platforms based on advanced electrode materials. In contrast to many published studies that rely on conventional bulk electrodes, this research focuses on the application of miniaturized sensor systems, suitable for low-cost, on-site, and routine analysis.

Two types of sensors were investigated: one based on a boron-doped diamond working electrode, and the other based on a multi-walled carbon nanotube working electrode. The research included the investigation of the applicability of the developed methods for analyzing real samples and comparing their performance with existing literature.

A key objective of the study was to physically and structurally characterize the selected sensors. This was carried out using field-emission scanning electron microscopy and Raman spectroscopy to confirm the morphology and crystal structure of the working electrode surfaces. Electrochemical characterization was then performed using cyclic voltammetry to assess the behavior and stability of the electrodes.

The next goal was the development of sensitive and reliable electroanalytical methods for quantifying xanthine alkaloids, specifically caffeine, theobromine, and theophylline, using differential pulse voltammetry and square wave voltammetry. Key electroanalytical parameters were determined, including the linear concentration range, limit of detection, limit of quantification, reproducibility, repeatability, accuracy, and precision.

Finally, special attention was given to the practical application of the developed methods in analyzing real samples, including coffee, energy drinks, soft drinks, chocolate, and pharmaceutical tablets. The validation of the proposed methods confirmed their suitability for routine analysis and their potential use in quality control and monitoring.

3. Experimental part

3.1 Materials, reagents, chemicals, and solutions

All chemicals used in these studies were of analytical grade. All aqueous solutions were prepared using demineralized water from a Milli-Q® deionization unit (Merck Millipore, Burlington, USA).

Potassium hexacyanoferrate(II) trihydrate ($K_4[Fe(CN)_6]\cdot 3H_2O$) in 0.1 mol L^{-1} KCl, used for investigating system reversibility and electrode characterization, was supplied by Merck (Germany).

As supporting electrolytes in these studies, 0.1 mol L^{-1} Britton-Robinson buffer and 0.5 mol L^{-1}, 0.1 mol L^{-1} phosphate buffer solution (PBS), hydrochloric acid (HCl) and sulfuric acid (H_2SO_4) were tested. 0.1 mol L^{-1} BRBS (1 L) was prepared by dissolving 2.80 mL of phosphoric acid (H_3PO_4) (16 mol L^{-1}), 2.40 mL of glacial acetic acid (CH_3COOH) (17 mol L^{-1}) and 2.48 g of boric acid (H_3BO_3). Na_2HPO_4 and NaH_2PO_4 were used for the preparation of PBS. All these substances were supplied by Alfa Aesar (Germany). 0.01 mol L^{-1} hydrochloric acid (HCl) was prepared by diluting 37 % hydrochloric acid produced by Alfa Aesar (Germany). 0.1 - 0.5 mol L^{-1} H_2SO_4 was prepared by diluting 96% sulfuric acid produced by Alfa Aesar (Germany). pH values were adjusted using sodium hydroxide (NaOH) obtained from Merck (Germany) and hydrochloric acid (HCl) from Alfa Aesar (Germany). Methanol (MeOH) was purchased from Alfa Aesar (Germany).

Standards of theophylline, caffeine, and theobromine were of analytical grade, supplied by Sigma Aldrich (USA), and used without further purification.

Coffee (Jacobs, Germany), chocolates (Lindt, Switzerland), energy drink (Crazy Wolf, Germany) and soft drink (Coca-Cola, USA) for real sample analysis were purchased at a nearby market. Pills (Durofilin®, Actavis Generics, Ireland) were purchased at a local drugstore.

3.2 Instrumentation

3.2.1 Characterization of boron-doped diamond

Scanning electron microscopy, manufactured by JEOL (7500F, Tokyo, Japan, 45° angle view), was used for morphological and structural examination of the electrode surfaces.

The chemical structure of the deposited films and boron incorporation in the BDD layer of the SP/BDD sensor were evaluated by Raman spectroscopy (633 nm Dilor system, 5 μm spot diameter, and 325 nm Spectroscopy & Imaging, Warstein, Germany, 2 μm spot diameter).

The actual appearance of both instruments is shown in *Figure 16.*

Figure 16. An actual look of the FE-SEM instrument (left) and the Raman instrument used in this research (right).

3.2.2 Electrochemical measurements

Cyclic voltammetry, differential pulse voltammetry, and square-wave voltammetry were performed with potentiostat/galvanostat Autolab PGSTAT 302 N (Metrohm Autolab, Czech Republic). The actual appearance of the instrument is shown in *Figure 17.*

Figure 17. The actual look of the Autolab instrument.

An SP/BDD sensor (Slovak Diamond Group, FEI STU, Slovakia) consists of BDD as the working and counter electrodes, and Ag/AgCl as the reference electrode. The WE surface area is 0.0707 cm^2, inner diameter of 3 mm, B/C 312 500 in the gas phase, and the resistivity was 0.017 Ω cm (O. Matvieiev et al., 2022). The SP/MWCNT sensor (Metrohm DropSens, model 110D, Llanera Asturias, Spain) was composed of a carbon working electrode modified with carboxyl-functionalized multi-walled carbon nanotubes (surface area 0.126 cm^2, inner diameter 4 mm), a carbon counter electrode, and a silver reference electrode. The actual appearance of both SP sensors is shown in *Figure 18.*

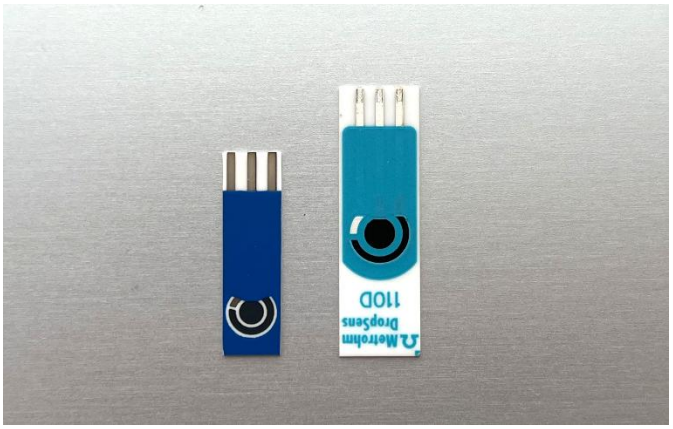

Figure 18. The actual look of SP/BDD (left) and SP/MWCNT (right) sensors.

A pH meter (Fisher Scientific, Pardubice, Czech Republic) equipped with a combined glass electrode (Metrohm, Pardubice, Czech Republic) was used to adjust the pH (*Figure 19*).

Figure 19. A pH meter used to adjust the pH.

A Bandelin Sonorex ultrasonic bath (Schalltec GmbH, Allmendingen, Germany) was used for preparing various solutions.

Statistical data analysis was performed using the corresponding software (OriginPro 8.0, OriginLab Corporation, USA). All experiments are done in a bulk electrolyte. The total volume of the voltammetric cell was 10 mL.

3.3 Preparation procedures

3.3.1 Electrochemical formation of the reference electrode of the SP/BDD sensor

The transformation of the silver reference electrode into a silver/silver chloride (Ag/AgCl) pseudo-reference was achieved through an electrochemical chlorination process (*Figure 20*). This modification was performed by chronoamperometric treatment, in which the Ag reference electrode of the SP/BDD sensor was connected as the working electrode in a standard three-electrode configuration.

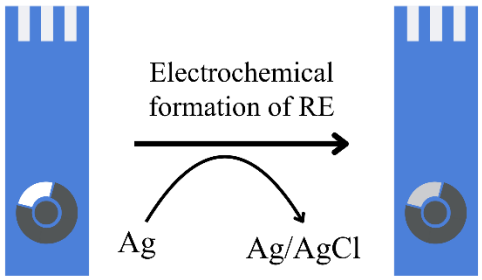

Figure 20. The transformation of Ag to Ag/AgCl by the chlorination process with the chronoamperometry technique.

The electrochemical cell contained a constantly stirred 0.1 mol L^{-1} KCl solution as the source of chloride ions. A constant potential of +700 mV (vs. external Ag/AgCl reference electrode) was applied for 30 seconds. Under these conditions, silver was oxidized to form a thin AgCl layer on the electrode surface, resulting in a stable Ag/AgCl quasi-reference electrode suitable for voltammetric measurements. This simple and rapid procedure ensures consistent potential behavior during electrochemical experiments.

3.3.2 Working electrode surface pretreatment of the SP/BDD sensor

Like other stationary electrodes, the SP/BDD sensor requires surface cleaning and electrochemical activation before use. Proper pretreatment of the working electrode is crucial for achieving optimal analytical performance. This process enhances electron transfer kinetics, increases sensitivity, improves signal stability, and contributes to better reproducibility and selectivity in electrochemical measurements.

The SP/BDD electrode surface was first thoroughly rinsed with highly purified distilled water to remove any surface contaminants. Following the initial rinse, a two-step electrochemical pretreatment was performed in a 0.5 mol L^{-1} sulfuric acid solution. The first step involved anodic polarization at +2.0 V for 120 seconds, followed by the second step, which consisted of cathodic polarization at -2.0 V for 120 seconds.

This pretreatment protocol ensures that the BDD surface is well-conditioned for future voltammetric measurements, contributing to higher signal quality and improved analytical reliability.

3.3.3. Preparation of real samples for analysis with SP sensors

Coca-Cola and energy drink samples were first subjected to 10 minutes of ultrasonic treatment to remove dissolved carbon dioxide. After degassing, a 1 mL aliquot of each beverage was mixed with 9 mL of 0.5 mol L^{-1} H_2SO_4 for subsequent analysis. For the coffee sample, 1 g of ground coffee was boiled in 100 mL of distilled water, and then a 1 mL portion of the resulting extract was combined with 9 mL of 0.5 mol L^{-1} H_2SO_4 prior to analysis.

A chocolate sample was prepared by dissolving 0.5 g of finely ground chocolate in 10 mL of hot distilled water, followed by ultrasonic treatment for one hour. Subsequently, 1 mL of this solution was mixed with 9 mL of 0.5 mol L^{-1} H_2SO_4,

The pill samples procedure involved extracting the drug powder from the capsule and dissolving 373 mg of powder in 5 mL of MeOH while stirring. After dissolving, the solution was transferred to a 250 mL flask and diluted with distilled water. Subsequently, 0.2 mL of this solution was added to 10 mL of 0.5 mol L^{-1} H_2SO_4.

3.4 Parameters optimization

3.4.1 Selection of supporting electrolyte or analysis with SP/BDD

According to published studies, the determination of xanthine alkaloids is most effective under highly acidic conditions. Such an environment promotes diffusion-controlled electrochemical processes at the electrode interface, particularly when boron-doped diamond electrodes are used, while simultaneously minimizing analyte adsorption onto the surface. This behaviour is typically observed at pH values lower than 3*(Spătaru et al., 2002)*.

During the electrochemical tests for the optimization of parameters and construction of the voltammetric protocol for determining xanthine alkaloids with an SP/BDD sensor, various supporting electrolytes, including BRB, PB, HNO_3, and H_2SO_4, were tested.

Due to all these facts and measurement confirmation, 0.5 mol L^{-1} sulfuric acid was chosen as the proper supporting electrolyte.

3.4.2 Selection of supporting electrolyte or analysis with SP/MWCNT

In the case of the SP/MWCNT sensor, the use of strong acidic media, such as sulfuric acid, proved to be unsuitable due to the sensor's limited physical and chemical resistance under these conditions. Therefore, only milder supporting electrolytes, BRB and PB, were evaluated during the optimization process. Among the tested options, BRB at pH 3 enabled the most stable and reproducible signal, providing a well-defined voltammetric response with minimal background interference. This mildly acidic environment was found to be optimal for ensuring sensitivity while preserving the structural integrity of the SP/MWCNT sensor.

As a result, BRB pH 2 was selected as the appropriate supporting electrolyte for all further measurements using this electrode.

3.4.3 Optimization of the working parameters of voltammetric methods

Differential pulse voltammetry was used for the determination of caffeine and theobromine, and for the quantification of theophylline with the SP/BDD sensor, square wave voltammetry was used. For the determination of caffeine with the SP/MWCNT sensor, DPV was used as a suitable electroanalytical technique.

Prior to evaluating the analytical parameters (linear concentration range, detection and quantification limits), it was necessary to determine the potential window and identify the optimal operating conditions under which the sensor exhibits its best electrochemical response.

DPV measurements for caffeine determination were performed using both SP/BDD and SP/MWCNT sensors in the potential range from +0.6 V to +1.4 V. For theobromine determination, DPV was employed in the potential range from +0.6 V to +1.1 V with the SP/BDD sensor. DPV and SWV measurements for theophylline determination were conducted in the potential range from +0.6 V to +1.6 V using a SP/BDD sensor.

DPV and SWV method parameters had to be optimized to achieve the best sensitivity and well-shaped peaks for every analyte.

4. Results and Discussion

4.1 Screen-printed boron-doped diamond sensor

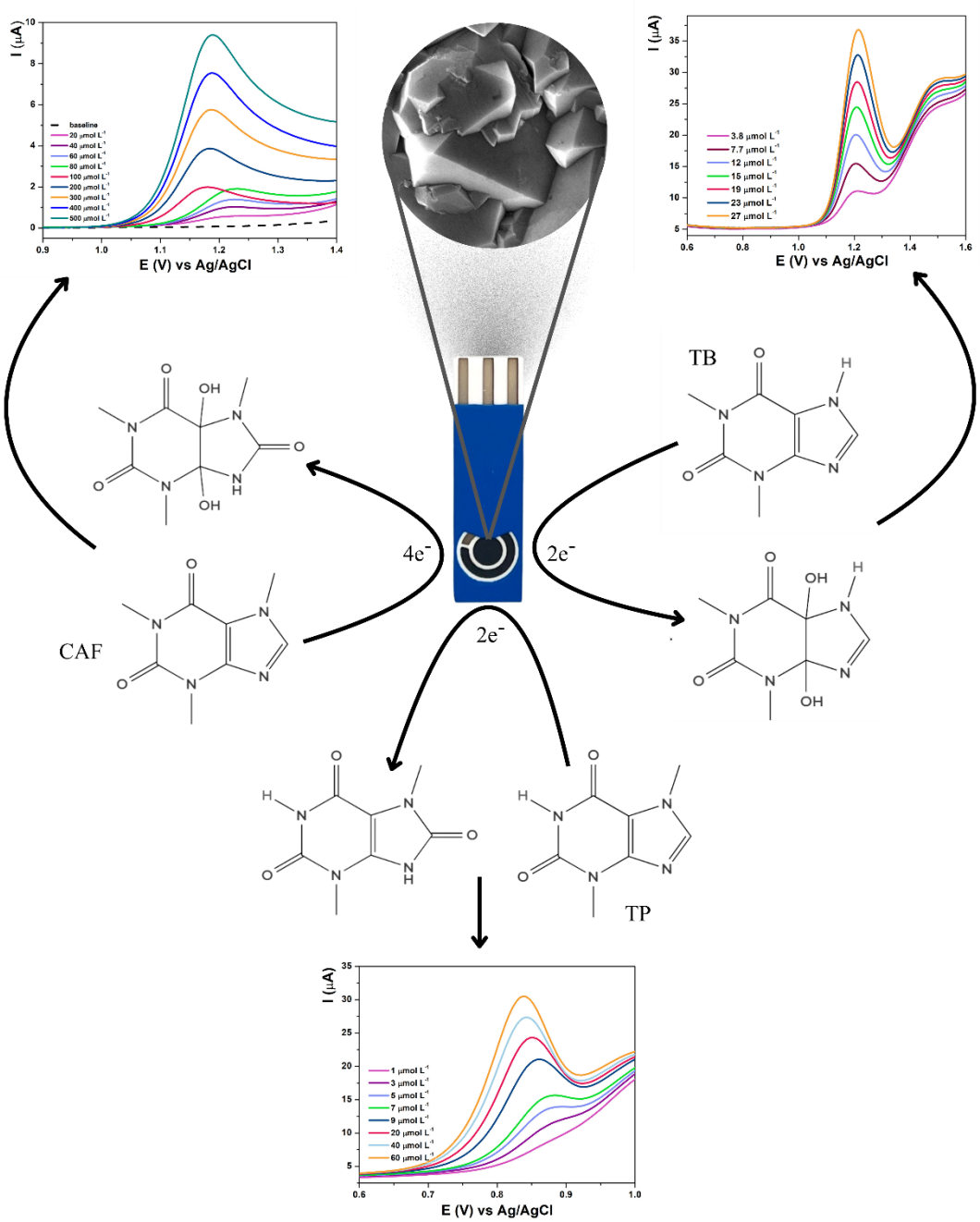

Figure 21. Main experimental points of developed methods and voltammetric response of the SP/BDD sensor to target analytes (xanthine alkaloids).

The main goal of this work was to obtain a method for the detection and quantification of caffeine, theobromine, and theophylline separately. The first part is focused on the results obtained during the optimization of the method for xanthine alkaloids determination and appropriate discussion.

The initial stage of this study utilized a screen-printed sensor incorporating a boron-doped diamond working electrode (SP/BDD). This sensor served for the optimization and establishment of a method applied to the simultaneous determination of all three xanthine alkaloids: caffeine, theobromine, and theophylline.

The surface characterization of the electrode was conducted using FE-SEM and Raman spectroscopy. FE-SEM provided detailed information about the morphology of the surface, including the shape, texture, and distribution of microcrystalline diamond structure on the electrode surfaces. Raman spectroscopy was employed to confirm the structural properties and composition of the materials, particularly the presence and quality of nanostructured diamond phases. Following structural characterization, electrochemical tests were performed.

The initial segment of the electrochemical results focuses on analyzing the electrochemical behavior of the SP/BDD electrode through cyclic voltammetry. The investigations encompassed evaluating system reversibility, determining the appropriate supporting electrolyte, and assessing how variations in scan rate influence the electrode's electrochemical response.

The second part of the results presents pulse voltammetric measurements related to the optimization of working parameters for the methods at the SP/BDD electrode. The aim was then to examine the electrochemical characteristics of the developed methods and compare them with the results reported in the literature, specifically with those of BDD and SP/BDD sensors.

The third section of the results is dedicated to evaluating the electrochemical performance of the newly developed methods based on the SP/BDD sensor. After optimizing the experimental conditions, the linear concentration ranges for quantifying xanthine alkaloids were established. Key analytical characteristics, including precision, limits of detection (LOD) and quantification (LOQ), as well as reproducibility and repeatability, were assessed. Furthermore, the influence of possible interfering species was investigated. The concluding section presents the application of the SP/BDD sensor to real sample analysis and the validation of the proposed methodology.

4.1.1 Characterization of electrode surface by FE-SEM and Raman spectroscopy method

The surface of the working electrode from SP/BDD was observed using FE-SEM. The SEM image (*Figure 22*) shows the boron-doped diamond thin film deposited on an Al_2O_3 (alumina) substrate, which serves as the base for the screen-printed sensor. The surface morphology reveals a compact and uniform microcrystalline structure, composed of faceted diamond grains with sizes ranging from approximately 0.5 to 2 µm. The individual crystallites are closely packed, forming a continuous layer with minimal visible porosity or structural defects. The total thickness of the BDD film is approximately 3.25 µm, providing a mechanically stable and electrically conductive surface ideal for electrochemical applications. The high-quality microstructure observed confirms the successful growth of a dense and adherent diamond layer.

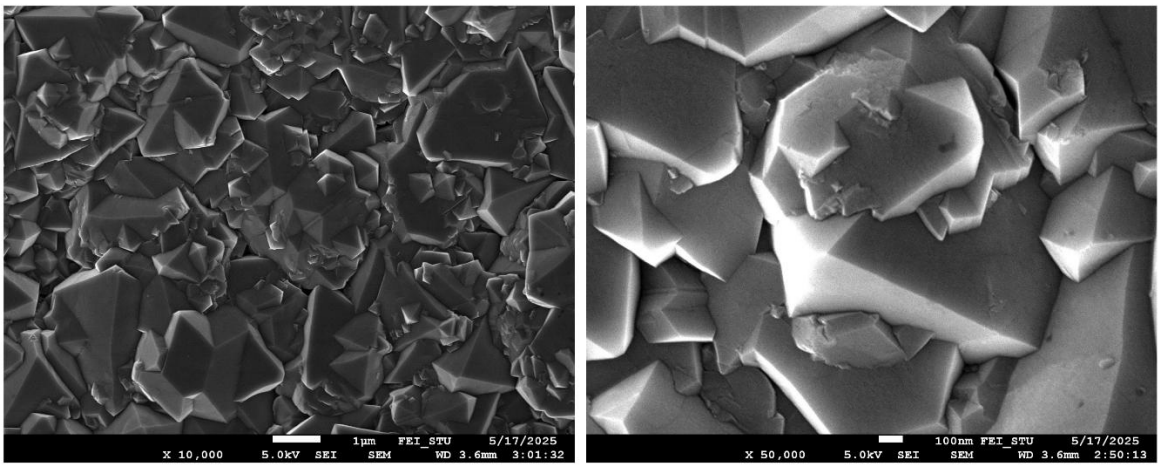

Figure 22. FE-SEM micrographs of boron-doped diamond thin film. Magnified $10*10^3$ times (left) and $50*10^3$ times (right).

Raman spectroscopy was employed to confirm the structural characteristics and boron incorporation in the BDD layer of the SP/BDD sensor. Spectra were recorded using two excitation wavelengths, 325 nm and 633 nm, to provide complementary insights into the bonding environment and electronic structure of the material (*Figure 23*). The obtained spectra exhibit the characteristic features of heavily boron-doped diamond. Specifically, prominent bands are observed at approximately 480 cm^{-1} (B_1), attributed to localized vibrations associated with boron clusters in the diamond lattice, and at 1200 cm^{-1} (B_2), a broad band commonly assigned to disordered diamond or boron-related vibrational modes. A peak near 1305 cm^{-1}, slightly shifted from the ideal diamond peak at 1332 cm^{-1}, indicates lattice distortion due to the high boron concentration. The combination of these spectral features confirms successful boron doping and the preservation of the diamond crystalline structure.

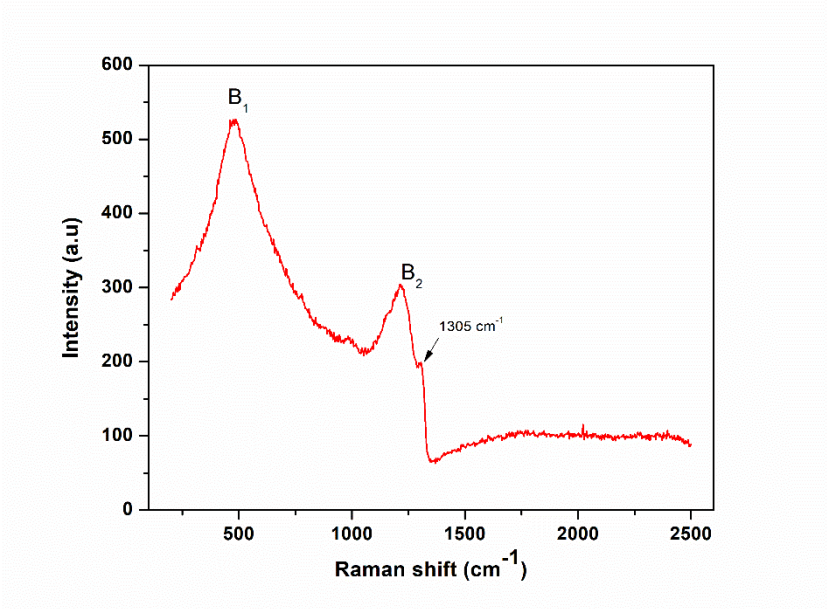

Figure 23. Raman spectra of the surface of the boron-doped diamond working electrode. B_1 - band attributed to localized vibrations associated with boron clusters in the diamond lattice; B_2 - band assigned to disordered diamond or boron-related vibrational modes.

4.1.2 Cyclic voltammetry study

4.1.2.1 Electrochemical behavior of SP/BDD sensor

This chapter outlines the electrochemical behavior of the SP/BDD sensor. The evaluation of its electrochemical characteristics includes examining the morphology of oxidation and reduction peaks, together with determining their corresponding current responses.

The electrochemical responses of SP/BDD were monitored in $K_4[Fe(CN)_6]$ solution (in order to test the system's reversibility), but more importantly, in solutions of each xanthine alkaloid separately.

The electrochemical characteristics of WE were investigated using cyclic voltammetry. Electrochemical response of WE was followed in 1 mmol L^{-1} $K_4[Fe(CN)_6]$ in 0.1 mol L^{-1} KCl. The applied potential ranged from -0.3 V to +0.8 V, while the scan rate varied from 5 to 100 mV s^{-1}. CV results show the presence of both oxidation and reduction peaks.

As a supporting electrolyte, 0.5 mol L^{-1} H_2SO_4 was used to test the electrochemical behavior of the SP/BDD sensor in the presence of xanthine alkaloids. The applied potential ranged from +0.8 V to +1.6 V, while the scan rate varied from 2 to 100 mV s^{-1}.

4.1.2.1.1 Electrochemical characterization of SP/BDD sensor

Electrochemical characterization is a critical step in understanding and optimizing the performance of SP sensors for analytical applications. Through the evaluation of key parameters such as the diffusion coefficient (D), charge transfer coefficient (α), and the heterogeneous electron transfer rate constant (k_s) and active surface of the electrode (mm^2), insight is gained into the kinetics and mechanisms governing redox reactions at the electrode surface. These parameters not only reflect the intrinsic electrochemical behavior of the sensor but also influence its sensitivity, selectivity, and analytical reliability. The electrochemical

characteristics of the SP/BDD sensor were systematically investigated. The results provide information about the efficiency and responsiveness of the sensor under experimental conditions.

The surface properties of SP/BDD were examined using a 1 mmol L^{-1} solution of $K_4[Fe(CN)_6]$ in 0.1 mol L^{-1} KCl, within a potential window ranging from –0.3 V to +0.8 V and at scan rates between 5 and 100 mV s^{-1} (Figure 24). As the scan rate increased, a proportional rise in the peak current was observed. The anodic peaks shifted slightly toward more positive potentials and the cathodic peaks toward more negative ones, with a peak separation of approximately 65 mV. These findings indicate that in this solution exhibits an efficient electrochemical response at the electrode interface, suggesting rapid electron transfer and high reversibility of the redox process.

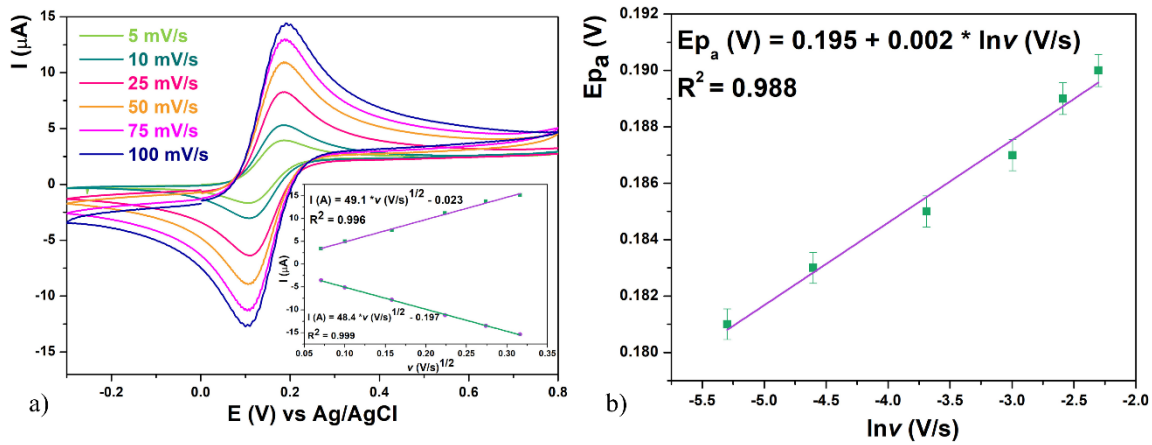

Figure 24. CVs of 1 mmol L^{-1} $K_4[Fe(CN)_6]$ in 0.1 mol L^{-1} KCl on increasing scan rates from 5 to 100 mV/s (Inset picture: Plots of anodic current (Ipa) and cathodic current (Ipc) vs. square root of the scan rate with SP/BDD).

Plots of anodic peak current (Ipa) and cathodic peak current (Ipc) versus square root of scan rate were generated, showing excellent linearity, which is consistent with the Randles-Shevchikov equation (Equation 2) for reversible systems and is expected for diffusion-controlled processes.

From this relation, the diffusion coefficient D was calculated to be 7.51×10^{-6} cm^2 s^{-1}.

The charge transfer coefficient (α) was calculated from the relations, where the slope was obtained from plotting Ep vs ln*v*:

$$slope = -\frac{RT}{\alpha nF}$$

where R is the gas constant, T is the temperature in K, n is the number of electrons, and F is Faraday's constant. A linear correlation between Epa vs. lnv was obtained, described by:

Epa (V) = 0.1951 + 0.0024 × ln*v* (V s^{-1}); $R^2 = 0.988$.

The charge transfer coefficient (α) is 0.45. This suggests a more symmetrical electron transfer process at this electrode, due to its good agreement with the theoretical value of 0.5 defined for an ideally reversible system.

Nicholson relation, shown in (*Equation 4*), was used for determination of heterogeneous electron transfer rate constant (k_s) was determined by the:

$$ks = \psi\left(\frac{D\pi nF\nu}{RT}\right)^{1/2} \qquad \textit{Equation 4}$$

where R is the gas constant, T temperature in K, D is the diffusion coefficient ($cm^2\ s^{-1}$), n is the number of electrons, F is Faraday's constant, and v is the scan rate. The calculated value is 1.05×10^{-2} cm s^{-1}.

Surface coverage (Γ*) was not considered because the process was diffusion-controlled.

The active surface area of the SP sensor was obtained based on testing the sweep rate on the electrochemical behaviour of the SP/BDD. *Figure 23* shows CV voltammograms measured at different scan rates (5-100 mV s^{-1}) in 0.1 mol L^{-1} KCl containing 1 mmol L^{-1} $K_4[Fe(CN)_6]$.

The active surface area of SP/BDD was calculated via *Equation 2* using the values of the anodic peak currents (Ip_a) with the applied sweep rates. The average value of the surface active area of SP/BDD was 6.62 mm^2. This value corresponds to 94% of the geometric surface area (7.07 mm^2), which can be the result of the non-porous nature of BDD thin films, where the electrochemically active area typically approaches the geometric area.

4.1.2.1.2 Electrochemical behavior of SP/BDD in the presence of caffeine

The oxidation pathway of caffeine involves a slow reaction of two electrons at the C-8-N-9 position, giving the substituted uric acid(1), followed by a two-electron oxidation, yielding the formation of 4,5-diol of uric acid analogue(2) through the primary two-electron and two-proton oxidation *(Hernandez-Aldave et al., 2019; Jose et al., 2021; Matteo et al., n.d.),* as illustrated in *Figure 25*.

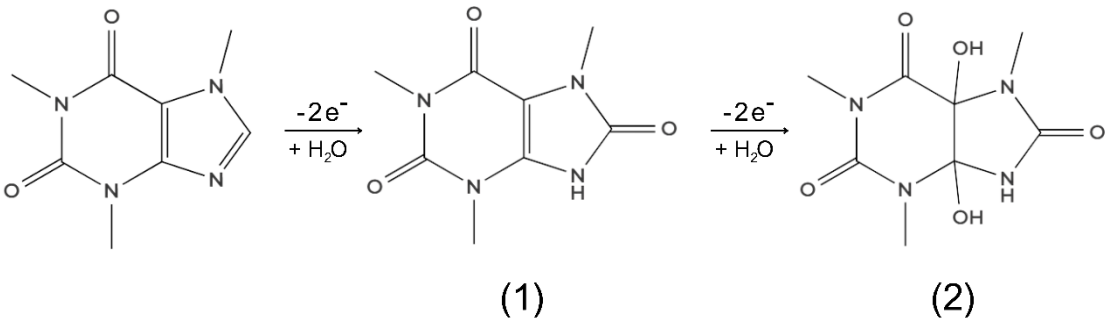

Figure 25. Mechanism of electrooxidation of caffeine.

The electrochemical oxidation kinetics of caffeine were investigated using an SP/BDD (*Figure 25a*). CV measurements were performed in 0.1 mmol L^{-1} caffeine in 0.5 mol L^{-1} H_2SO_4 over a range of scan rates from 2 to 100 mV s^{-1}. The log I vs log *v* relationship yielded a slope of 0.69 (R^2 = 0.988), indicating a mixed diffusion-adsorption controlled process with predominant diffusion control. This demonstrates efficient mass transport toward the SP/BDD electrode surface, with a minor contribution from surface adsorption or accumulation of caffeine species.

For each scan rate, the oxidation peak potential (Ep) was recorded (*Figure 26b*). In order to clarify the electron transfer mechanism and determine the kinetic parameters, the dependence

of Ep on the natural logarithm of the scan rate (ln v) was examined. The irreversible oxidation mechanism of caffeine was investigated using Laviron's equation (*Equation 5*) for non-reversible systems, which correlates the peak potential (Ep) with the scan rate (v):

$$E_p = E^0 + \frac{RT}{\alpha nF}\ln\left(\frac{RTk^0}{\alpha nF}\right) + \frac{RT}{\alpha nF} lnv \qquad \textit{Equation 5}$$

where Ep is the formal potential, R is the gas constant, T is the temperature, α is the electron transfer coefficient, n is the number of electrons, F is Faraday's constant, and k^0 is the standard rate constant.

Ep (V) = 1.25 + 0.032 × ln$v$ (V s^{-1}); R^2 = 0.996

The linear dependence between Ep and ln v indicates an irreversible kinetic process, reflected in a slight positive shift of Ep with increasing scan rate (*Figure 26a*). The obtained value αn = 0.86, assuming that the number of electrons involved in the rate-determining oxidation step is approximately n ≈ 2, gives a transfer coefficient α = 0.43. This value suggests a moderately asymmetric energy barrier, where the initial state (caffeine) exerts a somewhat greater influence on the activation energy than the product state (4,5-dihydroxyuric acid).

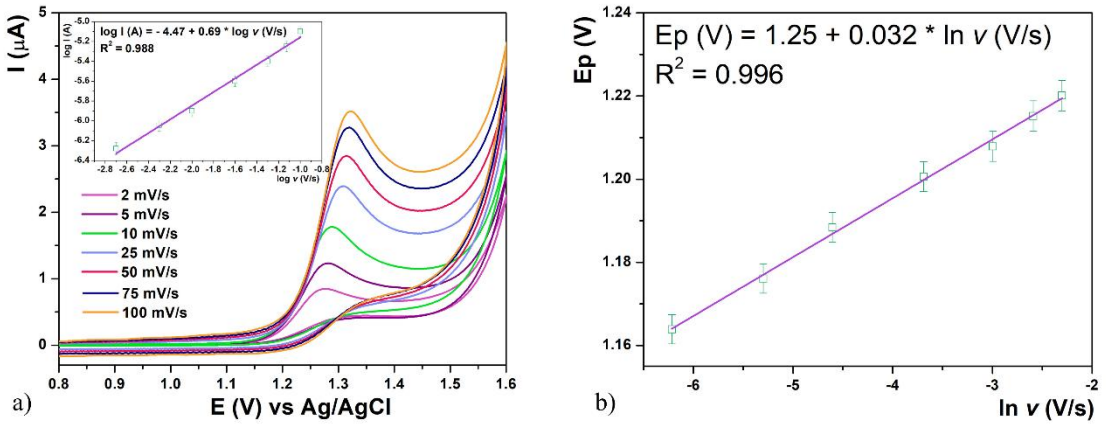

Figure 26. a) CVs of 0.1 mmol L^{-1} caffeine in 0.5 mol L^{-1} H_2SO_4 on increasing scan rates from 2 to 100 mV/s (Inset picture: Plots of log I vs. log v); b) Plots of Ep vs. ln$v$.

4.1.2.1.3 Electrochemical behavior of SP/BDD in the presence of theobromine

In an acidic medium, theobromine undergoes an irreversible electrochemical oxidation process involving the transfer of two electrons and two protons, forming an oxidized imidazolone-type derivative from the initial methylxanthine structure (*Figure 26*). The absence of a corresponding reduction peak and the linear dependence of current on the square root of the scan rate suggest a diffusion-controlled and irreversible oxidation mechanism characterized by a $2e^-/2H^+$ transfer.

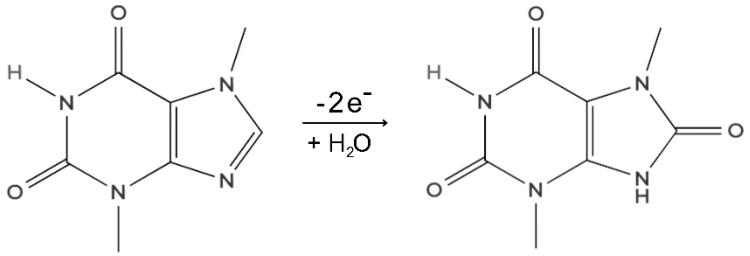

Figure 27. Mechanism of electrooxidation of theobromine.

Kinetic analysis of theobromine oxidation reveals fast electron-transfer kinetics on the SP/BDD electrode. The peak potential shows minimal dependence on scan rate, shifting only 60 mV across an increase in scan rate (2-100 mV/s). The linear relationship between Ep and ln v yields a slope of 0.01 (R^2 = 0.969), which is significantly smaller than typically observed for irreversible organic compound oxidations (*Figure 28b*). This small slope indicates that the heterogeneous electron transfer is rapid relative to the experimental timescale, approaching quasi-reversible behavior. Quantitative determination of the charge transfer coefficient (α) using the Laviron equation is not feasible for this system, as the minimal potential shift suggests the rate constant (k_s) is too high for conventional kinetic analysis at these scan rates.

The diffusion-controlled nature of the process is confirmed by the log I vs log *v* relationship (slope = 0.43, R^2 = 0.999), demonstrating efficient mass transport and fast interfacial kinetics at the SP/BDD electrode surface (*Figure 28a*).

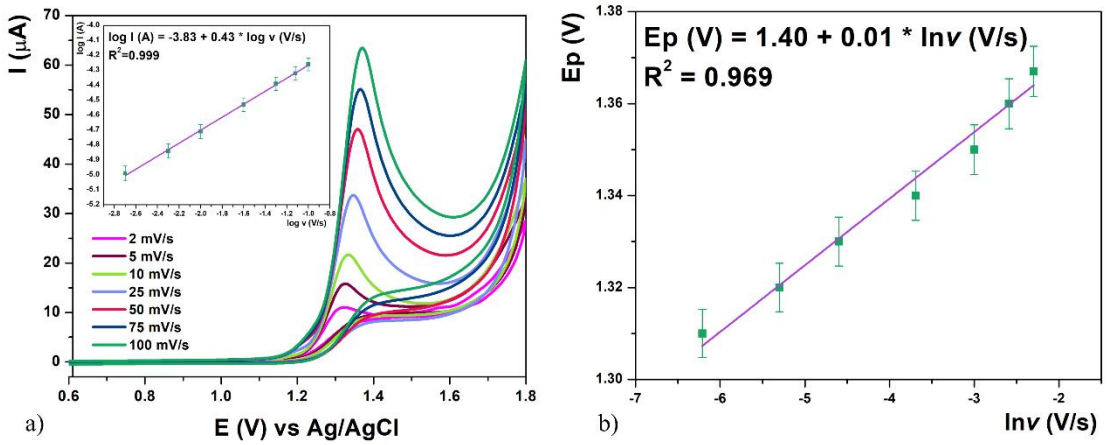

Figure 28. a) CVs of 0.1 mmol L^{-1} theobromine in 0.5 mol L^{-1} H_2SO_4 on increasing scan rates from 2 to 100 mV/s (Inset picture: Plots of log I vs. log *v*); b) Plots of Ep vs. ln*v*.

4.1.2.1.4 Electrochemical behavior of SP/BDD in the presence of theophylline

The oxidation of theophylline proceeds *via* a proton-coupled electron-transfer step at the xanthine ring. Under the acidic aqueous conditions, TP is oxidized on SP/BDD through an electron-transfer/chemical-step/electron-transfer sequence that constitutes a proton-coupled electron-transfer pathway centered at C4 of the xanthine ring (*Figure 29*). The first anodic step forms a π-delocalized radical cation; rapid nucleophilic addition of water at C4 gives a 4-

hydroxy intermediate (1). A second electron transfer leads, through further protonation and hydration, to the formation of the 4,5-diol intermediate (2).

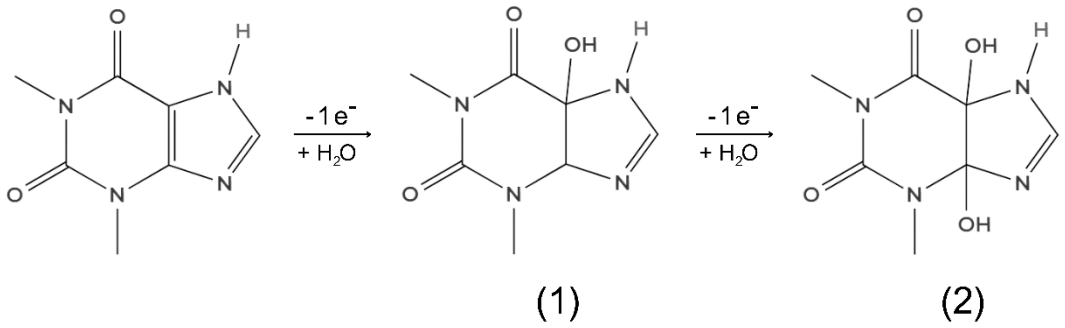

Figure 29. Mechanism of electrooxidation of theophylline.

CV was employed to investigate the electrochemical oxidation of 1 mmol L^{-1} TP in 0.5 mol L^{-1}, at the SP/BDD, with scan rates ranging from 5 to 100 mV s^{-1} (*Figure 30*a). The voltammograms exhibit an increase in peak current with increasing scan rate, accompanied by a slight positive shift in the oxidation peak, indicating some kinetic limitations in the electron transfer process. The slope value of the logarithmic plot of peak current (I_p) versus scan rate (v) is 0.42, which is close to the theoretical value of 0.5, implying that the oxidation process is diffusion-controlled, governed primarily by the mass transport of TP in solution rather than surface adsorption. These findings suggest that the oxidation of TP at the SP/BDD occurs through a diffusion-controlled mechanism, with the SP/BDD sensor providing a stable and reproducible platform for the electrochemical detection of TP.

At every applied scan rate, the corresponding oxidation peak potential (Ep) was measured. To elucidate the electron transfer pathway, Ep values were plotted against the natural logarithm of the scan rate (ln *v*) (*Figure 30b*). The irreversible oxidation behavior of TP was subsequently evaluated using Laviron's equation, as described earlier.:

$Ep\ (V) = 1.44 + 0.03 \times \ln v\ (V\ s^{-1})$; $R^2 = 0.999$

A straight-line correlation obtained from plotting Ep versus ln v indicates that the process follows an irreversible kinetic regime, evidenced by the gradual shift of Ep toward more positive potentials as the scan rate increases. From the slope, a value of $\alpha n = 0.84$ was determined, and assuming a two-electron transfer ($n = 2$) in the rate-limiting oxidation step, the charge transfer coefficient was calculated as $\alpha = 0.42$. This result points to a moderately asymmetric activation barrier, suggesting that the reactant state contributes slightly more to the activation energy than the product state. This α value suggests that the activation energy for the forward oxidation reaction is more favorable than that for the reverse process, consistent with the irreversible nature of theophylline oxidation.

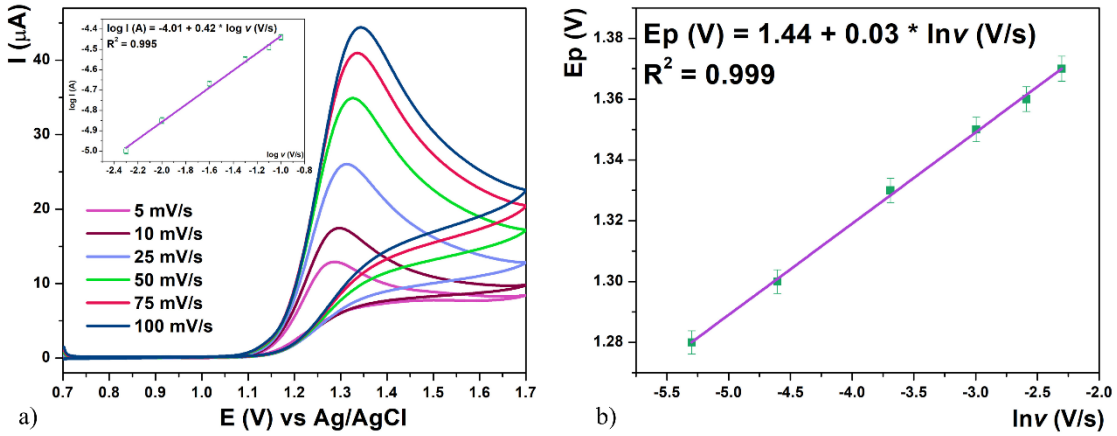

Figure 30. a) CVs of 0.1 mmol L^{-1} theophylline in 0.5 mol L^{-1} H_2SO_4 on increasing scan rates from 5 to 100 mV/s (Inset picture: Plots of log I vs. log *v*); b) Plots Ep vs. ln*v*.

4.1.2.2 Effect of supporting electrolyte

The choice of a suitable supporting electrolyte plays a crucial role in the electrochemical detection of the analyte. It directly influences the sensitivity, reproducibility, and clarity of the voltammetric signal. Due to the unique surface characteristics of BDD electrodes, such as low adsorption tendency, inertness, and a wide potential window, the choice of supporting electrolyte becomes crucial for electron transfer kinetics and minimizing background current.

4.1.2.2.1 Optimization of supporting electrolyte on the SP/BDD performances for the determination of caffeine

The electrolyte must provide a stable acidic environment that supports the oxidation of caffeine while preserving the sharpness and reproducibility of the voltammetric signal.

To determine the optimal electrolyte for caffeine detection, the electrochemical response of a 20 μmol L^{-1} caffeine solution was examined in various acidic media using the SP/BDD sensor (*Figure 31b*). The tested electrolytes included sulfuric acid (H_2SO_4), hydrochloric acid (HCl), BRBS at pH 2, and PB at the same pH. All media except hydrochloric acid produced a clearly visible and well-defined oxidation peak for caffeine. In HCl, the signal was significantly less distinct, and the oxidation peak was shifted toward more positive potentials.

The weaker signal observed in HCl can be explained by distinct molecular-level interactions. Although HCl and H_2SO_4 are both classified as strong acids, they differ markedly in their ionic makeup, which influences their interactions with caffeine as well as with the electrode interface. Literature reports indicate that protonation occurs exclusively for the monomeric form of caffeine, and the balance between the neutral species (caf) and its protonated counterpart ($Hcaf^+$) depends on the surrounding medium. This acid–base equilibrium impacts not only the oxidation peak profile but also its potential, owing to modifications in electron-transfer dynamics and the possible formation of ion pairs or other complexes. (*Spiro et al., 1989*).

Among the tested media, sulfuric acid provided the most favorable electrochemical profile, characterized by the highest peak current, a consistent oxidation potential, and a sharp,

symmetrical peak with minimal background noise. Based on these results, sulfuric acid was selected as the most suitable supporting electrolyte for subsequent measurements.

Further optimization was carried out to determine the ideal concentration of sulfuric acid (*Figure 31a*). At all concentrations tested, the oxidation of caffeine was marked by a distinct and oval-shaped peak. As the concentration of the acid increased, the oxidation peak gradually moved toward lower positive potentials. This behavior suggests that the electrochemical reaction proceeds more readily under strongly acidic conditions. With increasing acidity, the nitrogen sites in caffeine undergo greater protonation, which promotes more efficient electron transfer and reduces the additional potential needed to drive the oxidation process. As a result, a concentration of 0.5 mol L^{-1} H_2SO_4 was identified as optimal, offering the lowest oxidation potential and highest signal quality, and it was selected as the supporting electrolyte for all further voltammetric investigations of caffeine with the SP/BDD sensor.

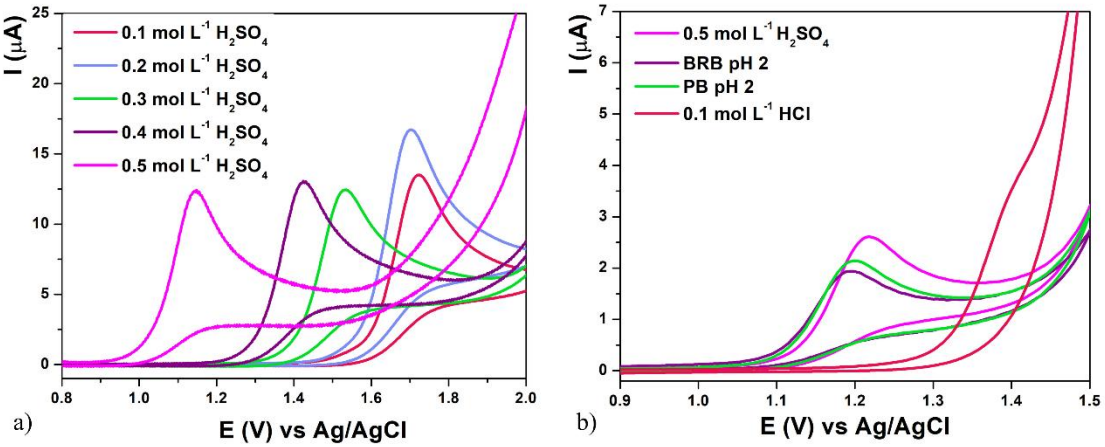

Figure 31. Electrochemical responses of SP/BDD sensor for 20 μmol L^{-1} CA obtained in a) 0.1 – 0.5 mol L^{-1} H_2SO_4 and b) 0.5 mol L^{-1} H_2SO_4, BRB pH 2, PB pH 2 and 0.1 mol L^{-1} HCl.

4.1.2.2.2 Optimization of supporting electrolyte on the SP/BDD performances for the determination of theobromine

According to the literature, optimal electrochemical detection of theobromine is typically achieved under strongly acidic conditions. Acidic media promote diffusion-controlled processes at the electrode surface and help prevent surface fouling. These favorable conditions are typically observed at pH values below 3 (*Ľubomír Švorc et al., 2018; Spătaru et al., 2002*).

Based on these findings, sulfuric acid was tested as the candidate supporting electrolyte for further evaluation. The electrochemical behavior of 0.1 mmol L^{-1} theobromine standard was investigated using a SP/BDD sensor in a concentration range of 0.1-0.5 mol L^{-1} H_2SO_4. As shown in *Figure 32*, increasing the concentration of H_2SO_4 led to a progressive shift in the oxidation peak toward lower potentials. This trend is consistent with enhanced protonation of the analyte and facilitated electron transfer in a more acidic environment.

In parallel, a rise in the background current was observed with increasing acid concentration, likely due to the enhanced oxygen evolution reaction (OER) in highly acidic media. This effect was particularly evident at 0.5 mol L^{-1} H_2SO_4, where both the peak shift and background current increase were most pronounced.

Nonetheless, the voltammogram recorded in 0.5 mol L^{-1} H_2SO_4 exhibited a clearly defined and sharp oxidation peak for theobromine at approximately 0.9 V vs Ag/AgCl. This signal is consistent with prior studies involving similar BDD-based electrode systems (*Peng et al., 2017; Vinoth and Wang, 2024*). The observed peak suggests a single-step electrochemical oxidation mechanism involving the transfer of two protons and two electrons, as previously illustrated in *Figure 26.*

Given the superior sensitivity, peak definition, and favorable oxidation potential observed, 0.5 mol L^{-1} H_2SO_4 was selected as the optimal supporting electrolyte for the determination of theobromine and used in all subsequent measurements.

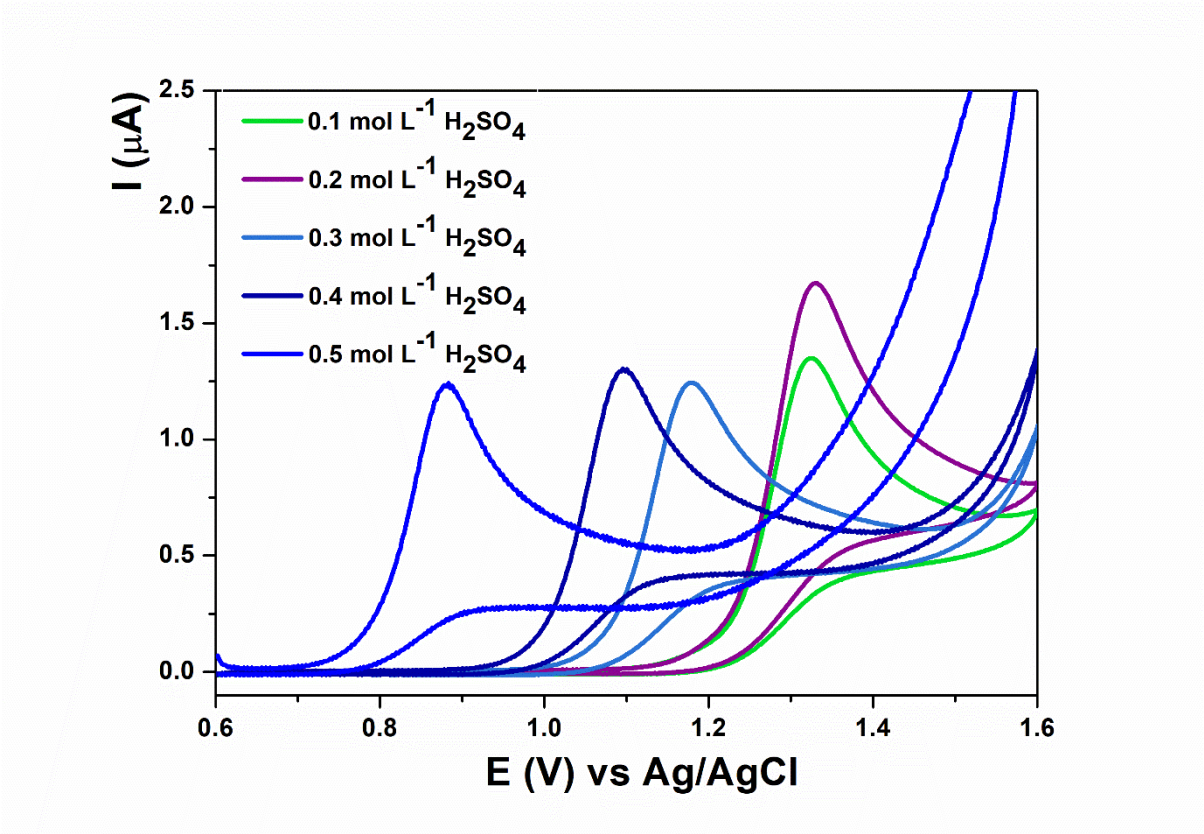

Figure 32. Electrochemical responses of SP/BDD sensor for 0.1 mmol L^{-1} TB obtained in 0.1 – 0.5 mol L^{-1} H_2SO_4

4.1.2.2.3 Optimization of supporting electrolyte on the SP/BDD performances for the determination of theophylline

According to literature data, theophylline exhibits the most favorable electrochemical response under strongly acidic conditions. To identify the optimal supporting electrolyte, three acidic media were selected: BRB pH2, 0.1 mol L^{-1} HCl, and 0.5 mol L^{-1} H_2SO_4. The electrochemical behavior of TP (0.1 mmol L^{-1}) was examined using cyclic voltammetry with the SP/BDD sensor in each of these solutions.

Figure 33 shows a shift of the peaks to higher potential values in strongly acidic media, such as 0.1 mol L^{-1} HCl and 0.5 mol L^{-1} H_2SO_4, which is consistent with the stabilization of the protonated form of TP. These shifts are due to the proton-coupled nature of TP oxidation, as well as specific electrolyte effects *(Wang et al., 2014).*

In contrast, for the BRB buffer pH 2, the Ep value is lower, reflecting weaker protonation and reduced interfacial interactions. The peak currents are also electrolyte-dependent. The highest current is obtained in 0.5 mol L^{-1} H_2SO_4 due to its high ionic strength and conductivity, which minimizes iR drop, and due to possible specific adsorption of sulfate anions that facilitates charge transfer. Lower currents are recorded in HCl and BRB buffer, where conductivity is lower or where buffer components may partially block the electrode surface. These results confirm that both pH and the nature of the supporting electrolyte strongly influence the electrooxidation of TP. The peak obtained in 0.5 mol L^{-1} H_2SO_4 had an oxidation potential value of 1.20 V. It has the highest peak current value and a well-defined peak. Considering this, we concluded that 0.5 mol L^{-1} H_2SO_4 would be the preferred supporting solution for TP detection with SP/BDD.

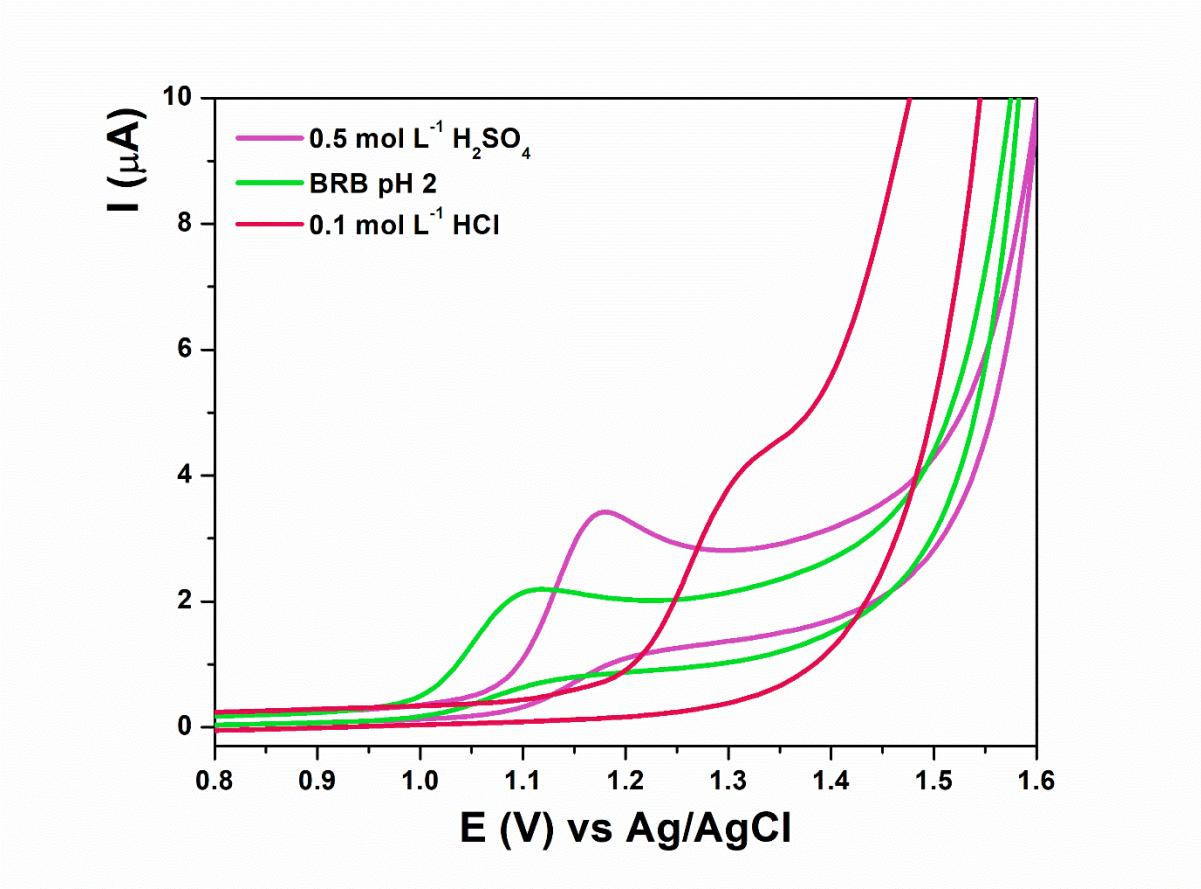

Figure 33. Electrochemical responses of SP/BDD sensor for 0.1 mmol L^{-1} TP obtained in 0.5 mol L^{-1} H_2SO_4, BRB pH 2 and 0.1 mol L^{-1} HCl.

4.1.3 Pulse methods

Differential pulse voltammetry (DPV) and square wave voltammetry (SWV) are widely recognized for their strong suppression of background (capacitive) currents and their capability to enable fast and reliable electroanalytical measurements. Owing to their high sensitivity and low detection limits, these techniques are particularly suitable for trace and ultra-trace quantification of a broad range of analytes (*Joseph Wang and Bassam A. Freiha, 1983; Laborda et al., 2014*)

To assess the relative performance of DPV and SWV with SP/BDD sensor and under controlled and comparable conditions, preliminary experiments were conducted for each of the three analytes caffeine, theobromine, and theophylline, using a fixed analyte concentration of 0.1 mmol L^{-1} prepared in their respective optimized supporting electrolytes. The aim was to compare signal quality, peak sharpness, background current suppression, and overall analytical performance under standardized, non-optimized parameters. Differential pulse voltammetry was applied in a potential range from +0.4 V to +1.6 V with a modulation amplitude of 50 mV and a modulation time of 25 ms, while square-wave voltammetry was tested in a potential range from +0.4 V to +1.6 V at a frequency of 25 Hz and a modulation amplitude of 50 mV.

For caffeine, both techniques yielded detectable oxidation signals. However, DPV produced a sharper, more defined peak with visibly lower background currents, resulting in better signal clarity and easier peak identification. SWV, while operationally simpler and faster, exhibited broader peaks and elevated baseline currents, which slightly compromised the resolution (*Figure 34a*).

Similar observations were made in the case of theobromine. Although both techniques provided measurable responses, DPV demonstrated a clear advantage in terms of peak intensity, symmetry, and signal-to-noise ratio, and the electrochemical response was more stable and better suited for quantitative analysis (*Figure 34b*).

In contrast, theophylline showed different behavior under the same measurement conditions. While DPV produced a detectable signal, the peak was flatter and less defined. SWV, on the other hand, yielded a clearer, more reproducible signal with improved peak visibility and baseline separation. In this case, SWV proved to be the more appropriate technique for the analytical determination of theophylline (*Figure 34c*).

Based on this comparative evaluation, DPV was selected as the final method for caffeine and theobromine, and for theophylline, SWV was retained as the method of choice. This highlights the necessity of method-specific optimization even when using the same electrode material, and confirms that both voltammetric techniques, when appropriately selected, can offer reliable and sensitive detection for different xanthine derivatives.

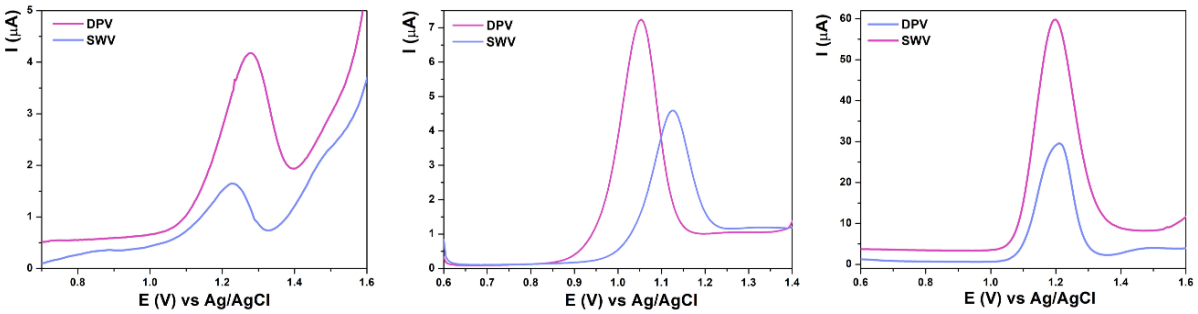

Figure 34. Comparison of DPV and SWV techniques for the determination of 0.1 mmol L^{-1} of a) caffeine, b) theobromine and c) theophylline.

4.1.3.1 Optimization of working parameters of pulse techniques

To achieve the best sensitivity and well-shaped peaks for every analyte, the parameters of both techniques have to be optimized.

4.1.3.1.1 Optimization of working parameters for the differential pulse voltammetry (DPV) method

The DPV procedure was optimized by varying the modulation amplitude (V) and modulation time (s).

In the presence of 0.01 mmol L^{-1} caffeine in 0.5 mol L^{-1} H_2SO_4 on the SP/BDD, DPV parameters optimization was carried out. The pulse amplitude was adjusted between 10 and 200 mV while maintaining a fixed modulation time of 25 ms. Among the tested values, 100 mV provided the most favorable signal response and was therefore chosen for subsequent experiments (*Figure 35a*). Following this, the modulation time was optimized while keeping the amplitude constant at 100 mV (*Figure 35b*). This parameter was examined over the interval from 10 to 200 ms, and 25 ms yielded the optimal performance. Consequently, this modulation time was adopted for all further measurements.

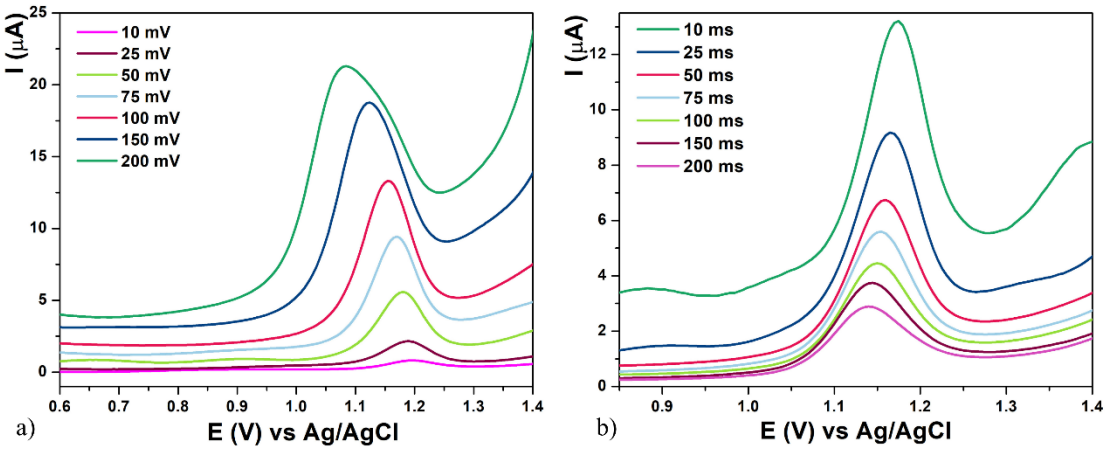

Figure 35. Optimization of DPV parameters: a) amplitude and b) modulation time, in the presence of 0.01 mmol L^{-1} caffeine. The optimization procedure was carried out using a solution containing 0.01 mmol L^{-1} TB in 0.5 mol L^{-1} H_2SO_4 at the SP/BDD electrode, where each parameter was varied individually while the others were kept constant. As illustrated in *Figure 36*, increasing the modulation amplitude from 10 to 150 mV (with the modulation time maintained at 25 ms) caused only a slight rise in the background current, while peak potentials for TB shifted toward more negative values when the amplitude exceeded 125 mV. Based on these observations, 125 mV was selected as the optimal modulation amplitude. Further investigation of modulation times in the range of 10–200 ms demonstrated a progressive increase in background current (*Figure 36a*). Beyond 50 ms, this effect became more pronounced and was accompanied by a considerable shift of the oxidation peak toward higher potentials. Although the peak current continued to increase at longer times, a modulation time of 50 ms was ultimately chosen as optimal (*Figure 36b*).

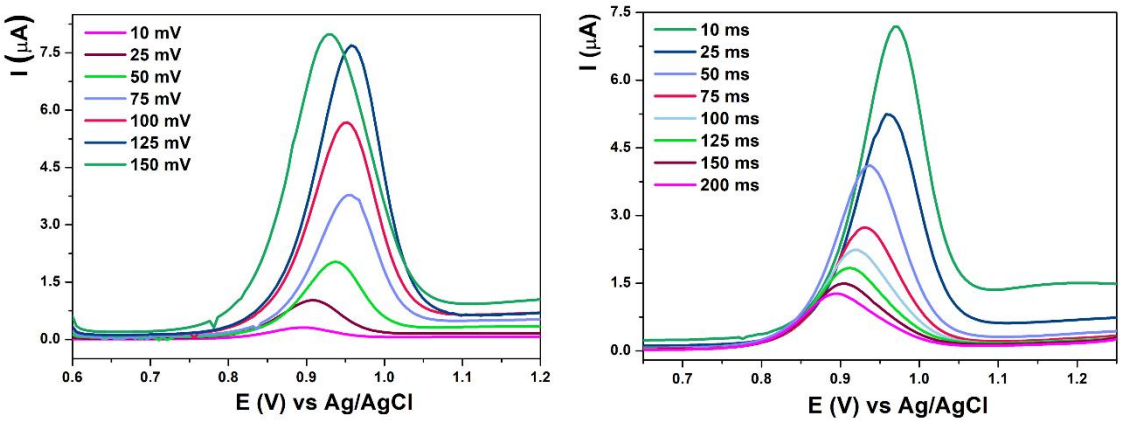

Figure 36. Optimization of DPV parameters: a) amplitude and b) modulation time, in the presence of 0.01 mmol L^{-1} theobromine.

4.1.3.1.2 Optimization of working parameters for the square wave voltammetry (SWV) method

The optimization of the SWV method was performed by adjusting the modulation amplitude and frequency parameters. The experiments were conducted in a solution containing 0.01 mmol L^{-1} TP in 0.5 mol L^{-1} H_2SO_4 at the SP/BDD electrode, with each variable modified individually while the remaining parameters were kept constant. As presented in *Figure 37a*, increasing the modulation amplitude from 10 to 100 mV (at a constant frequency of 25 Hz) resulted in a higher background current and a noticeable shift of the TP peak potential toward more negative values when the amplitude exceeded 50 mV. Based on these findings, 50 mV was selected as the optimal modulation amplitude for further measurements. Regarding frequency, which was studied in the range from 10 to 150 Hz, an increase resulted in a steady increase in background current, as demonstrated in *Figure 37b*. Based on these findings, we identified 75 Hz as the optimal frequency.

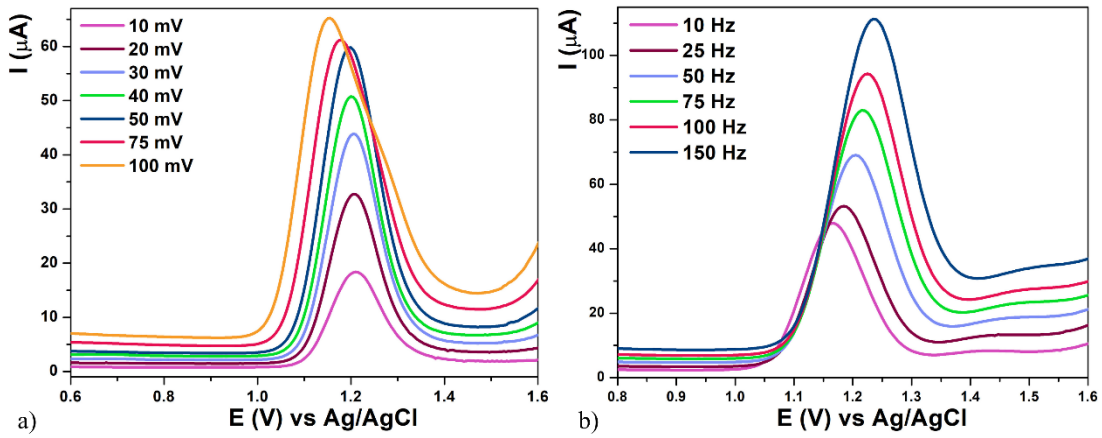

Figure 37. Optimization of SWV parameters: a) amplitude and b) frequency, in the presence of 0.01 mmol L^{-1} theophylline.

4.1.3.2 Analytical performance of the proposed method with SP/BDD sensor

The sensitivity of an electrochemical sensor is defined by its ability to reliably detect and quantify low concentrations of the analyte. Key performance indicators include the limit of detection and limit of quantification. These parameters were calculated from the slope (*m*) of the calibration curve and the standard deviation (*S*) of the blank signal, using the standard formulas *(Đurđić et al., 2024)*:

- $LOD = 3\ S\ m^{-1}$ *Equation 6*
- $LOQ = 10\ S\ m^{-1}$ *Equation 7*

During the development of electroanalytical methods, it is not uncommon to get two distinct linear ranges within the calibration curve. This phenomenon, well-documented in literature (*Dorraji and Jalali, 2016; Stanković, 2015; Stanković et al., 2015a, 2015b)*, is attributed to the concentration-dependent electrochemical behavior of the analyte. At lower concentrations, the response is typically governed by a diffusion-controlled process, resulting in a well-defined linear range. However, as the concentration increases, adsorption of the analyte or its oxidation products on the electrode surface may begin to dominate, leading to changes in the redox mechanism and a new linear relationship. This trapping effect on the electrode surface alters the slope of the calibration curve, reflecting a shift from diffusion-driven to adsorption-influenced processes.

Caffeine detection was performed using DPV in 0.5 mol L^{-1} H_2SO_4, in the potential window of +0.9 V to +1.4 V, with a pulse amplitude of 100 mV and a modulation time of 25 ms. The voltammetric response was recorded across a concentration range of 20 to 500 µmol L^{-1} (*Figure 38*).

Concentration range: 20–500 µmol L^{-1}
Equation: I (µA) = 0.015·c (µmol L^{-1}) – 0.091 (R^2 = 0.996)

LOD: **2.80 µmol L^{-1}** | ***LOQ:*** **8.40 µmol L^{-1}**

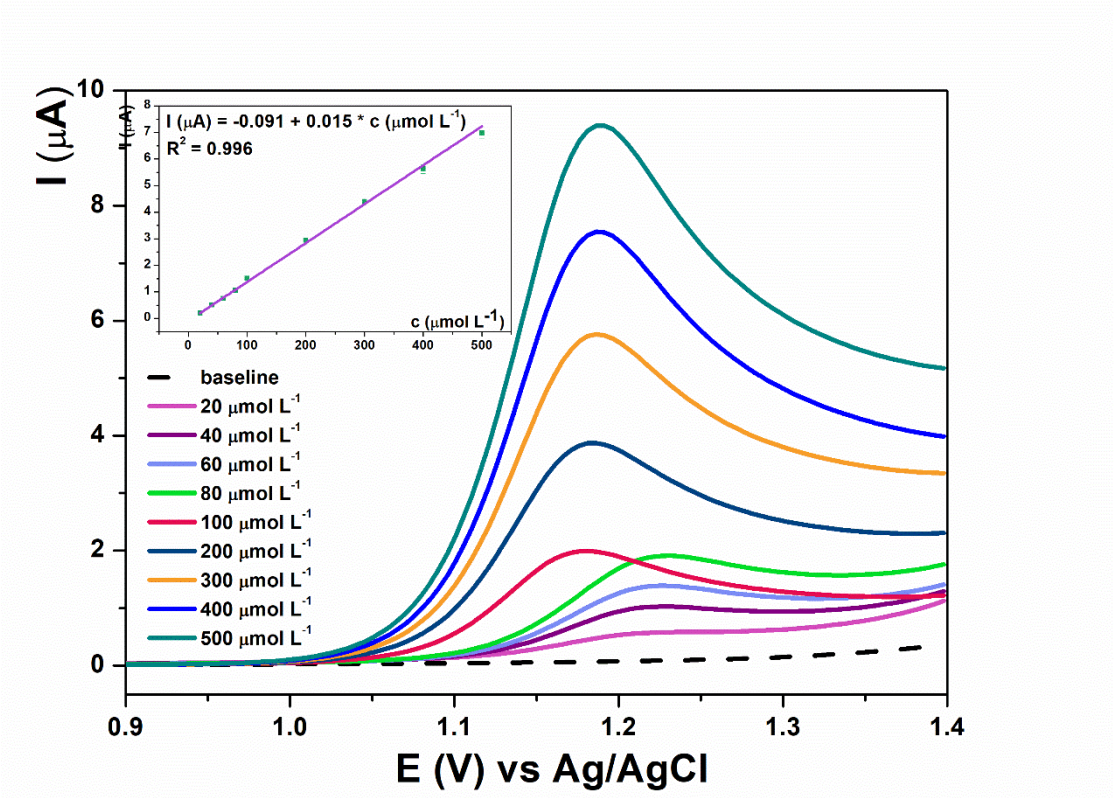

Figure 38. Voltammetric response of SP/BDD for the addition of different aliquots of caffeine standard to a 0.5 mol L^{-1} H_2SO_4. (Inset picture: Calibration graphs with corresponding error bars).

Theobromine detection was performed using DPV in 0.5 mol L^{-1} H_2SO_4, within the potential window +0.6 V to +1.2 V, with a pulse amplitude of 125 mV and modulation time of 50 ms. The voltammetric response was recorded across a concentration range of 1 to 60 μmol L^{-1} *(Figure 39).* The calibration curve showed two linear ranges:

1. Low concentration range: 1–7 μmol L^{-1}
   Equation: I (μA) = 7.61 + 1.10·c (μmol L^{-1}) (R^2 = 0.998)

2. High concentration range: 7–60 μmol L^{-1}
   Equation: I (μA) = 19 + 0.19·c (μmol L^{-1}) (R^2 = 0.989)

   ***LOD:* 0.51 μmol L^{-1} | *LOQ:* 1.55 μmol L^{-1}**

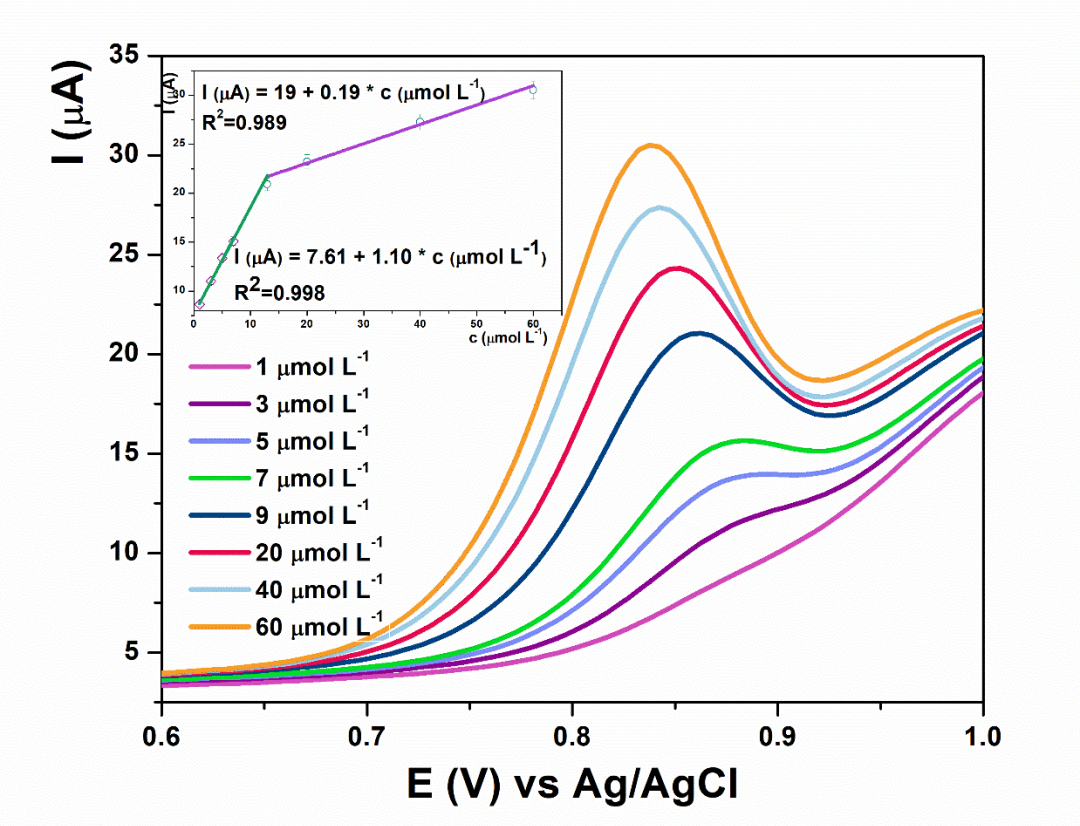

Figure 39. Voltammetric response of SP/BDD for the addition of different aliquots of theobromine standard to a 0.5 mol L^{-1} H_2SO_4. (Inset picture: Calibration graphs with corresponding error bars).

Theophylline detection was performed using SWV in 0.5 M H_2SO_4, in a potential window from +0.6 to +1.7 V, with an amplitude of 50 mV and a frequency of 75 Hz. The voltammetric response was recorded across a concentration range of 3.85 to 26.92 μmol L^{-1} (*Figure 40*). A single linear range was obtained:

1. Concentration range: 3.8–27 μmol L^{-1}
   Equation: I (μA) = –1.36 + 0.96·c (μmol L^{-1}) (R^2 = 0.999)

   ***LOD:* 0.24 μmol L^{-1} | *LOQ:* 0.73 μmol L^{-1}**

All obtained data with the SP/BDD sensor are summarized in *Table 3.*

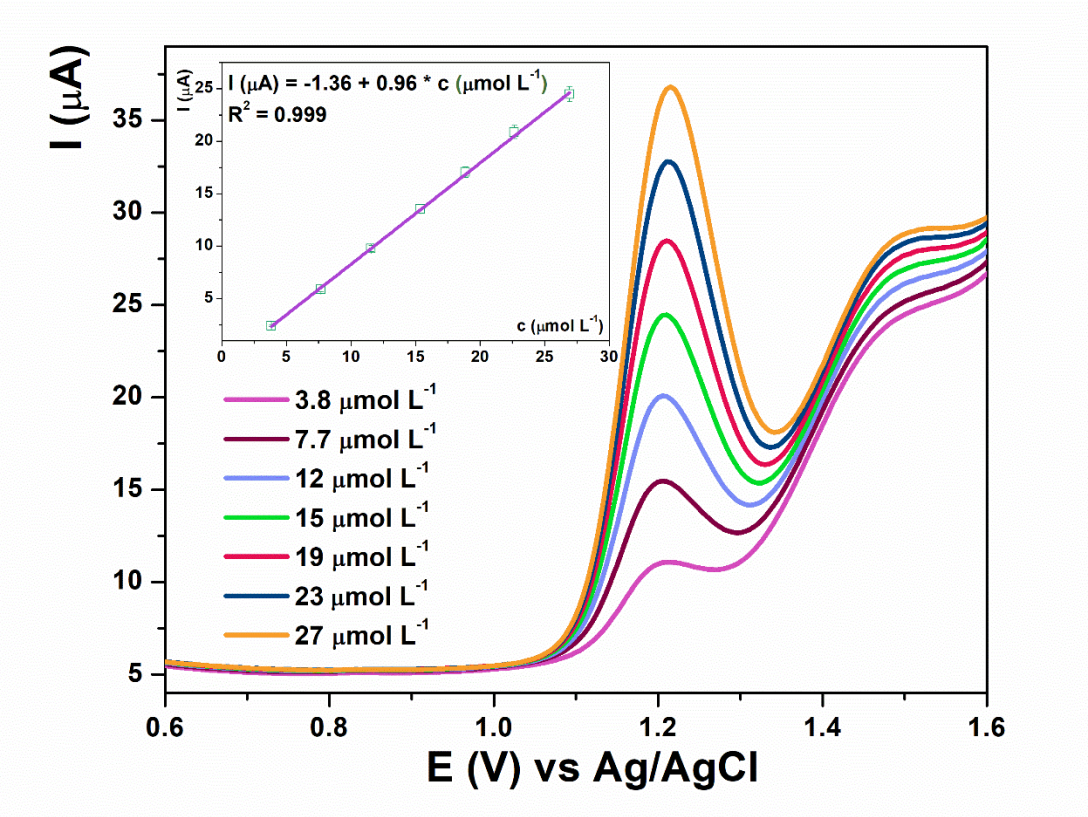

Figure 40. Voltammetric response of SP/BDD for the addition of different aliquots of theophylline standard to a 0.5 mol L^{-1} H_2SO_4. (Inset picture: Calibration graphs with corresponding error bars).

Xanthine Alkaloid	**Linear Range [μmol L^{-1}]**	**LOD [μmol L^{-1}]**	**LOQ [μmol L^{-1}]**
Caffeine	20 - 500	2.80	8.40
Theobromine	1-7 7-60	0.51	1.55
Theophylline	3.8 - 27	0.24	0.73

Table 3. Obtained analytical parameters with the SP/BDD sensor toward xanthine alkaloids.

4.1.3.2.1 Lifetime, reproducibility, and repeatability of SP/BDD sensor

Reliable electrochemical sensors, particularly those intended for disposable or point-of-care applications, must demonstrate high stability, reproducibility, and repeatability to ensure consistent analytical performance across multiple uses and units. These parameters are critical not only for method validation, but also for potential real-world implementation.

To evaluate these characteristics, a series of experiments was conducted using the SP/BDD sensor to detect caffeine, theobromine, and theophylline. For each analyte, sensor performance was evaluated through repeated measurements at defined concentrations, over both short- and long-term periods.

The morphological and electrochemical stability of both the working and reference electrodes was monitored throughout repeated measurements. *Figures 41a* show SEM micrographs of the SP/BDD working electrode (left) and the AgCl quasi-reference (right) electrode, respectively, before any use (a) and after 100 continuous measurement cycles in 0.5 mol L^{-1} H_2SO_4, with CV (b). It is noticeable that working electrode surfaces have not changed after prolonged use. This confirms the robustness and durability of the BDD material. However, a slight variation in the crystalline surface structure is observed for the Ag/AgCl quasi-reference electrode, with a sharper grain boundary contrast in *Figure 41b* (right) compared to its initial state, *Figure 41a* (right). This phenomenon could be attributed to partial metal or salt dissolution processes occurring during repeated sensor operation.

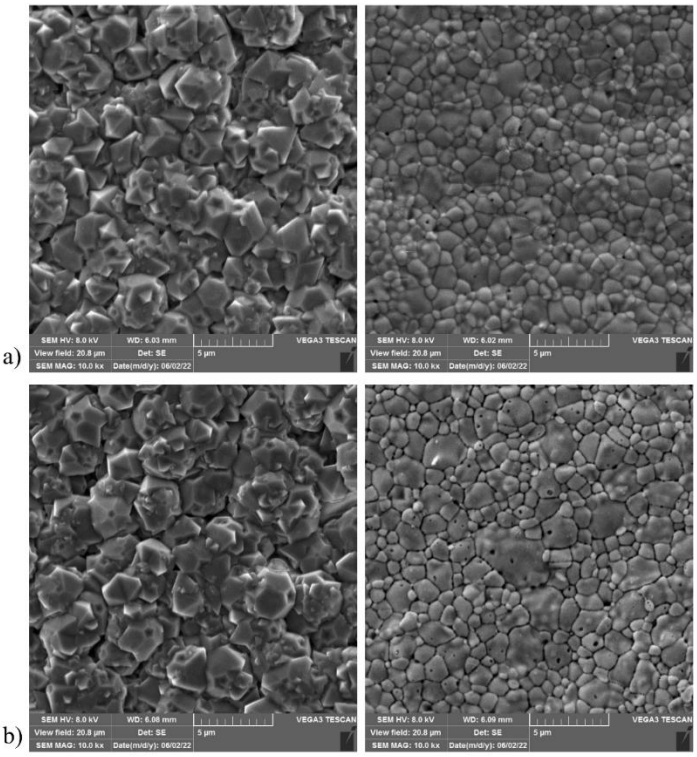

Figure 41. FE-SEM micrographs of a) new BDD working electrode (left) and quasi-reference Ag/AgCl electrode (right); and b) BDD working electrode (left) and quasi-reference Ag/AgCl electrode (right) used in 100 continuous measurements in 0.5 mol L^{-1} H_2SO_4, with CV.

Sensor lifetime was tested by storing the sensors at room temperature in ambient air for a period of two months, during which repeated measurements were taken regularly. Throughout this

period, no significant changes were observed in either the electrochemical response or the surface morphology of the electrodes, confirming their structural and functional stability.

Reproducibility (sensor-to-sensor variation) and repeatability (same-sensor precision) were assessed by performing ten replicate measurements of a fixed concentration for each analyte, using both a single electrode and five different electrodes under the same conditions.

Ten consecutive measurements at 10 μmol L^{-1} caffeine using the same sensor showed a variation in peak current of 5.0%, indicating good intra-electrode precision. Across five sensors variation was 2.1%.

At a concentration of 10 μmol L^{-1} of theobromine, the repeatability across ten measurements on the same sensor showed a 1.41% variation, while reproducibility across five sensors yielded 1.78% variation. These low values confirm excellent consistency and robustness of the sensor for TB detection.

Ten replicate measurements of 10 μmol L^{-1} theophylline on a single electrode showed a variation of 2.3%, while five different sensors yielded a variation of 1.9%.

The current responses remained stable over the whole one-month testing period, demonstrating long-term electrochemical reliability.

Although the SP/BDD sensor is intended for single-use scenarios, the results demonstrate that it offers robust electrochemical stability over prolonged usage, with minimal signal drift or degradation. This stability, combined with the low variability in repeated and cross-sensor measurements, strongly supports its potential for practical deployment in routine electroanalytical applications.

4.1.3.2.2 Interferences study

Interference studies, also known as selectivity assessments, are a crucial component in the development and validation of analytical methods. They are conducted to evaluate the ability of a sensor or method to distinguish the target analyte in the presence of potentially interfering substances that may coexist in complex sample matrices. Without proper evaluation of selectivity, the accuracy and reliability of analytical results may be compromised, particularly in real-world applications such as clinical diagnostics, food analysis, or environmental monitoring. Therefore, interference studies are essential to ensure that the analytical method maintains its precision, accuracy, and reproducibility even in a complex sample matrix *(Dorkó et al., 2015*) .

To assess the sensors' ability to selectively detect caffeine, an interference study was conducted using SP/BDD electrodes (*Figure 42*). The goal was to determine how various substances commonly present in real beverages—such as energy drinks, coffee, and soft drinks—might affect the caffeine signal. A range of inorganic ions and organic compounds was examined, including glucose, sucrose, fructose, ascorbic acid, and citric acid. Additionally, inorganic salts frequently found in these matrices—such as sodium nitrate, sodium carbonate, sodium chloride, sodium sulfate, potassium chloride, and magnesium chloride—were tested. It is important to consider that typical beverage components like caffeine, tannins, proteins, oils, sugars, sweeteners, and plant extracts (as reported in coffee, energy drinks, and Coca-Cola matrices) can adsorb onto electrode surfaces, potentially causing passivation and altering electrochemical behavior *(Filik et al., 2017; Silva et al., 2017)*. Each potential interferent was

added at 1.0 mmol L^{-1}, which is ten times higher than the caffeine concentration (0.1 mmol L^{-1}), in order to challenge the sensor's selectivity under realistic conditions. The interference experiments were performed using DPV in 0.5 mol L^{-1} H_2SO_4, applying the optimized measurement settings described earlier. The results showed that none of the tested substances affected the caffeine response. No additional peaks or significant signals attributable to the interferents were detected, confirming that the SP/BDD sensors exhibit strong selectivity for caffeine determination under the conditions tested.

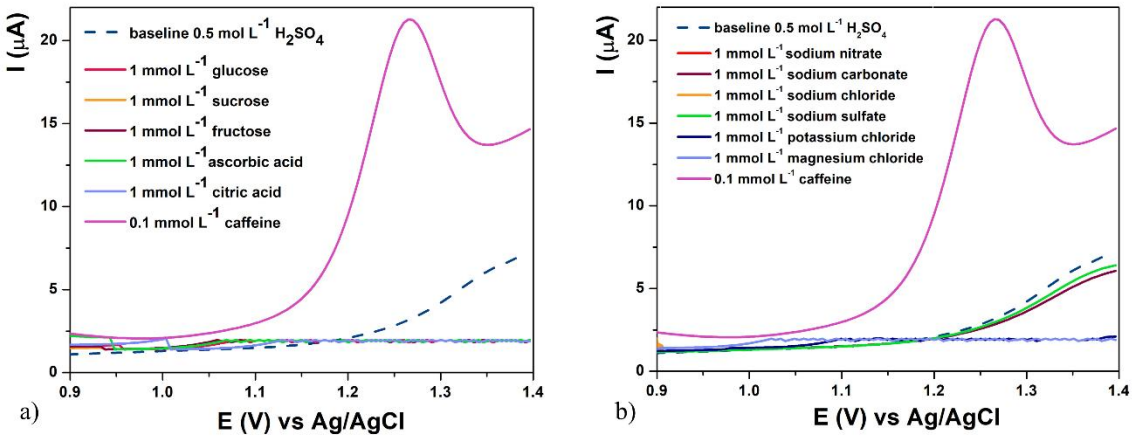

Figure 42. DPV response of SP/BDD for caffeine in the presence of potential interfering compounds.

The selectivity of the SP/BDD electrode toward TB was evaluated using DPV measurements under optimized conditions in the presence of typical interfering compounds found in chocolate. The study was divided into two parts to assess the effects of both organic and inorganic substances commonly present in real samples. In the first part, the electrochemical response of 10 μmol L^{-1} and 0.1 mmol L^{-1} organic interferents, specifically glucose and sucrose, was examined after being added to the same 0.5 mol L^{-1} H_2SO_4 matrix. For comparison, a DPV measurement of 1 μmol L^{-1} TB was recorded in the presence of all interferents. As shown in *Figure 43*, these organic compounds were electrochemically inactive under the optimized conditions, allowing for accurate quantification of TB. In the second part, 0.1 mmol L^{-1} solutions of calcium chloride, sodium chloride, and ammonium acetate were tested, and 1 μmol L^{-1} TB was successfully detected in the mixture containing all salts. From these results (*Figure 43*), it is evident that the tested inorganic salts do not interfere with the determination of TB.

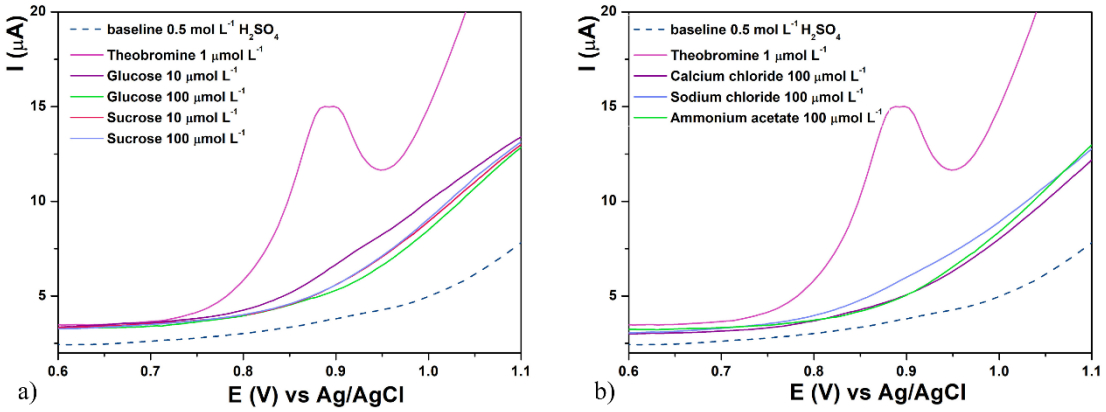

Figure 43. DPV response of SP/BDD for theobromine in the presence of potential interfering compounds.

The specificity of the SP/BDD SPE for TP was evaluated using SWV measurements under the optimized experimental conditions, in the presence of typical interfering compounds found in pharmaceutical tablets. The study was carried out in two stages to assess the effects of both organic and inorganic substances commonly encountered in real samples. In the first stage, the electrochemical response of 10 μmol L^{-1} and 0.1 mmol L^{-1} organic interferents, specifically glucose and sucrose, was examined after being sequentially introduced into the same matrix (0.5 mol L^{-1} H_2SO_4). For reference, a SWV of 1 μmol L^{-1} TP was recorded at the end of the solution containing all interferents. In *Figure 44*, we can see that the selected interfering compounds are not electroactive under the optimized conditions and that TP can be quantitatively determined in their presence. In the other part of the experiment, SWV of 0.1 mmol L^{-1} solutions of calcium chloride, sodium chloride, and ammonium acetate were measured, and 1 μmol L^{-1} TP was detected in the solution containing all salts. From *Figure 44*, we conclude that salts do not interfere with the TP determination.

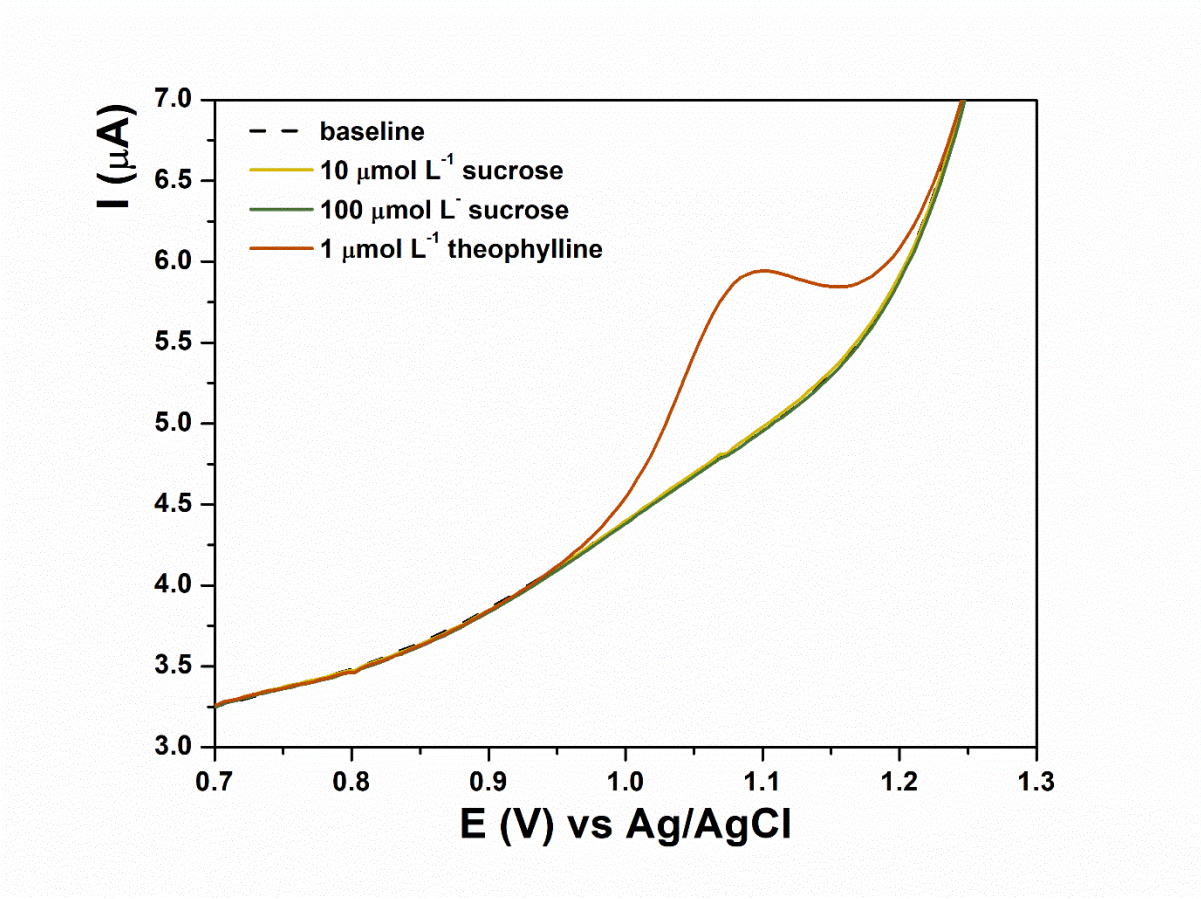

Figure 44. DPV response of SP/BDD for theophylline in the presence of potential interfering compounds.

4.1.4 Application of SP/BDD sensors and proposed methods in the real sample analysis

To evaluate the practical applicability of the developed methods using the SP/BDD sensor, various commercially available products were selected as real samples. These included soft drinks, energy drinks, and coffee for caffeine determination; chocolate products for theobromine analysis; and pharmaceutical tablets for theophylline detection. All samples were prepared following the procedure previously described.

All measurements were done in triplicate. Results for both the electroanalytical measurement and reference (confirmation) methods are summarized in *Table 7*.

4.1.4.1 Application of SP/BDD sensor and proposed method in the coffee sample

The caffeine was quantified in two different coffee samples using the SP/BDD and the DPV method in 0.5 mol L^{-1} H_2SO_4 within the potentials from 0.6 V to 1.6 V. A standard caffeine solution of known concentration (10 mmol L^{-1}) was added 5 times per 40 µL in the prepared real sample solution. The obtained values of caffeine concentration were 38 mg in 100 g of coffee for the first sample (*Figure 45a*) and 49 mg in 100 g of coffee for the second sample (*Figure 45b*). The indicated concentration of caffeine on the packaging was 40 mg and 50 mg per 100 g.

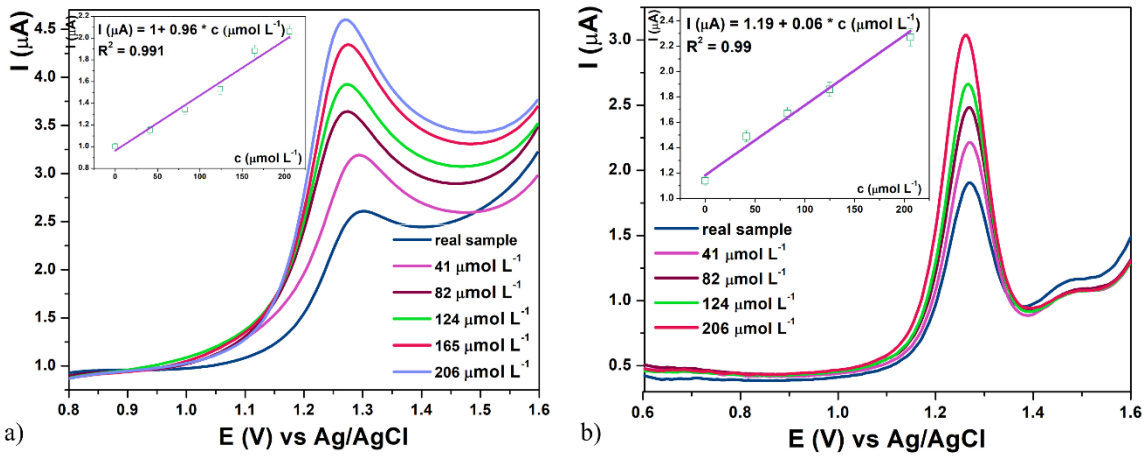

Figure 45. Standard addition method for coffee samples obtained by SP/BDD; (Inset pictures: Plot of current intensity (I) vs. concentration of caffeine (c)). The prepared solution of the real sample was spiked five times with aliquots of 40 µL of (10 mmol L^{-1}) caffeine standard.

4.1.4.2 Application of SP/BDD sensor and proposed method in energy drink sample

Caffeine content in the energy drink was measured using the SP/BDD electrode and DPV in 0.5 mol L^{-1} H_2SO_4, scanning the potential range from 0.6 V to 1.6 V. The concentration was determined by the standard addition technique: first 20 µL, followed by four successive additions of 50 µL each, of a 10 mmol L^{-1} caffeine standard solution were introduced into the prepared sample. A standard addition plot was then generated (*Figure 46*). From this analysis, the caffeine concentration was calculated to be 34 mg per 100 mL of the energy drink. The product label reports a caffeine content of 30 mg per 100 mL.

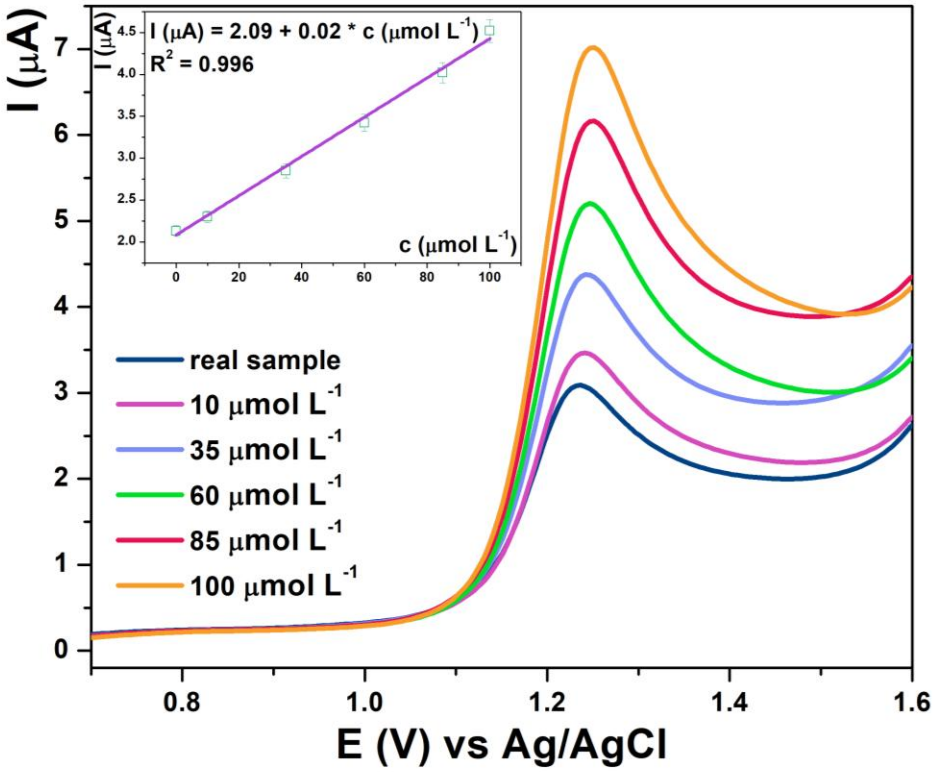

Figure 46. Standard addition method for energy drink sample obtained by SP/BDD; (Inset pictures: Plot of current intensity (I) vs. concentration of caffeine (c)). The prepared solution of the real sample was spiked five times with aliquots of 10 mmol L^{-1} caffeine standard.

4.1.4.3 Application of SP/BDD sensor and proposed method in soft drink sample

The quantification of caffeine in Coca-Cola was conducted utilizing the SP/BDD with the DPV method in 0.5 mol L^{-1} H_2SO_4 as a supporting electrolyte. The measurement was carried out over the potential window of 0.6 V to 1.6 V. Caffeine quantification was performed using the standard addition approach: 20 µL portions of a 10 mmol L^{-1} caffeine standard solution were added to the prepared real sample solution three times. A calibration graph was then plotted (*Figure 47*), from which the caffeine concentration was calculated as 0.0526 mmol L^{-1}, equivalent to 9.96 mg of caffeine per 100 mL of *Coca-Cola*. The label on the product lists a caffeine content of 8.50 mg per 100 mL.

Comparing our sensor's results with those obtained using two established reference methods (*Table 7*) shows that the values are consistent within the standard deviation range. This indicates that the SP/BDD-based sensor provides reliable, accurate, and rapid caffeine determination in this type of beverage sample.

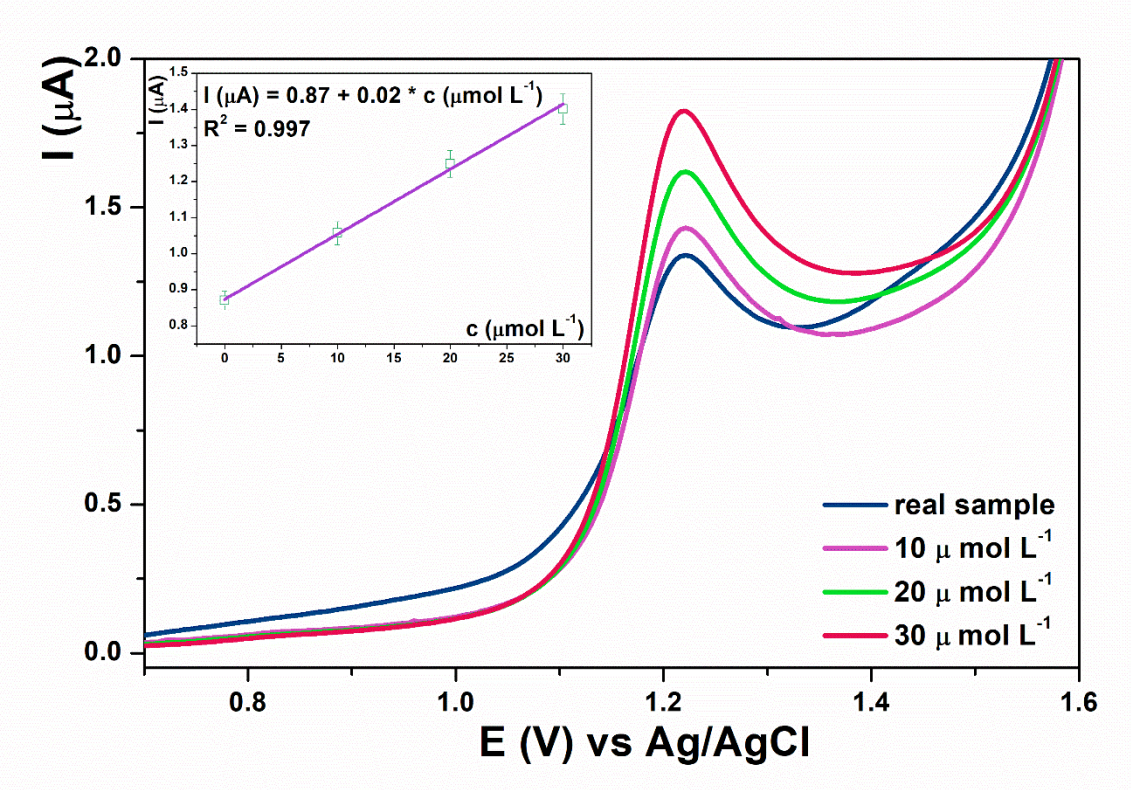

Figure 47. Standard addition method for soft drink sample obtained by SP/BDD; (Inset pictures: Plot of current intensity (I) vs. concentration of caffeine (c)). The prepared solution of the real sample was spiked three times with aliquots of 10 mmol L^{-1} caffeine standard.

Measurement	Coca-Cola [mg/100 mL]	Coffee 1 [mg/100 g]	Coffee 2 [mg/100 g]	Energy drink [mg/100 mL]
I	9.99	39	48	34.70
II	9.92	38	48	33.20
III	9.97	38	49	33.00
Average	**9.96**	**38.33**	**48.33**	**33.63**

Table 4. Obtained results with SP/BDD sensor, for caffeine quantification, in real sample analysis.

4.1.4.4 Application of SP/BDD sensor and proposed method in the chocolate sample

The determination of theobromine (TB) in chocolate was carried out using the SP/BDD electrode with the DPV technique, employing 0.5 mol L^{-1} H_2SO_4 as the supporting electrolyte. Measurements were performed over a potential range of 0.6–1.2 V. Quantification was achieved using the standard addition approach, where 20 µL aliquots of a 10 mmol L^{-1} TB standard solution were added sequentially five times to the prepared real sample solutions. From the resulting calibration curves, the TB content was calculated as 0.45 µmol L^{-1} (155 mg per 100 g) in chocolate with 30% cocoa (*Figure 48a*) and 0.19 µmol L^{-1} (748 mg per 100 g) in chocolate with 70% cocoa (*Figure 48b*).

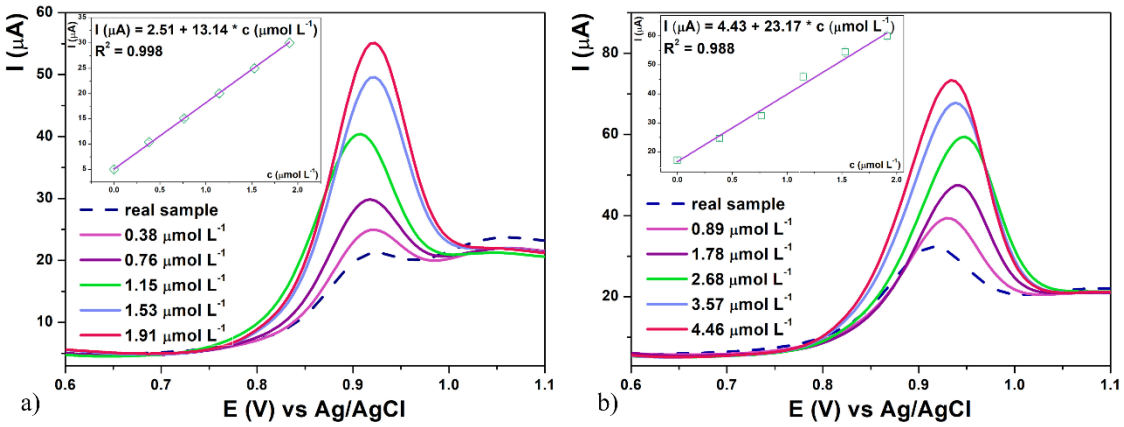

Figure 48. Standard addition method for chocolate samples obtained by SP/BDD; (Inset pictures: Plot of current intensity (I) vs. concentration of caffeine (c)). The prepared solution of the real sample was spiked five times with aliquots of 10 mmol L^{-1} theobromine standard.

Measurement	Chocolate 30% [mg/100 g]	Chocolate 70% [mg/100 g]
I	153.0	753.5
II	155.3	745.5
III	156.7	745.0
Average	**155**	**748**

Table 5. Obtained results with SP/BDD sensor, for theobromine quantification, in real sample analysis

4.1.4.5 Application of SP/BDD sensor and proposed method in the pill sample

The determination of theophylline (TP) in pharmaceutical tablets was performed using BDD SPEs combined with the SWV technique, with 0.5 mol L^{-1} H_2SO_4 serving as the supporting electrolyte. Measurements were carried out over a potential range of 0.7–1.6 V. For quantification, the standard addition method was applied, adding 20 µL portions of a 10 mmol L^{-1} TP standard solution five times to the prepared sample solutions. A calibration curve was generated, from which the TP content in a single capsule was calculated as 108 µmol L^{-1}, equivalent to 243.75 mg. This result is in close agreement with the labeled amount of 250 mg per capsule (*Figure 49*).

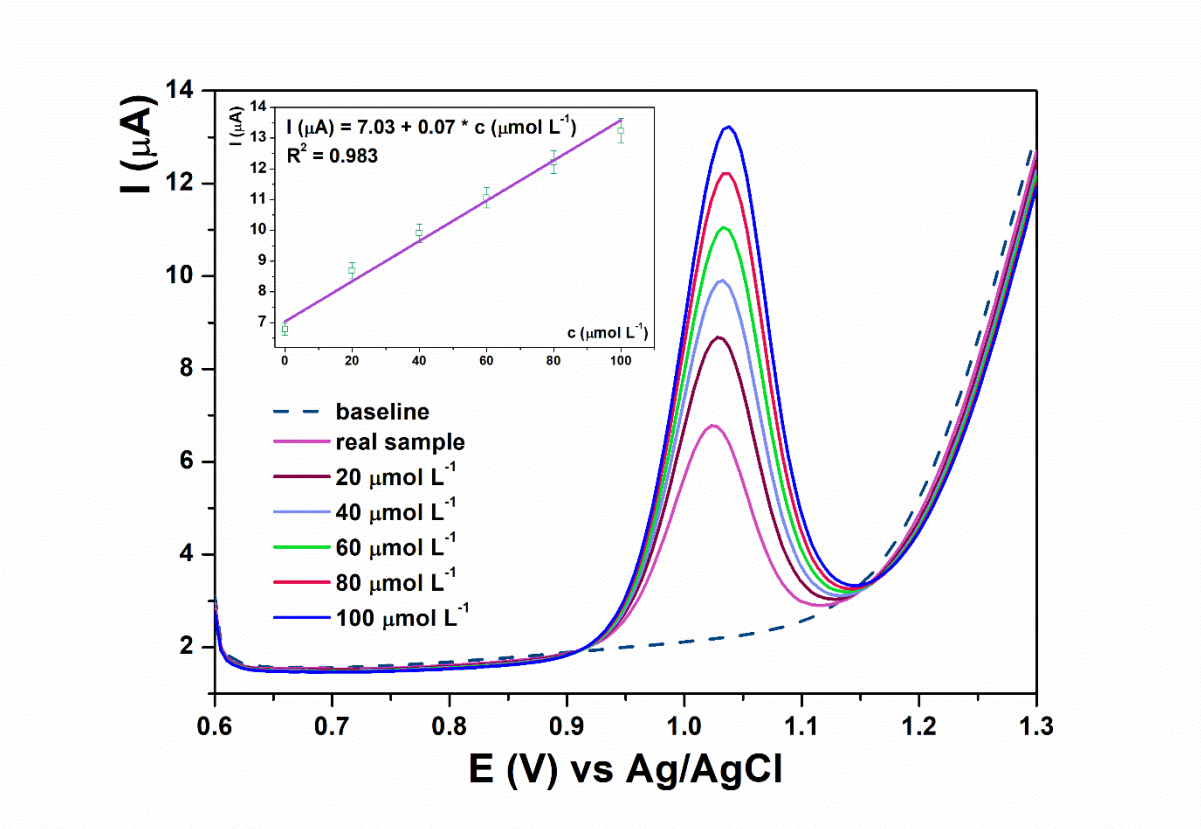

Figure 49. Standard addition method for chocolate samples obtained by SP/BDD; (Inset pictures: Plot of current intensity (I) vs. concentration of caffeine (c)). The prepared solution of the real sample was spiked five times with aliquots of 10 mmol L^{-1} theophylline standard.

Measurement	Pill I [mg]	Pill II [mg]	Pill III [mg]
I	244.00	243.50	239.80
II	246.00	244.75	241.50
III	247.25	246.25	241.70
Average	**245.75**	**244.50**	**241.00**

Table 6. Obtained results with SP/BDD sensor, for theophylline quantification, in real sample analysis.

Method	Coffee 1 (CAF) [mg/100 g]	Coffee 2 (CAF) [mg/100 g]	Energy drink (CAF) [mg/100 mL]	Soft drink (CAF) [mg/100 mL]	Chocolate 1 (TB) [mg/100 g]	Chocolate 2 (TB) [mg/100 g]	Pills (TP) [mg]
Declared value	40	50	30 mg	8.5	/	/	250
SP/BDD	38.33±0.47	48.33±0.47	33.63±0.76	9.96±0.03	155±3	748±15	243.75±5.61
HPLC	35	51	31.94	10.23	148.95	710.40	/
Spectro-photometric method	/	/	/	10.2	/	/	/

Table 7. The obtained results with electroanalytical measurements with the SP/BDD sensor and with reference (confirmation) methods.

4.2 Screen-printed multi-walled carbon nanotube sensor

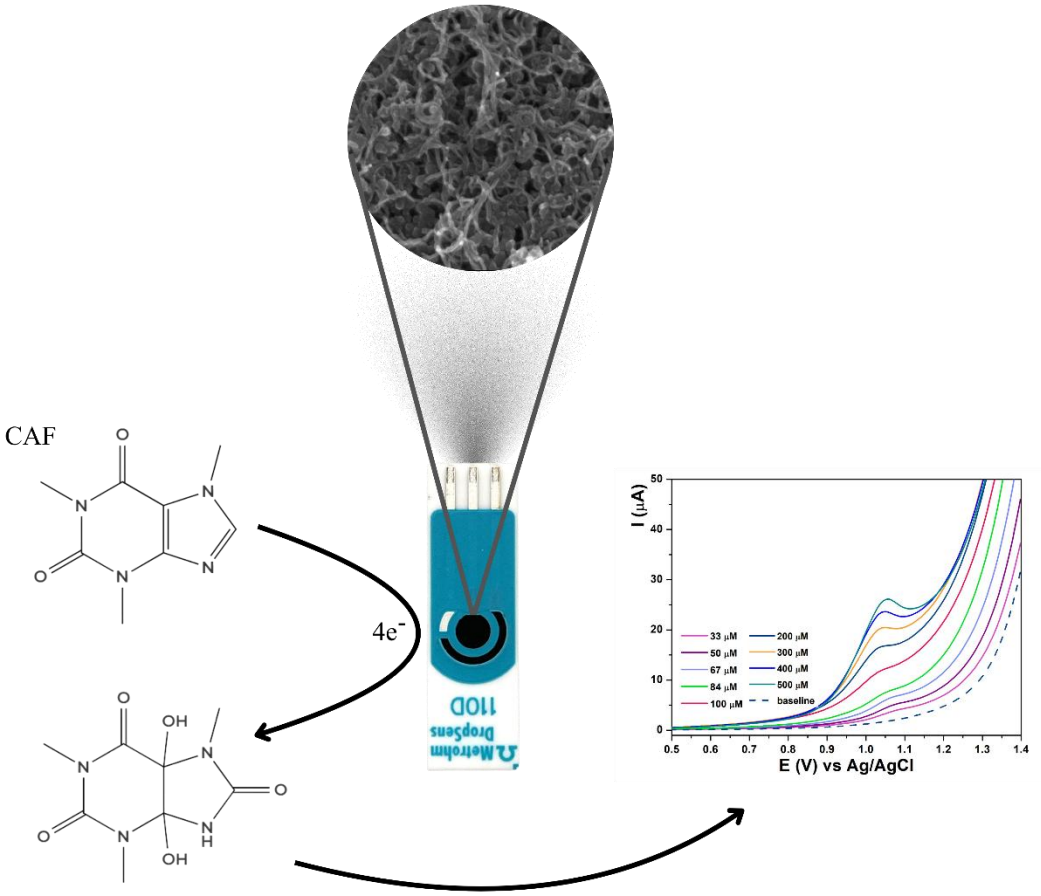

Figure 50. Main experimental points of the developed methods and voltammetric response of the SP/MWCNT sensor to the target analyte (caffeine).

The second part of this research was based on a screen-printed sensor with a multi-walled carbon nanotube working electrode (SP/MWCNT). This sensor was used to optimize and develop of a analytical protocol that could be used to caffeine determination.

The surface characterization of the electrode was conducted using FE-SEM. FE-SEM provided detailed information about the morphology of the surface, including the shape, texture, and distribution of nanostructured features on the electrode surfaces. Following structural characterization, electrochemical measurements were applied.

The initial section of the electrochemical results addresses the investigation of the electrochemical properties of the SP/MWCNT electrode by means of cyclic voltammetry. The study comprised evaluating the reversibility of the system, choosing an appropriate supporting electrolyte, and examining the influence of scan rate on the electrode's electrochemical behavior.

The following part of the study presents pulse voltammetric measurements with the aim to do optimization of operating parameters for the methods at the SP/MWCNT electrode.

The subsequent objective was to evaluate the electrochemical performance of the developed methods and compare the obtained findings with those available in the literature.

The third principal section of the results focuses on assessing the electrochemical characteristics of the proposed methods using the SP/MWCNT sensor. After optimizing both experimental and instrumental parameters, the linear concentration range for caffeine determination was established. Key analytical figures of merit—including precision, limits of detection (LOD) and quantification (LOQ), as well as reproducibility and repeatability—were determined. In addition, the influence of potential interfering species was investigated.

The final section presents the application of the SP/MWCNT sensor to real sample analysis and the validation of the proposed methodology.

4.2.1 Characterization of electrode surface by FE-SEM method

Surfaces of working and reference electrodes of SP/MWCNT were observed using the FE-SEM method. And this analysis reveals a fibrous, entangled network of tubular structures with a high aspect ratio (*Figure 51*). The nanotubes appear as long, thread-like cylinders with diameters ranging from 10 to 50 nm and lengths extending from 1 to 3 μm. Due to their hollow concentric-wall structure, they form dense bundles or aggregates. The surface morphology generally shows a relatively smooth texture along the tube walls, while the overall arrangement appears randomly oriented, forming a porous and interconnected mesh. This morphology contributes significantly to the large surface area and high conductivity of the SP/MWCNT sensor.

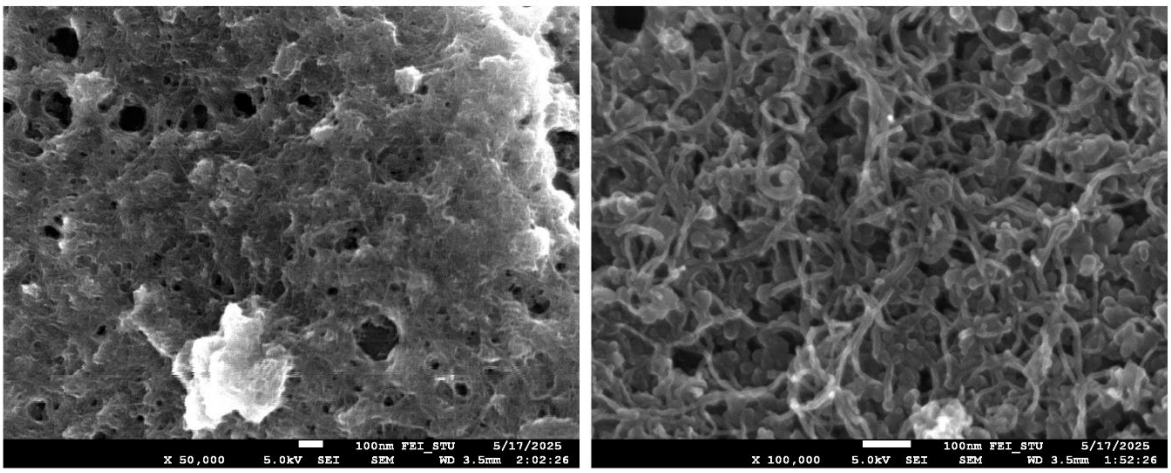

Figure 51. FE-SEM micrographs of multi-walled carbon nanotube. Magnified $50*10^3$ times (left) and $100*10^3$ times (right).

4.2.2 Cyclic voltammetry study

4.2.2.1 Electrochemical behavior of SP/MWCNT sensor

This chapter presents a detailed evaluation of the electrochemical performance of the SP/MWCNT sensor. The assessment of its electrochemical characteristics includes examining the shape and definition of oxidation and reduction peaks, as well as determining their corresponding current intensities. Particular attention is given to how these peak features reflect the sensor's sensitivity, stability, and overall analytical capability.

The electrocatalytic responses of SP/MWCNT were tested in $K_4[Fe(CN)_6]$ solution, and in the standard solution of every xanthine alkaloid separately.

The electrochemical characteristics of WE were investigated using cyclic voltammetry. Electrochemical response of WE was followed in 0.1 mmol L^{-1} $K_4[Fe(CN)_6]$ in 0.1 mol L^{-1} KCl. The applied potential ranged from -0.3 V to +0.8 V, while the scan rate varied from 5 to 100 mV s^{-1}.

As a supporting electrolyte, BRB pH 2 was used to test the electrochemical behavior of the SP/MWCNT sensor in the presence of the xanthine alkaloid caffeine. The applied potential ranged from +0.8 V to +1.5 V, while the scan rate varied from 2 to 100 mV s^{-1}. Cyclic

voltammograms reveal the presence of oxidation peaks from xanthine alkaloid, which are slightly shifted to more positive potential values as the scan rate increases.

4.2.2.1.1 Electrochemical characterization of SP/BDD sensor

Electrochemical characterization of the SP/MWCNT sensor was performed using the same approach as previously described for the SP/BDD electrode. All measurements were conducted under identical experimental conditions, employing the same electrochemical equations and evaluation protocols. The surface area of SP/MWCNT was probed using 1 mmol L^{-1} $K_4[Fe(CN)_6]$ in 0.1 mol L^{-1} KCl in a potential range from -0.3 V to +0.8 V, at different scan rates ranging from 5 to 100 mV s^{-1} *(Figure 52)*.

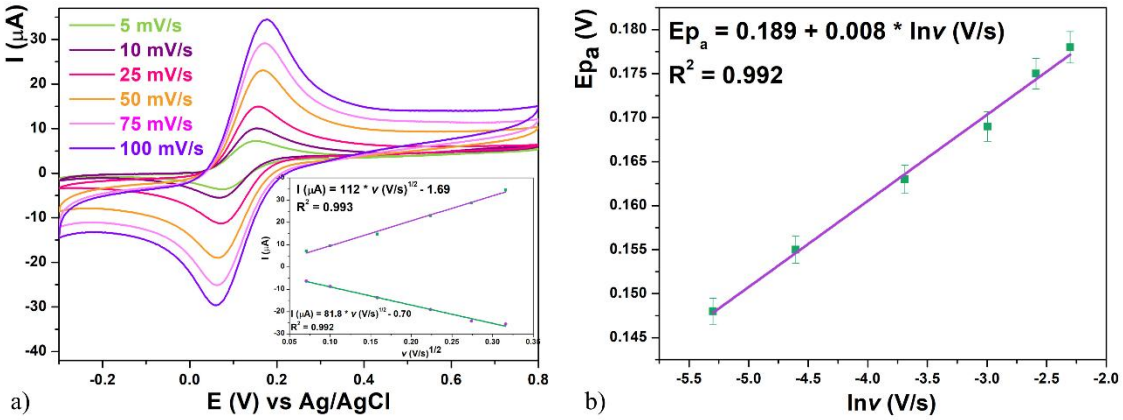

Figure 52. CVs of 1 mmol L^{-1} $K_4[Fe(CN)_6]$ in 0.1 mol L^{-1} KCl on increasing scan rates from 5 to 100 mV/s (Inset picture: Plots of anodic current (Ipa) and cathodic current (Ipc) vs. square root of the scan rate with SP/BDD).

The diffusion coefficient D was calculated to be 7.24×10^{-6} cm^2 s^{-1}.

A linear correlation between Epa vs. lnv was obtained *(Figure 52b)*:

Ep_a (V) = 0.189 + 0.008 × ln$v$ (V s^{-1}); R^2 = 0.992.

The charge transfer coefficient (α) is 0.32. In comparison with the value of charge transfer coefficient calculated for SP/BDD (α=0.45), this suggests a more symmetrical electron transfer process on the SP/BDD, because the value approaches the theoretical value of 0.5 for a fully reversible system.

The heterogeneous electron transfer rate constant (k_s) was calculated to be 6.8×10^{-3} cm s^{-1}. Considering the calculated value for the SP/BDD sensor (1.05×10^{-2} cm s^{-1}), these results indicate approximately 35% faster electron transfer kinetics at SP/BDD compared to the SP/MWCNT electrode.

Surface coverage (Γ*) was not considered, again, due to the diffusion-controlled nature of the process.

The active surface area of the SP/MWCNT sensor was determined following the testing of the sweep rate versus the electrocatalytic response of the MWCNT WEs. *Figure 52a* shows CV results recorded with the sensor at different scan rates (5-100 mV s^{-1}) in 0.1 mol L^{-1} KCl containing 1 mmol L^{-1} $K_4[Fe(CN)_6]$.

The active surface area of SP/MWCNT was investigated via *Equation 2* using the results of the response of the anodic signal (Ipa) with the appropriate sweep rates. The obtained value of the active surface area of SP/MWCNT was 1.51 cm² (151 mm^2), which represents approximately a 12-fold increase compared to the geometric area (0.126 cm²). This significant enhancement demonstrates the effective contribution of carbon nanotubes in increasing the available surface for electrochemical reactions, which is characteristic of nanomaterial-modified electrodes.

4.2.2.1.2 Electrochemical behavior of SP/MWCNT in the presence of caffeine

The electrochemical oxidation behavior of 0.1 mmol L^{-1} caffeine was examined on an SP/MWCNT electrode at scan rates ranging from 2 to 100 mV s^{-1} in BRB at pH 2 (*Figure 53a*). By plotting the peak potential against the natural logarithm of the scan rate, a linear trend was obtained, allowing the calculation of the electron transfer coefficient product using Laviron's equation, which resulted in a value of 0.86 (*Figure 53b*).

This larger α value, closer to unity, indicates a more symmetric activation barrier than that observed for SP/BDD (α = 0.43), suggesting more rapid electron transfer and a greater contribution of the product state to the activation energy. Such behavior may reflect a different transition-state configuration on the SP/MWCNT surface, possible specific adsorption of the oxidized caffeine species, or a combination of electron transfer and chemical reaction steps.

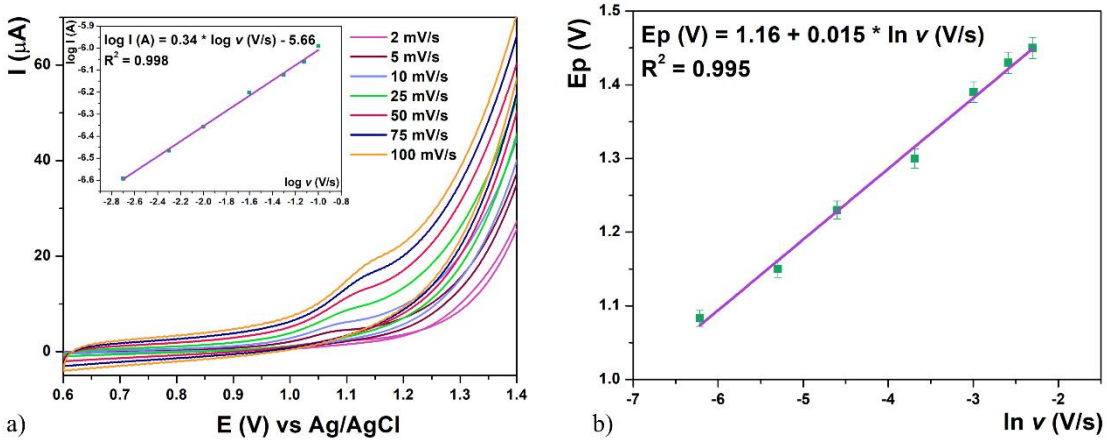

Figure 53. Figure 25. a) CVs of 0.1 mmol L^{-1} caffeine in BRB pH 2 on increasing scan rates from 2 to 100 mV/s (Inset picture: Plots of log I vs. log *v*); b) Plots of Ep vs. ln*v*.

4.2.2.2 Effect of pH of supporting electrolyte

The selection of an appropriate supporting electrolyte is a crucial step in the development of reliable and sensitive electrochemical methods. The nature, pH, and ionic strength of the electrolyte can significantly influence the kinetics and thermodynamics of redox processes, as well as the shape and position of voltammetric peaks and the level of background current. An optimal electrolyte not only enhances the analytical signal but also ensures reproducibility and stability of measurements by reducing background (capacitive) current and preserving optimal conditions for analyte determination.

4.2.2.2.1 Optimization of pH of supporting electrolyte on the SP/MWCNT performances for the determination of caffeine

To determine the optimal pH conditions for caffeine detection using the SP/MWCNT sensor, a series of voltammetric measurements was conducted in BRBS across a pH range from 2 to 6, with a fixed caffeine concentration of 20 μmol L^{-1}. The results, shown in *Figure 54,* revealed a clear pH dependence of the electrochemical response. The most intense and sharply defined oxidation peak was observed at pH 2. As the pH increased, the peak current progressively decreased, and after pH 4 disappeared, indicating that the oxidation mechanism is strongly influenced by the availability of protons. Moreover, higher pH values resulted in a rise in background current, which further compromised signal clarity and detection sensitivity. Considering all these observations, BRB at pH 2 was chosen as the appropriate pH value for the electrolyte for further studies using the SP/MWCNT sensor. This choice is also supported by literature findings, which confirm that caffeine exhibits its most favorable electrochemical behavior in strongly acidic environments *(Alessandro Trani et al., 2017; Yanwei Wang et al., 2014)*.

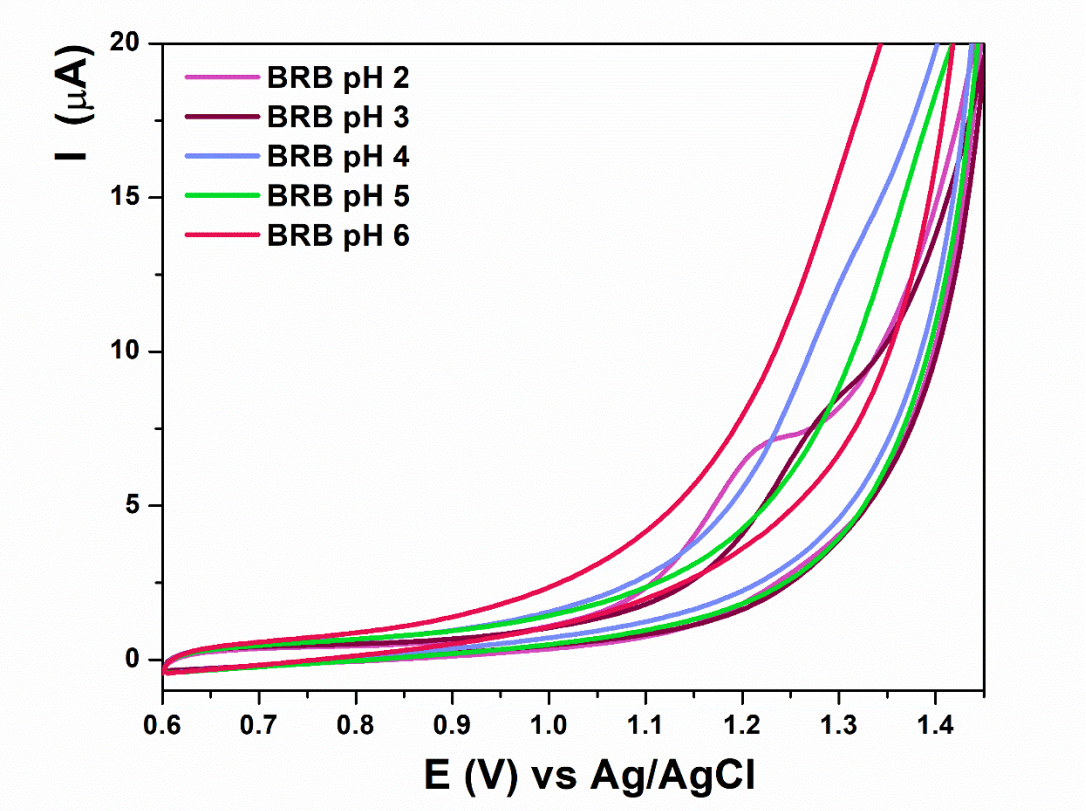

Figure 54. Electrochemical responses of SP/MWCNT sensor for 20 μmol L^{-1} CA obtained in BRB at different pH values (2-6).

4.2.3 Pulse methods

To assess the relative performance of DPV and SWV with SP/MWCNT sensor and under controlled and comparable conditions, preliminary experiments were conducted for caffeine using a fixed analyte concentration of 0.1 mmol L^{-1} prepared in respective optimized supporting electrolytes, BRB pH 2. The aim was to compare signal quality, peak sharpness, background current suppression, and overall analytical performance under standardized, non-optimized parameters.

Differential pulse voltammetry was applied in a potential range from +0.4 V to +1.4 V with a modulation amplitude of 50 mV and a modulation time of 25 ms, while square-wave voltammetry was tested in a potential range from +0.4 V to +1.4 V at a frequency of 25 Hz and a modulation amplitude of 50 mV.

With the SP/MWCNT sensor in the presence of caffeine, both techniques yielded detectable oxidation signals. However, DPV produced a sharper, more defined peak, resulting in better signal clarity and easier peak identification. SWV, while operationally simpler and faster, exhibited a broader peak, which slightly compromised the resolution (*Figure 55).* After choosing the DPV technique, parameters had to be optimized to achieve the best sensitivity and well-shaped peaks for the analyte.

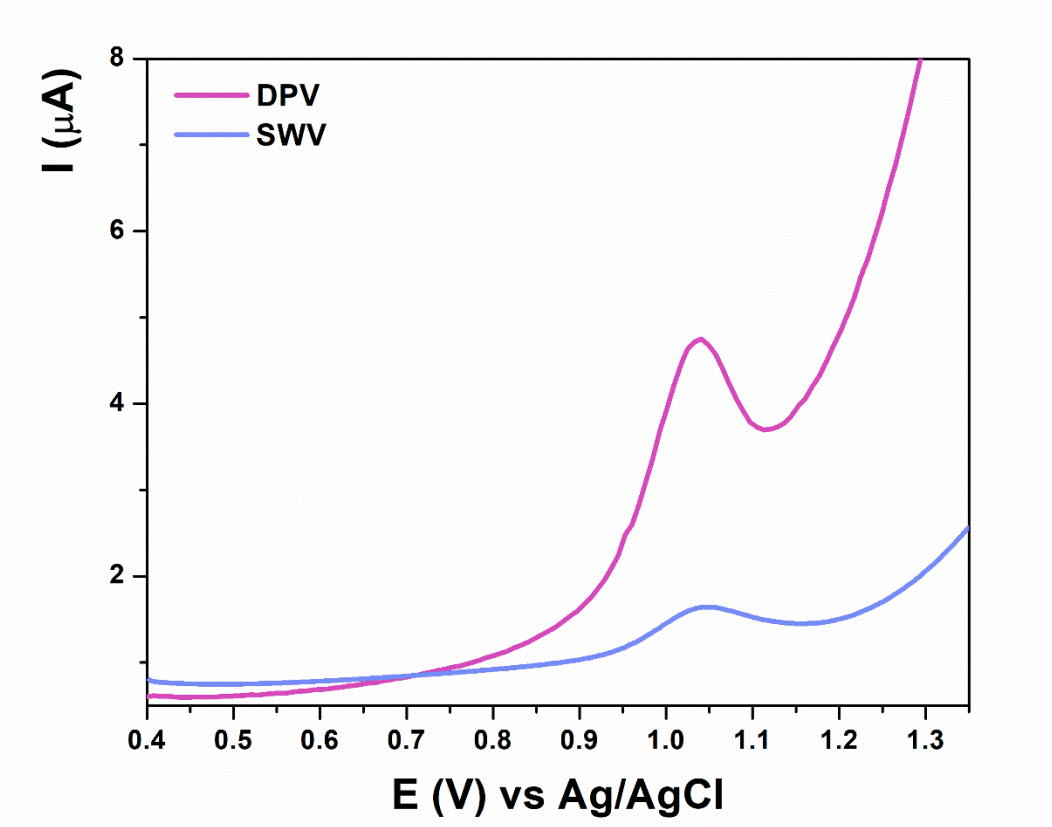

Figure 55. Comparison of DPV and SWV techniques for the determination of 0.1 mmol L^{-1} caffeine with SP/MWCNT sensor.

4.2.3.1 Optimization of working parameters for the differential pulse voltammetry (DPV) method

The DPV procedure was optimized by varying the modulation amplitude and modulation time.

With 0.01 mmol L^{-1} caffeine in BRB at pH 2 on the SP/BDD electrode, the DPV settings were optimized. First, the pulse amplitude was adjusted between 10 and 200 mV while keeping the modulation time fixed at 25 ms. The most favorable signal was achieved at 100 mV, so this value was chosen for subsequent experiments (*Figure 56a*).

Next, with the amplitude fixed at 100 mV, the modulation time was varied from 10 to 200 ms (*Figure 56b*). The optimal response occurred at 25 ms, and this modulation time was adopted for all further measurements.

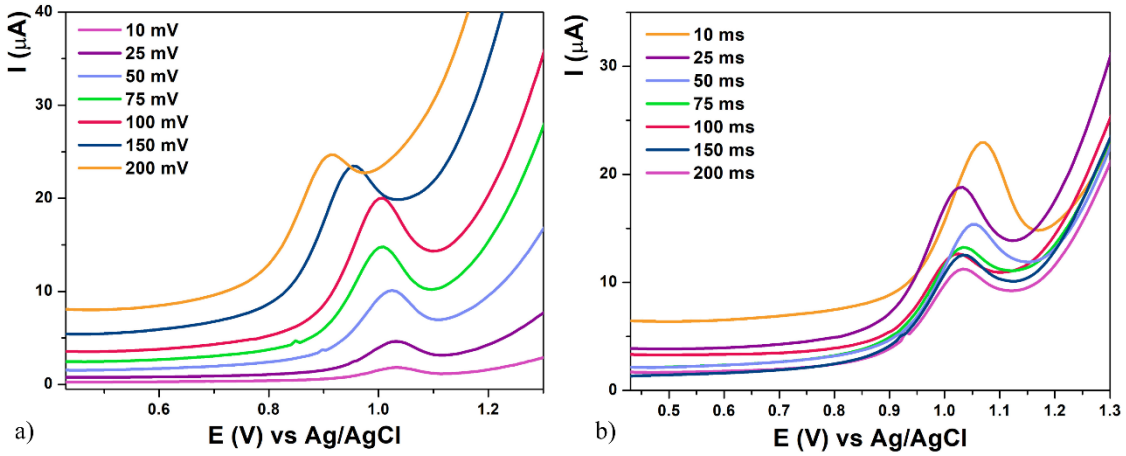

Figure 56. Optimization of DPV parameters: a) amplitude and b) modulation time, in the presence of 0.01 mmol L^{-1} caffeine.

4.2.3.1.1 Analytical performance of the proposed method with SP/MWCNT sensor

To evaluate the analytical performance of the SP/MWCNT sensor, DPV measurements were conducted in a potential range from +0.5 V to +1.4 V in BRB pH 2, under previously optimized parameters of amplitude 100 mV and modulation time 25 ms. The LOD and LOQ were calculated using the same approach described earlier, based on the calibration curve parameters. The obtained results are presented below, allowing for direct comparison with the SP/BDD sensor performance.

After obtaining the voltammetric response at various concentrations of caffeine, a calibration curve was constructed (*Figure 57).* The response was linear in the concentration range of 33 to 500 μmol L^{-1} and is described by the regression equation:

1. Concentration range: 33-500 μmol L^{-1}
   Equation: I (μA) = 0.14 + 0.02 · c (μmol L^{-1}) (R^2 = 0.992)

   ***LOD:* 9.40 μmol L^{-1} | *LOQ:* 28.50 μmol L^{-1}**

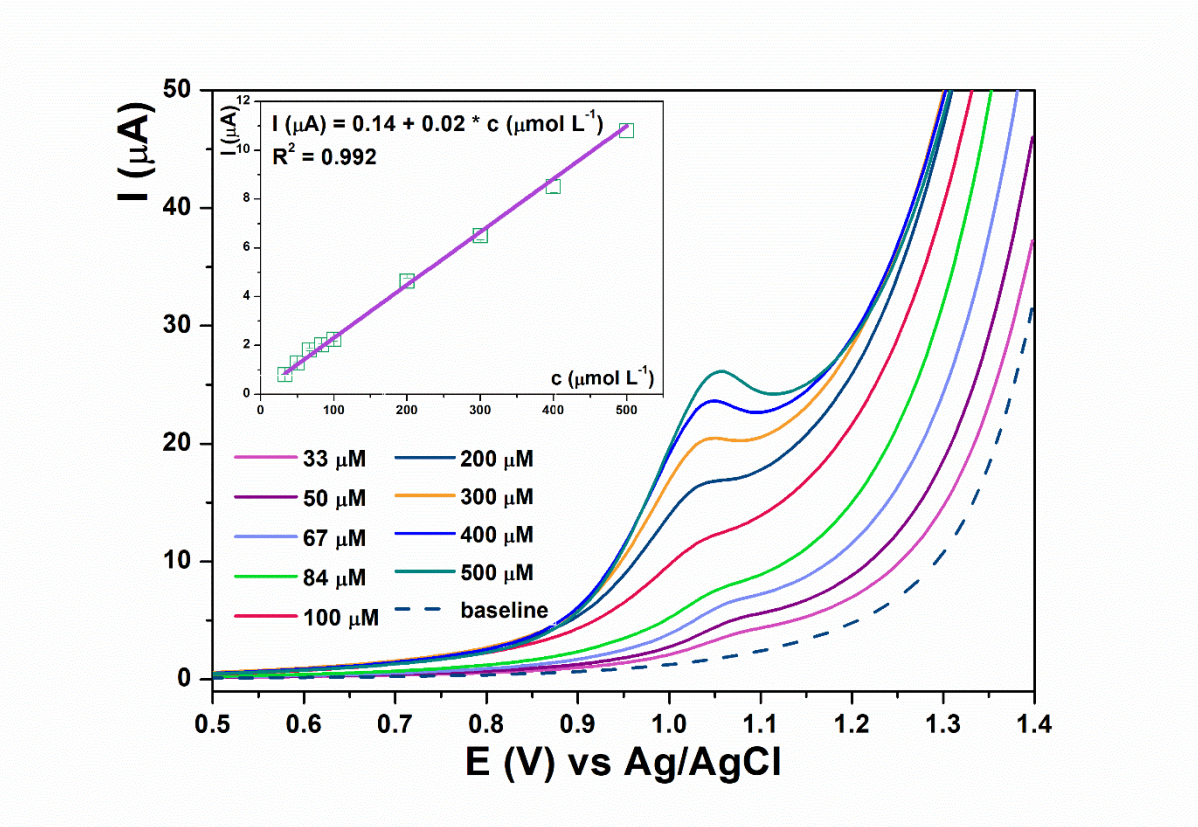

Figure 57. Voltammetric response of SP/MWCNT for the addition of different aliquots of caffeine standard to a BRB pH 2 (Inset picture: Calibration graph with corresponding error bars).

Although the SP/MWCNT sensor exhibits a satisfactory analytical performance for caffeine detection, its sensitivity and signal definition are lower than those observed with the SP/BDD sensor. In particular, the background current was more pronounced and the oxidation peak less sharp, which may reflect differences in surface structure, electron transfer kinetics, or surface fouling tendencies between the two materials.

A comparative summary of analytical parameters, including linear range, LOD, LOQ, oxidation peak potential, and supporting electrolyte for both sensors, is presented in *Table 8.* These results clearly highlight the superior performance of SP/BDD for electrochemical detection of caffeine, offering a more favorable detection profile for practical applications.

Sensor	**Linear range**	**LOD**	**LOQ**
SP/BDD	20-500	2.80	8.40
SP/MWCNT	33-500	9.40	28.50

Table 8. A comparative summary of analytical parameters for SP/BDD and SP/MWCNT sensors in caffeine determination.

4.2.3.1.2 Lifetime, reproducibility, and repeatability of the sensor

The reproducibility of the SP/MWCNT sensor was evaluated using a caffeine concentration of 50 µmol L^{-1}, under conditions optimized during method development. Ten consecutive measurements at this concentration yielded an oxidation peak current variation of approximately 6%, indicating satisfactory reproducibility for analytical purposes.

The operational lifetime of the SP/MWCNT sensors was determined to be at least one month without significant deterioration in performance. The electrodes were stored at room temperature, exposed to air, during this period. These results suggest that SP/MWCNT sensors are suitable for routine electrochemical analysis over a reasonable period of time, provided they are used within their validated lifespan.

4.2.3.1.3 Interferences study

To evaluate the selectivity of the SP/MWCNT sensor for caffeine determination, an interference study was conducted *(Figure 58)*. The purpose was to assess the influence of various potentially coexisting species commonly present in real beverage samples, such as energy drinks, coffee, and soft drinks. The selectivity evaluation included a broad range of both inorganic and organic compounds known to be present in such matrices. Specifically, the tested organic species included glucose, sucrose, fructose, ascorbic and citric acid. In addition, inorganic substances such as sodium nitrate, sodium carbonate, sodium chloride, sodium sulfate, potassium chloride and magnesium chloride were selected due to their frequent occurrence in commercial beverage formulations.

Each potential interfering species was introduced at a concentration of 1.0 mmol L^{-1}, ten times higher than the caffeine concentration (0.1 mmol L^{-1}), to create a stringent testing environment for evaluating sensor selectivity. DPV was employed as the detection technique, utilizing the previously optimized parameters. All measurements were conducted in BRB at pH 2 to ensure consistency with the established conditions for caffeine detection.

The results demonstrated that none of the tested substances produced additional peaks or significant signal alterations in the voltammograms. No measurable interference with the caffeine signal was observed, indicating that the SP/MWCNT sensor maintains high selectivity for caffeine even in the presence of potentially interfering compounds under simulated real-sample conditions.

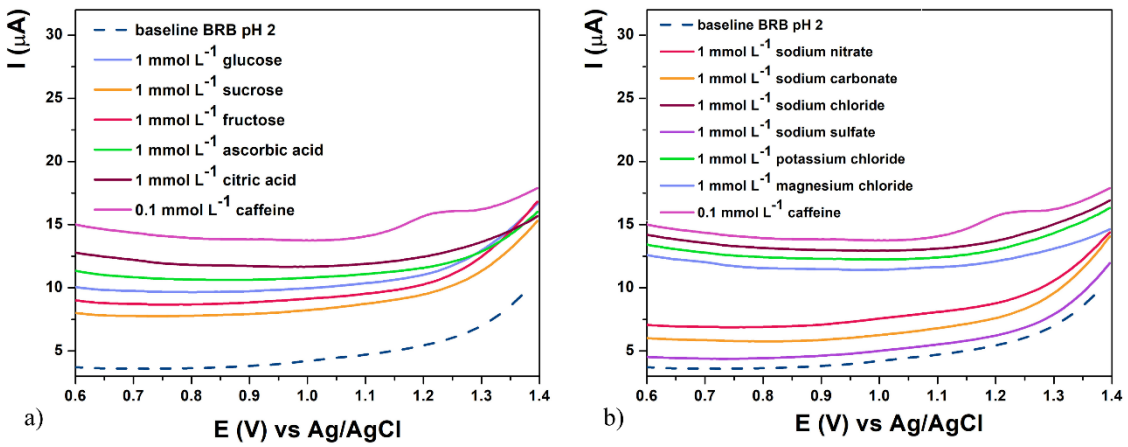

Figure 58. DPV response of SP/MWCNT for caffeine in the presence of potential interfering compounds.

4.2.4 Application of SP/MWCNT sensor and proposed methods in the real sample analysis

To evaluate the practical applicability of the developed methods using the SP/MWCNT sensor, commercially available products were selected as real samples. These included energy drinks and coffee for the determination of caffeine. All samples were prepared following the procedure previously described.

All measurements were done in triplicate. Results for both the electroanalytical measurement and reference (confirmation) methods are summarized in *Table 10.*

4.2.4.1 Application of SP/MWCNT sensor and proposed method in the coffee sample

Caffeine content was measured again in two different coffee samples using the SP/MWCNT electrode and DPV in BRB at pH 2, scanning from 0.6 V to 1.4 V. A 10 mmol L^{-1} caffeine standard solution was added to each prepared sample four times, with 50 µL per addition. Using the SP/MWCNT sensor, the caffeine concentrations were found to be 32 mg per 100 g of coffee for the first sample (*Figure 59a*) and 49 mg per 100 g for the second sample (*Figure 59b*). The product labels listed caffeine contents of 40 mg and 50 mg per 100 g, respectively.

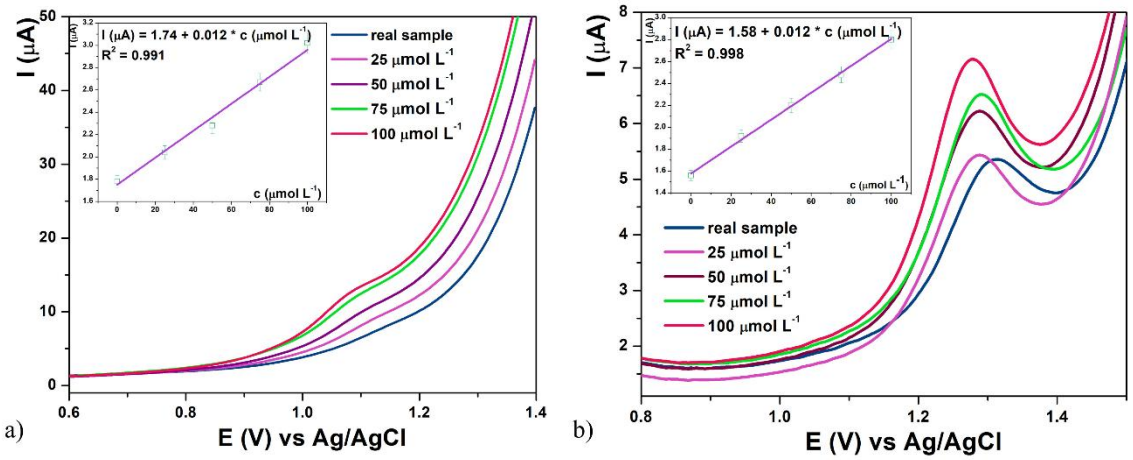

Figure 59. Standard addition method for coffee samples obtained by SP/MWCNT; (Inset pictures: Plot of current intensity (I) vs. concentration of caffeine (c)). The prepared solution of the real sample was spiked four times with aliquots of 50 µL of (10 mmol L^{-1}) caffeine standard.

4.2.4.2 Application of SP/MWCNT sensor and proposed method in soft drink sample

Quantification of caffeine in Coca-Cola using the SP/MWCNT electrode was not feasible because the acidic components of the beverage quickly degraded the silver pseudo-reference electrode surface, leading to unstable and non-reproducible measurements.

4.2.4.3 Application of SP/MWCNT sensor and proposed method in energy drink sample

Using the SP/MWCNT electrode and DPV in BRB at pH 2, caffeine was quantified in an energy drink within the potential window of 0.9 V to 1.4 V. A 10 mmol L^{-1} caffeine standard solution was added to the sample solution in five increments of 50 µL each, and a standard

addition plot was created (*Figure 60*). The analysis yielded a caffeine concentration of 21 mg per 100 mL of energy drink, while the label indicates 30 mg per 100 mL.

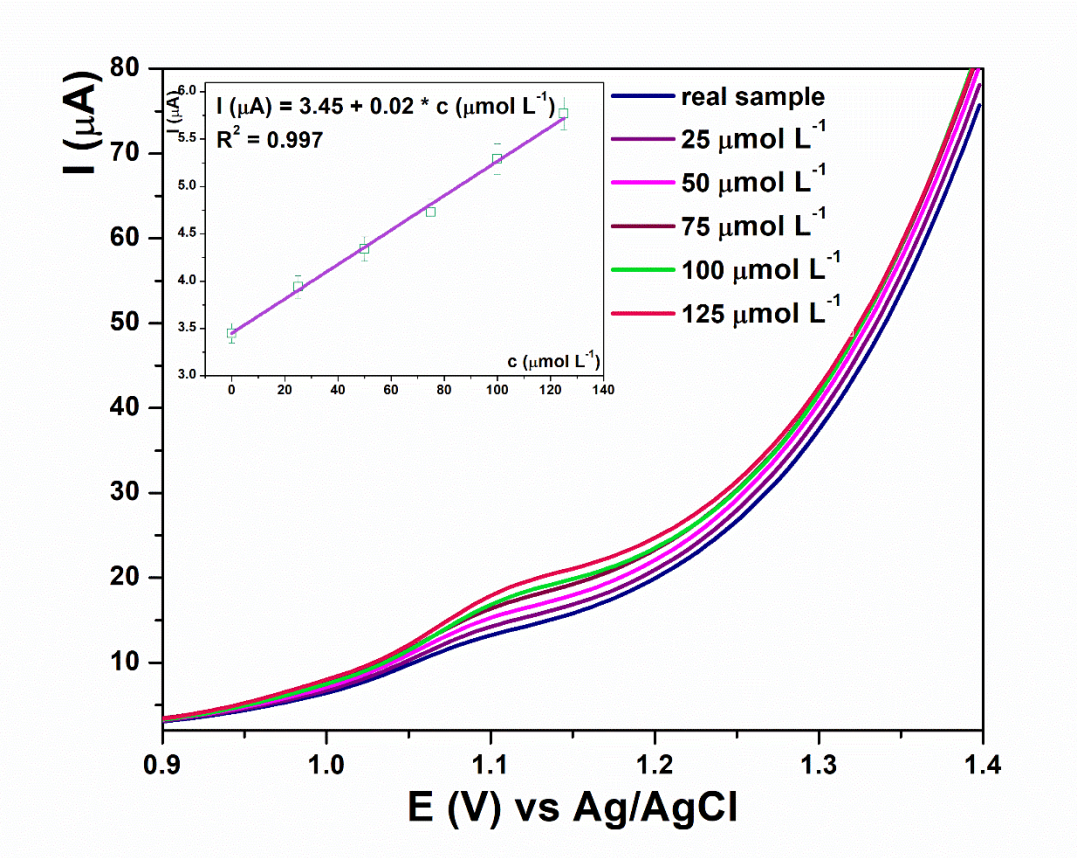

Figure 60. Standard addition method for coffee samples obtained by SP/MWCNT; (Inset pictures: Plot of current intensity (I) vs. concentration of caffeine (c)). The prepared solution of the real sample was spiked five times with aliquots of 50 μL of (10 mmol L^{-1}) caffeine standard.

The SP/BDD sensor produced results that align well with the labeled values, falling within the method's standard deviation range. Based on this comparison, the SP/BDDE is the more suitable electrode for analyzing these types of samples. The issues previously observed with the SP/MWCNT surface when testing Coca-Cola samples likely explain the lower accuracy seen in energy drink measurements, since the composition of these beverages is quite similar.

Measurement	Coffee 1 [mg/100 g]	Coffee 2 [mg/100 g]	Energy drink [mg/100 mL]
I	33.10	47.20	21.20
II	31.60	49.10	23.00
III	32.00	50.00	20.00
Average	**32.23**	**48.77**	**21.40**

Table 9. Obtained results with SP/MWCNT sensor, for theophylline quantification, in real sample analysis.

Method	Coffee 1 [mg/100 g]	Coffee 2 [mg/100 g]	Energy drink [mg/100 mL]
Declared value	40	50	30
SP/MWCNT	32.23±0.63	48.77±1.17	21.40±1.23
HPLC	35.00	51.00	31.94

Table 10. The obtained results with electroanalytical measurements with the SP/MWCNT sensor and with reference (confirmation) methods.

5. Conclusion

In this doctoral dissertation, new voltammetric methods for the determination of xanthine alkaloids in food samples and pharmaceutical products were developed and validated. Two different types of sensors were investigated, screen-printed platforms with chemically deposited boron-doped diamond working electrode (SP/BDD) and a sensor with multi-walled carbon nanotube (SP/MWCNT) working electrode, each offering specific electrochemical advantages.

The sensors tested in this research were selected for their advanced material properties, miniaturized format, and suitability for rapid, low-cost, and sensitive detection. Both sensor types demonstrated excellent potential for developing electrochemical methods capable of detecting a wide range of chemical compounds in complex matrices.

The SP/BDD sensor, in particular, proved highly suitable for voltammetric analysis due to its wide working potential window, excellent chemical and mechanical stability, and low background current. These characteristics enabled the development of reliable methods with improved sensitivity, lower limits of detection (LOD), and enhanced selectivity for xanthine alkaloids in the presence of common interferents.

The SP/MWCNT sensor demonstrated strong potential for voltammetric analysis owing to the high surface area, excellent electrical conductivity, and electrocatalytic activity of multi-walled carbon nanotubes. These properties contributed to enhanced signal intensity, enabling the development of effective methods for caffeine determination. The sensor also showed satisfactory selectivity in the presence of common interferents and exhibited stable performance across multiple measurements, confirming its suitability for practical applications in real-sample analysis.

Overall, the SP/BDD sensor outperformed the SP/MWCNT platform in several key aspects. It provided significantly lower LOD and LOQ values, demonstrated superior physical and chemical stability, and maintained reliable performance under more demanding analytical conditions. Owing to its robustness and wide potential window, a broader range of real samples could be successfully analyzed with SP/BDD, whereas the SP/MWCNT sensor showed limitations in harsher environments and could not be applied to all matrices included in this study.

SP/BDD Sensor

A screen-printed sensor with a chemically deposited boron-doped diamond (BDD) working electrode was employed for the development of voltammetric methods for the detection and quantification of xanthine alkaloids: caffeine, theobromine, and theophylline. The crystal structure and morphology of the BDD electrode surface were characterized using field emission scanning electron microscopy (FE-SEM) and Raman spectroscopy.

The key findings obtained from the method development with the SP/BDD sensor can be summarized as follows:

- The calculated electrochemically active surface area of the SP/BDD working electrode was 0.0662 cm^2 = 6.62 mm^2.

- Cyclic voltammetry experiments at different scan rates confirmed that the oxidation of all three xanthine alkaloids at the SP/BDD surface is governed by a diffusion-controlled mechanism.
- 0.5 mol L^{-1} H_2SO_4 was identified as the optimal supporting electrolyte for the detection of caffeine, theobromine, and theophylline using the SP/BDD sensor.
- Comparative evaluation of DPV and SWV techniques revealed that DPV provided better sensitivity for caffeine and theobromine, and SWV was more suitable for the determination of theophylline.
- The optimal DPV parameters were:
    - For caffeine: 100 mV pulse amplitude, 25 ms pulse time.
    - For theobromine: 125 mV pulse amplitude, 50 ms pulse time.
- The optimal SWV parameters for theophylline were 50 mV amplitude and 75 Hz frequency.
- The developed methods showed the following linear working ranges:
    - Caffeine: 20 - 500 µmol L^{-1}
    - Theobromine: 1 - 60 µmol L^{-1}
    - Theophylline: 3.8 - 27 µmol L^{-1}
- The calculated limit of detection (LOD) and limit of quantification (LOQ) were:
    - Caffeine: LOD = 2.80 µmol L^{-1}; LOQ = 8.40 µmol L^{-1}
    - Theobromine: LOD = 0.51 µmol L^{-1}; LOQ = 1.55 µmol L^{-1}
    - Theophylline: LOD = 0.24 µmol L^{-1}; LOQ = 0.73 µmol L^{-1}
- The SP/BDD sensor demonstrated excellent reproducibility, repeatability, and measurement precision during the detection of all target analytes.
- High selectivity was confirmed in the presence of common potential interferents, indicating reliable performance in complex sample matrices.
- The developed method showed high accuracy and practical applicability, as verified through real sample analysis:
    - Caffeine in two types of coffee, a soft drink, and an energy drink;
    - Theobromine in two chocolate samples;
    - Theophylline in pharmaceutical tablets.

SP/MWCNT Sensor

The key findings obtained from the method development with the SP/MWCNT sensor can be summarized as follows:

- The calculated electrochemically active surface area of the SP/MWCNT working electrode was 1.51 cm^2 = 155 mm^2.
- Cyclic voltammetry experiments at different scan rates confirmed that the oxidation of caffeine at the SP/MWCNT surface is governed by a diffusion-controlled mechanism.
- BRB pH 2 was identified as the optimal supporting electrolyte for the detection of caffeine using the SP/MWCNT sensor.
- Comparative evaluation of DPV and SWV techniques revealed that DPV provided better sensitivity for the determination of caffeine with the SP/MWCNT sensor.
- The optimal DPV parameters were 100 mV pulse amplitude, 25 ms pulse time.
- The developed method showed the following linear working range 33-500 μmol L^{-1}.
- The calculated limit of detection (LOD) and limit of quantification (LOQ) were 9.40 μmol L^{-1} and 28.50 μmol L^{-1}.
- The SP/MWCNT sensor demonstrated great reproducibility, repeatability, and measurement precision during the detection of all target analytes.
- High selectivity was confirmed in the presence of common potential interferents, indicating reliable performance in complex sample matrices.
- The developed method showed high accuracy and practical applicability, as verified through real sample analysis in two types of coffee and an energy drink.

6. References

Antonio, J., Newmire, D.E., Stout, J.R., Antonio, B., Gibbons, M., Lowery, L.M., Harper, J., Willoughby, D., Evans, C., Anderson, D., Goldstein, E., Rojas, J., Monsalves-Álvarez, M., Forbes, S.C., Gomez Lopez, J., Ziegenfuss, T., Moulding, B.D., Candow, D., Sagner, M. & Arent, S.M. (2024). *Common questions and misconceptions about caffeine supplementation: what does the scientific evidence really show? Journal of the International Society of Sports Nutrition*, 21(1), 2323919. https://doi.org/10.1080/15502783.2024.2323919

A. Douglas Kinghorn, Heinz Falk, Simon Gibbons, Jun'ichi Kobayashi, 2017. Progress in the Chemistry of Organic Natural Products.

Abbasi, S., Peerzada, M.H., Nizamuddin, S., Mubarak, N.M., 2020. Chapter 25 - Functionalized nanomaterials for the aerospace, vehicle, and sports industries, in: Mustansar Hussain, C. (Ed.), Handbook of Functionalized Nanomaterials for Industrial Applications, Micro and Nano Technologies. Elsevier, pp. 795–825. https://doi.org/10.1016/B978-0-12-816787-8.00025-9

Abdalla, S., Al-Marzouki, F., Al-Ghamdi, A.A., Abdel-Daiem, A., 2015. Different Technical Applications of Carbon Nanotubes. Nanoscale Res. Lett. 10, 358. https://doi.org/10.1186/s11671-015-1056-3

Abdel-Haleem, F.M., Gamal, E., Rizk, M.S., Madbouly, A., El Nashar, R.M., Anis, B., Elnabawy, H.M., Khalil, A.S.G., Barhoum, A., 2021. Molecularly Imprinted Electrochemical Sensor-Based Fe2O3@MWCNTs for Ivabradine Drug Determination in Pharmaceutical Formulation, Serum, and Urine Samples. Front. Bioeng. Biotechnol. 9. https://doi.org/10.3389/fbioe.2021.648704

Abdulla, S., Mathew, T.L., Pullithadathil, B., 2015. Highly sensitive, room temperature gas sensor based on polyaniline-multiwalled carbon nanotubes (PANI/MWCNTs) nanocomposite for trace-level ammonia detection. Sens. Actuators B Chem. 221, 1523–1534. https://doi.org/10.1016/j.snb.2015.08.002

Ajayan, P.M., Zhou, O.Z., 2001. Applications of Carbon Nanotubes, in: Dresselhaus, M.S., Dresselhaus, G., Avouris, P. (Eds.), Carbon Nanotubes: Synthesis, Structure, Properties, and Applications. Springer, Berlin, Heidelberg, pp. 391–425. https://doi.org/10.1007/3-540-39947-X_14

Al-Ahmed, A., Sarı, A., Mazumder, M.A.J., Hekimoğlu, G., Al-Sulaiman, F.A., Inamuddin, 2020. Thermal energy storage and thermal conductivity properties of Octadecanol-MWCNT composite PCMs as promising organic heat storage materials. Sci. Rep. 10, 9168. https://doi.org/10.1038/s41598-020-64149-3

Alam, A.U., Qin, Y., Catalano, M., Wang, L., Kim, M.J., Howlader, M.M.R., Hu, N.-X., Deen, M.J., 2018. Tailoring MWCNTs and β-Cyclodextrin for Sensitive Detection of Acetaminophen and Estrogen. ACS Appl. Mater. Interfaces 10, 21411–21427. https://doi.org/10.1021/acsami.8b04639

Alcaide, M., Taylor, A., Fjorback, M., Zachar, V., Pennisi, C.P., 2016. Boron-Doped Nanocrystalline Diamond Electrodes for Neural Interfaces: In vivo Biocompatibility Evaluation. Front. Neurosci. 10. https://doi.org/10.3389/fnins.2016.00087

Aleksanyan, M.S., Sayunts, A.G., Shahkhatuni, G.H., Simonyan, Z.G., Aroutiounian, V.M., Shahnazaryan, G.E., 2022. Flexible sensor based on multi-walled carbon nanotube-SnO2 nanocomposite material for hydrogen detection. Adv. Nat. Sci. Nanosci. Nanotechnol. 13, 035003. https://doi.org/10.1088/2043-6262/ac8671

Alkahtani, M., Zharkov, D.K., Leontyev, A.V., Shmelev, A.G., Nikiforov, V.G., Hemmer, P.R., 2022. Lightly Boron-Doped Nanodiamonds for Quantum Sensing Applications. Nanomaterials 12, 601. https://doi.org/10.3390/nano12040601

Allen J. Bard, Larry R. Faulkner, 2000. Electrochemical Methods: Fundamentals and Applications.

Althagafi, A., 2022. Effects of Caffeine, Theophylline, and Aminophylline on Electroconvulsive Therapy: A Review of Evidence. J. Microsc. Ultrastruct. 10, 103. https://doi.org/10.4103/jmau.jmau_19_21

Ando, Y., Zhao, X., Shimoyama, H., Sakai, G., Kaneto, K., 1999. Physical properties of multiwalled carbon nanotubes. Int. J. Inorg. Mater. 1, 77–82. https://doi.org/10.1016/S1463-0176(99)00012-5

Andrews, R., Jacques, D., Qian, D., Rantell, T., 2002. Multiwall Carbon Nanotubes: Synthesis and Application. Acc. Chem. Res. 35, 1008–1017. https://doi.org/10.1021/ar010151m

Ashihara, H., Mizuno, K., Yokota, T., Crozier, A., 2017. Xanthine Alkaloids: Occurrence, Biosynthesis, and Function in Plants.

Baral, A., Bose, N., Show, B., Bandyopadhyay, N.R., Mukherjee, N., 2023. ZnO/f-MWCNT as a potential candidate for supercapacitive energy storage and piezoelectric energy generation. Mater. Today Chem. 31, 101627. https://doi.org/10.1016/j.mtchem.2023.101627

Behul, M., Marton, M., Chvála, A., Michniak, P., Pifko, M., Honig, H., Scheler, T., Kurniawan, M., Vojs, M., 2025. Nanoscale Engineering of Si/BDD/TiO2 heterostructure interfaces to enhance photoelectrochemical performance. Appl. Surf. Sci. Adv. 27, 100757. https://doi.org/10.1016/j.apsadv.2025.100757

Bekyarova, E., Ni, Y., Malarkey, E.B., Montana, V., McWilliams, J.L., Haddon, R.C., Parpura, V., 2005. Applications of Carbon Nanotubes in Biotechnology and Biomedicine. J. Biomed. Nanotechnol. 1, 3–17. https://doi.org/10.1166/jbn.2005.004

Bianco, A., Kostarelos, K., Prato, M., 2005. Applications of carbon nanotubes in drug delivery. Curr. Opin. Chem. Biol., Biopolymers / Model systems 9, 674–679. https://doi.org/10.1016/j.cbpa.2005.10.005

Bogdanowicz, R., 2014. Characterization of Optical and Electrical Properties of Transparent Conductive Boron-Doped Diamond thin Films Grown on Fused Silica. Metrol. Meas. Syst. 2014 No 4 685-698.

Boylan, P.M., Abdalla, M., Bissell, B., Malesker, M.A., Santibañez, M., Smith, Z., 2023. Theophylline for the management of respiratory disorders in adults in the 21st century: A scoping review from the American College of Clinical Pharmacy Pulmonary

Practice and Research Network. Pharmacother. J. Hum. Pharmacol. Drug Ther. 43, 963–990. https://doi.org/10.1002/phar.2843

Brian R. Eggins, 2002. Chemical Sensors and Biosensors (Analytical Techniques in the Sciences).

Cao, Q., Rogers, J.A., 2008. Random networks and aligned arrays of single-walled carbon nanotubes for electronic device applications. Nano Res. 1, 259–272. https://doi.org/10.1007/s12274-008-8033-4

Chen, K., Gao, W., Emaminejad, S., Kiriya, D., Ota, H., Nyein, H.Y.Y., Takei, K., Javey, A., 2016. Printed Carbon Nanotube Electronics and Sensor Systems. Adv. Mater. 28, 4397–4414. https://doi.org/10.1002/adma.201504958

Chung, J.H., Hasyimah, N., Hussein, N., 2022. Application of Carbon Nanotubes (CNTs) for Remediation of Emerging Pollutants - A Review. Trop. Aquat. Soil Pollut. 2, 13–26. https://doi.org/10.53623/tasp.v2i1.27

Cinková, K., Zbojeková, N., Vojs, M., Marton, M., Samphao, A., Švorc, Ľ., 2015. Electroanalytical application of a boron-doped diamond electrode for sensitive voltammetric determination of theophylline in pharmaceutical dosages and human urine. Anal. Methods 7, 6755–6763. https://doi.org/10.1039/C5AY01493J

Costa, D.J.E., Santos, J.C.S., Sanches-Brandão, F.A.C., Ribeiro, W.F., Salazar-Banda, G.R., Araujo, M.C.U., 2017. Boron-doped diamond electrode acting as a voltammetric sensor for the detection of methomyl pesticide. J. Electroanal. Chem. 789, 100–107. https://doi.org/10.1016/j.jelechem.2017.02.036

Crapnell, R.D., Banks, C.E., 2021. Electroanalytical overview: The electroanalytical detection of theophylline. Talanta Open 3, 100037. https://doi.org/10.1016/j.talo.2021.100037

Crawford, K.G., Maini, I., Macdonald, D.A., Moran, D.A.J., 2021. Surface transfer doping of diamond: A review. Prog. Surf. Sci. 96, 100613. https://doi.org/10.1016/j.progsurf.2021.100613

Czupryniak, J., Fabiańska, A., Stepnowski, P., Ossowski, T., Bogdanowicz, R., Gnyba, M., Siedlecka, E.M., 2012. Application of BDD thin film electrode for electrochemical decomposition of heterogeneous aromatic compounds. Cent. Eur. J. Phys. 10, 1183–1189. https://doi.org/10.2478/s11534-012-0058-3

da Costa, L.P., 2020. Chapter 14 - Engineered nanomaterials in the sports industry, in: Hussain, C.M. (Ed.), Handbook of Nanomaterials for Manufacturing Applications, Micro and Nano Technologies. Elsevier, pp. 309–320. https://doi.org/10.1016/B978-0-12-821381-0.00014-4

Dai, H., 2002. Carbon nanotubes: opportunities and challenges. Surf. Sci. 500, 218–241. https://doi.org/10.1016/S0039-6028(01)01558-8

Dalmas, F., Chazeau, L., Gauthier, C., Masenelli-Varlot, K., Dendievel, R., Cavaillé, J.Y., Forró, L., 2005. Multiwalled carbon nanotube/polymer nanocomposites: Processing and properties. J. Polym. Sci. Part B Polym. Phys. 43, 1186–1197. https://doi.org/10.1002/polb.20409

Das, D., Banerjee, A., 2015. Further improvements of nano-diamond structures on unheated substrates by optimization of parameters with secondary plasma in MW-PECVD. Surf. Coat. Technol. 272, 357–365. https://doi.org/10.1016/j.surfcoat.2015.03.042

Das, D., Raj, R., Jana, J., Chatterjee, S., Ganapathi, K.L., Chandran, M., Ramachandra Rao, M.S., 2022. Diamond—the ultimate material for exploring physics of spin-defects for quantum technologies and diamondtronics. J. Phys. Appl. Phys. 55, 333002. https://doi.org/10.1088/1361-6463/ac6d89

David Harvey, 1999. Modern Analytical Chemistry.

de las Casas, C., Li, W., 2012. A review of application of carbon nanotubes for lithium ion battery anode material. J. Power Sources 208, 74–85. https://doi.org/10.1016/j.jpowsour.2012.02.013

De Volder, M.F.L., Tawfick, S.H., Baughman, R.H., Hart, A.J., 2013. Carbon Nanotubes: Present and Future Commercial Applications. Science 339, 535–539. https://doi.org/10.1126/science.1222453

Di Matteo, P., Bortolami, M., Feroci, M., Scarano, V., Petrucci, R., 2021. Electrochemical Transformations of Methylxanthines in Non-Aqueous Medium. ChemElectroChem 8, 2754–2763. https://doi.org/10.1002/celc.202100320

Diaconu, M., Litescu, S.C., Radu, G.L., 2011. Bienzymatic sensor based on the use of redox enzymes and chitosan–MWCNT nanocomposite. Evaluation of total phenolic content in plant extracts. Microchim. Acta 172, 177–184. https://doi.org/10.1007/s00604-010-0486-y

Dineshkumar, B., Krishnakumar, K., Bhatt, A.R., Paul, D., Cherian, J., John, A., Suresh, S., 2015. Single-walled and multi-walled carbon nanotubes based drug delivery system: Cancer therapy: A review. Indian J. Cancer 52, 262. https://doi.org/10.4103/0019-509X.176720

Dorkó, Z., Verbić, T., Horvai, G., 2015. Selectivity in analytical chemistry: Two interpretations for univariate methods. Talanta 132, 680–684. https://doi.org/10.1016/j.talanta.2014.10.018

Dorraji, P.S., Jalali, F., 2016. Differential pulse voltammetric determination of nanomolar concentrations of antiviral drug acyclovir at polymer film modified glassy carbon electrode. Mater. Sci. Eng. C 61, 858–864. https://doi.org/10.1016/j.msec.2016.01.030

Dragan Manojlović, Jelena Mutić, Dejan Šegan, 2010. Osnove Elektroanaliticke Hemije. Belgrade.

Dresselhaus, M.S., Dresselhaus, G., Eklund, P.C., Rao, A.M., 2000. Carbon Nanotubes, in: Andreoni, W. (Ed.), The Physics of Fullerene-Based and Fullerene-Related Materials. Springer Netherlands, Dordrecht, pp. 331–379. https://doi.org/10.1007/978-94-011-4038-6_9

Đurđić, S., Vlahović, F., Ognjanović, M., Gemeiner, P., Sarakhman, O., Stanković, V., Mutić, J., Stanković, D., Švorc, Ľ., 2024. Nano-size cobalt-doped cerium oxide

particles embedded into graphitic carbon nitride for enhanced electrochemical sensing of insecticide fenitrothion in environmental samples: An experimental study with the theoretical elucidation of redox events. Sci. Total Environ. 909, 168483. https://doi.org/10.1016/j.scitotenv.2023.168483

E R Strachan, A Bennett, 1994. Theobromine poisoning in dogs. Vet. Rec. https://doi.org/10.1136/vr.134.11.284.

Einaga, Y. (Ed.), 2022. Diamond Electrodes: Fundamentals and Applications. Springer, Singapore. https://doi.org/10.1007/978-981-16-7834-9

Elvira Gonzalez de Mejia, Marco Vinicio Ramirez-Mares, 2014. Impact of caffeine and coffee on our health. Trends Endocrinol. Amp Metab. 25, 489–492. https://doi.org/10.1016/j.tem.2014.07.003

Eva Martínez Pinilla, Ainhoa Oñatibia-Astibia, Rafael Franco, 2015. The relevance of theobromine for the beneficial effects of cocoa consumption. Front. Pharmacol. https://doi.org/10.3389/fphar.2015.00030

F. Estelle R Simons, Cathy A. Gillespie, Allan B. Becker, Keith J. Simons, n.d. The bronchodilator effect and pharmacokinetics of theobromine in young patients with asthma 703–707. https://doi.org/10.1016/0091-6749(85)90674-8

Fang, K., Zhang, X., Deng, M., Gai, Z., Zhang, M., Yang, Y., 2025. Effect of boron doping levels on the piezoresistive properties of boron-doped diamond films prepared by HFCVD. Vacuum 231, 113768. https://doi.org/10.1016/j.vacuum.2024.113768

Favero, G., Fusco, G., Mazzei, F., Tasca, F., Antiochia, R., 2015. Electrochemical Characterization of Graphene and MWCNT Screen-Printed Electrodes Modified with AuNPs for Laccase Biosensor Development. Nanomaterials 5, 1995–2006. https://doi.org/10.3390/nano5041995

Feier, B., Florea, A., Cristea, C., Săndulescu, R., 2018. Electrochemical detection and removal of pharmaceuticals in waste waters. Curr. Opin. Electrochem., Environmental Electrochemistry ● Solar Cells 11, 1–11. https://doi.org/10.1016/j.coelec.2018.06.012

Ferrier, D.C., Honeychurch, K.C., 2021. Carbon Nanotube (CNT)-Based Biosensors. Biosensors 11, 486. https://doi.org/10.3390/bios11120486

Filik, H., Avan, A.A., Mümin, Y., 2017. Simultaneous Electrochemical Determination of Caffeine and Vanillin by Using Poly(Alizarin Red S) Modified Glassy Carbon Electrode. Food Anal. Methods 10, 31–40. https://doi.org/10.1007/s12161-016-0545-z

Flores-Lasluisa, J.X., Cazorla-Amorós, D., Morallón, E., 2024. Deepening the Understanding of Carbon Active Sites for ORR Using Electrochemical and Spectrochemical Techniques. Nanomaterials 14, 1381. https://doi.org/10.3390/nano14171381

Fortin, E., Chane-Tune, J., Delabouglise, D., Bouvier, P., Livache, T., Mailley, P., Marcus, B., Mermoux, M., Petit, J.-P., Szunerits, S., Vieil, E., 2005. Interfacing Boron Doped Diamond and Biology: An Insight on Its Use for Bioanalytical Applications. Electroanalysis 17, 517–526. https://doi.org/10.1002/elan.200403190

Ganiyu, S.O., dos Santos, E.V., Martínez-Huitle, C.A., Waldvogel, S.R., 2022. Opportunities and challenges of thin-film boron-doped diamond electrochemistry for valuable resources recovery from waste: Organic, inorganic, and volatile product electrosynthesis. Curr. Opin. Electrochem. 32, 100903. https://doi.org/10.1016/j.coelec.2021.100903

Ganiyu, S.O., Martínez-Huitle, C.A., 2019. Nature, Mechanisms and Reactivity of Electrogenerated Reactive Species at Thin-Film Boron-Doped Diamond (BDD) Electrodes During Electrochemical Wastewater Treatment. ChemElectroChem 6, 2379–2392. https://doi.org/10.1002/celc.201900159

Garrett, D.J., Saunders, A.L., McGowan, C., Specks, J., Ganesan, K., Meffin, H., Williams, R.A., Nayagam, D.A.X., 2016. In vivo biocompatibility of boron doped and nitrogen included conductive-diamond for use in medical implants. J. Biomed. Mater. Res. B Appl. Biomater. 104, 19–26. https://doi.org/10.1002/jbm.b.33331

Gastel, A.V., 2022. Drug-Induced Insomnia and Excessive Sleepiness. Sleep Med. Clin. 17, 471–484. https://doi.org/10.1016/j.jsmc.2022.06.011

Giuseppe Maruccio, Jagriti Narang, 2022. Electrochemical Sensors: From Working Electrodes to Functionalization and Miniaturized Devices.

Goh, J.W., Thaw, M.M., Ramim, J.U., Mukherjee, R., 2023. Theophylline Toxicity: A Differential to Consider in Patients on Long-Term Theophylline Presenting With Nonspecific Symptoms. Cureus. https://doi.org/10.7759/cureus.48480

Goldstein, J.I., Newbury, D.E., Echlin, P., Joy, D.C., Lyman, C.E., Lifshin, E., Sawyer, L., Michael, J.R., 2003. Scanning Electron Microscopy and X-ray Microanalysis: Third Edition. Springer US, Boston, MA. https://doi.org/10.1007/978-1-4615-0215-9

Gonçalves, A.G., Figueiredo, J.L., Órfão, J.J.M., Pereira, M.F.R., 2010. Influence of the surface chemistry of multi-walled carbon nanotubes on their activity as ozonation catalysts. Carbon 48, 4369–4381. https://doi.org/10.1016/j.carbon.2010.07.051

Gong, H., Peng, R., Liu, Z., 2013. Carbon nanotubes for biomedical imaging: The recent advances. Adv. Drug Deliv. Rev., Carbon Nanotubes in Medicine and Biology: Therapy and Diagnostics & Safety and Toxicology 65, 1951–1963. https://doi.org/10.1016/j.addr.2013.10.002

Granger, M.C., Witek, M., Xu, J., Wang, J., Hupert, M., Hanks, A., Koppang, M.D., Butler, J.E., Lucazeau, G., Mermoux, M., Strojek, J.W., Swain, G.M., 2000. Standard Electrochemical Behavior of High-Quality, Boron-Doped Polycrystalline Diamond Thin-Film Electrodes. Anal. Chem. 72, 3793–3804. https://doi.org/10.1021/ac0000675

Griesbach, U., Zollinger, D., Pütter, H., Comninellis, C., 2005. Evaluation of boron doped diamond electrodes for organic electrosynthesis on a preparative scale⋆. J. Appl. Electrochem. 35, 1265–1270. https://doi.org/10.1007/s10800-005-9038-2

Hafaiedh, I., Elleuch, W., Clement, P., Llobet, E., Abdelghani, A., 2013. Multi-walled carbon nanotubes for volatile organic compound detection. Sens. Actuators B Chem. 182, 344–350. https://doi.org/10.1016/j.snb.2013.03.020

Hans-Rudolf Buser, Markus D. Müller, Thomas Poiger, Ignaz J. Buerge, 2003. Caffeine, an anthropogenic marker for wastewater contamination of surface waters. Environ. Sci. Technol. 37, 691–700. https://doi.org/10.1021/es020125z

Helbling, T., Roman, C., Hierold, C., 2010. Signal-to-Noise Ratio in Carbon Nanotube Electromechanical Piezoresistive Sensors. Nano Lett. 10, 3350–3354. https://doi.org/10.1021/nl101031e

Hendrik J. Smit., Rachel J. Blackburn, 2005. Reinforcing effects of caffeine and theobromine as found in chocolate. Psychopharmacology (Berl.) 101–106. https://doi.org/10.1007/s00213-005-2209-3

Hendrik Jan Smit, n.d. Theobromine and the Pharmacology of Cocoa. https://doi.org/10.1007/978-3-642-13443-2_7

Hernández-Rivera, M., Zaibaq, N.G., Wilson, L.J., 2016. Toward carbon nanotube-based imaging agents for the clinic. Biomaterials 101, 229–240. https://doi.org/10.1016/j.biomaterials.2016.05.045

Hu, X., Dong, S., 2008. Metal nanomaterials and carbon nanotubes—synthesis, functionalization and potential applications towards electrochemistry. J. Mater. Chem. 18, 1279–1295. https://doi.org/10.1039/B713255G

Ichikawa, K., Wada, T., Nishihara, T., Tsuji, M., Mori, A., Yokohama, F., Hasegawa, D., Kawamoto, K., Tanakaya, M., Katyama, Y., Sakuragi, S., Ito, H., 2017. A case of life-threatening supraventricular tachycardia storm associated with theophylline toxicity. J. Cardiol. Cases 15, 125–128. https://doi.org/10.1016/j.jccase.2016.12.004

Ilaria Cova, V. Leta, C. Mariani, & L. Pantoni, S. Pomati, 2019. Exploring cocoa properties: is theobromine a cognitive modulator? Psychopharmacology (Berl.). https://doi.org/10.1007/s00213-019-5172-0

Ishii, K., Ogata, G., Einaga, Y., 2022. Electrochemical detection of triamterene in human urine using boron-doped diamond electrodes. Biosens. Bioelectron. 217, 114666. https://doi.org/10.1016/j.bios.2022.114666

Ivan Senta, Emma Gracia-Lor, Andrea Borsotti, Ettore Zuccato, Sara Castiglioni, 2015. Wastewater analysis to monitor use of caffeine and nicotine and evaluation of their metabolites as biomarkers for population size assessment. Water Res. 74, 23–33. https://doi.org/10.1016/j.watres.2015.02.002

Ivandini, T.A., Sato, R., Makide, Y., Fujishima, A., Einaga, Y., 2005. Pt-implanted boron-doped diamond electrodes and the application for electrochemical detection of hydrogen peroxide. Diam. Relat. Mater., Proceedings of the 10th International Conference on New Diamond Science and Technology (ICNDST-10) 14, 2133–2138. https://doi.org/10.1016/j.diamond.2005.08.022

Jain, S., Thakare, V.S., Das, M., Godugu, C., Jain, A.K., Mathur, R., Chuttani, K., Mishra, A.K., 2011. Toxicity of Multiwalled Carbon Nanotubes with End Defects Critically Depends on Their Functionalization Density. Chem. Res. Toxicol. 24, 2028–2039. https://doi.org/10.1021/tx2003728

Jiang, K., Gerhardt, R.A., 2021. Fabrication and Supercapacitor Applications of Multiwall Carbon Nanotube Thin Films. C 7, 70. https://doi.org/10.3390/c7040070

Jin, J., Guo, Jiuchuan, Guo, Jinhong, Li, D., 2024. Carbon-Based Biosensor in Point of Care Setting. Adv. Sens. Res. 3, 2400037. https://doi.org/10.1002/adsr.202400037

Jin, S.H., 2016. Single-walled carbon nanotubes (SWNTs); history and future prospects for electronic applications, in: 2016 23rd International Workshop on Active-Matrix Flatpanel Displays and Devices (AM-FPD). Presented at the 2016 23rd International Workshop on Active-Matrix Flatpanel Displays and Devices (AM-FPD), pp. 38–41. https://doi.org/10.1109/AM-FPD.2016.7543611

Jishou Xu, Michael C. Granger, Qingyun Chen, Jerzy W. Strojek, 1997. Boron-Doped Diamond Thin-Film Electrodes. Anal. Chem. 69, 591A-597A. https://doi.org/10.1021/ac971791z

Joseph Wang, 2023. Analytical Electrochemistry, 4th ed.

Joseph Wang, Bassam A. Freiha, 1983. Subtractive differential pulse voltammetry following adsorptive accumulation of organic compounds. Talanta 30, 837–840. https://doi.org/10.1016/0039-9140(83)80193-3

Juliana dePaula, Adriana Farah, 2019. Caffeine Consumption through Coffee: Content in the Beverage, Metabolism, Health Benefits and Risks. Beverages 5, 37. https://doi.org/10.3390/beverages5020037

Kapri, A., Pant, S., Gupta, N., Nain, S., 2022. Recent Advances in the Biological Significance of Xanthine and its Derivatives: A Review. Pharm. Chem. J. 56, 461–474. https://doi.org/10.1007/s11094-022-02661-8

Katz, E., Willner, I., 2004. Biomolecule-Functionalized Carbon Nanotubes: Applications in Nanobioelectronics. ChemPhysChem 5, 1084–1104. https://doi.org/10.1002/cphc.200400193

Kaur, J., Gill, G.S., Jeet, K., 2019. Chapter 5 - Applications of Carbon Nanotubes in Drug Delivery: A Comprehensive Review, in: Mohapatra, S.S., Ranjan, S., Dasgupta, N., Mishra, R.K., Thomas, S. (Eds.), Characterization and Biology of Nanomaterials for Drug Delivery, Micro and Nano Technologies. Elsevier, pp. 113–135. https://doi.org/10.1016/B978-0-12-814031-4.00005-2

Khan, A., Alamry, K.A., 2022. Surface Modified Carbon Nanotubes: An Introduction, in: Surface Modified Carbon Nanotubes Volume 1: Fundamentals, Synthesis and Recent Trends, ACS Symposium Series. American Chemical Society, pp. 1–25. https://doi.org/10.1021/bk-2022-1424.ch001

Kiamahalleh, M.V., Zein, S.H.S., Najafpour, G., Sata, S.A., Buniran, S., 2012. Multiwalled carbon nanotubes based nanocomposites for supercapacitors: a review of electrode materials. Nano 07, 1230002. https://doi.org/10.1142/S1793292012300022

Killard, A.J., 2017. Disposable sensors. Curr. Opin. Electrochem. 3, 57–62. https://doi.org/10.1016/j.coelec.2017.06.013

Kim, S.N., Rusling, J.F., Papadimitrakopoulos, F., 2007. Carbon Nanotubes for Electronic and Electrochemical Detection of Biomolecules. Adv. Mater. 19, 3214–3228. https://doi.org/10.1002/adma.200700665

Kissinger, P., Hieneman, W.R., 2018. Laboratory Techniques in Electroanalytical Chemistry, Revised and Expanded, 2nd ed. CRC Press.

Knittel, P., Stach, R., Yoshikawa, T., Kirste, L., Mizaikoff, B., Kranz, C., E. Nebel, C., 2019. Characterisation of thin boron-doped diamond films using Raman spectroscopy and chemometrics. Anal. Methods 11, 582–586. https://doi.org/10.1039/C8AY02468E

Kolesov, B.A., 2022. An Introduction to Raman Spectroscopy. Cambridge Scholars Publishing, S.l.

Kordás, K., Mustonen, T., Tóth, G., Jantunen, H., Lajunen, M., Soldano, C., Talapatra, S., Kar, S., Vajtai, R., Ajayan, P.M., 2006. Inkjet Printing of Electrically Conductive Patterns of Carbon Nanotubes. Small 2, 1021–1025. https://doi.org/10.1002/smll.200600061

Kramplová, Z., Ferancová, A., Maliar, T., Purdešová, A., 2023. Tuneable properties of boron-doped diamond working electrodes and their advantages for the detection of pesticides. J. Electroanal. Chem. 949, 117846. https://doi.org/10.1016/j.jelechem.2023.117846

Kukovecz, Á., Kozma, G., Kónya, Z., 2013. Multi-Walled Carbon Nanotubes, in: Vajtai, R. (Ed.), Springer Handbook of Nanomaterials. Springer, Berlin, Heidelberg, pp. 147–188. https://doi.org/10.1007/978-3-642-20595-8_5

Kumar, S., K. Sidhu, H., K. Paul, A., Bhardwaj, N., S. Thakur, N., Deep, A., 2023. Bioengineered multi-walled carbon nanotube (MWCNT) based biosensors and applications thereof. Sens. Diagn. 2, 1390–1413. https://doi.org/10.1039/D3SD00176H

Kumar, S., Priyadarshan, Ghosh, S.K., 2021. Statistical and computational analysis of an environment-friendly MWCNT/NiSO4 composite materials. J. Manuf. Process. 66, 11–26. https://doi.org/10.1016/j.jmapro.2021.04.001

L. J. Dorfman, M. E. Jarvik, n.d. Comparative stimulant and diuretic actions of caffeine and theobromine in man. Clin. Pharmacol. Ther. 869–872. https://doi.org/10.1002/cpt1970116869

Laborda, E., González, J., Molina, Á., 2014. Recent advances on the theory of pulse techniques: A mini review. Electrochem. Commun. 43, 25–30. https://doi.org/10.1016/j.elecom.2014.03.004

Laschi, S., Bulukin, E., Palchetti, I., Cristea, C., Mascini, M., 2008. Disposable electrodes modified with multi-wall carbon nanotubes for biosensor applications. IRBM 29, 202–207. https://doi.org/10.1016/j.rbmret.2007.11.002

Levi-Polyachenko, N.H., Merkel, E.J., Jones, B.T., Carroll, D.L., Stewart, J.H.I., 2009. Rapid Photothermal Intracellular Drug Delivery Using Multiwalled Carbon Nanotubes. Mol. Pharm. 6, 1092–1099. https://doi.org/10.1021/mp800250e

Li, S., Huang, S., Ke, Y., Chen, H., Dang, J., Huang, C., Liu, W., Cui, D., Wang, J., Zhi, X., Ding, X., 2021. A HiPAD Integrated with rGO/MWCNTs Nano-Circuit Heater

for Visual Point-of-Care Testing of SARS-CoV-2. Adv. Funct. Mater. 31, 2100801. https://doi.org/10.1002/adfm.202100801

Lin, Y., Shen, W., Fang, C., Wang, Y., Zhang, Y., Chen, L., Wang, Q., Wan, B., Zhang, Z., Jia, X., 2024. High pressure and high temperature synthesized boron-doped diamond electrodes for effective waste water treatment. J. Eur. Ceram. Soc. 44, 4570–4579. https://doi.org/10.1016/j.jeurceramsoc.2024.01.097

Liu, G., Lin, Y., Tu, Y., Ren, Z., 2005. Ultrasensitive voltammetric detection of trace heavy metal ions using carbon nanotube nanoelectrode array. Analyst 130, 1098–1101. https://doi.org/10.1039/B419447K

Liu, H., Dandy, D.S., 1995. 3 - Diamond CVD Techniques, in: Liu, H., Dandy, D.S. (Eds.), Diamond Chemical Vapor Deposition. William Andrew Publishing, Park Ridge, NJ, pp. 14–45. https://doi.org/10.1016/B978-081551380-3.50004-9

Liu, S., An, L., Chen, X., Li, Z., Duan, M., Deng, F., Ju, B.-F., Chen, Y.-L., 2024. A locally boron-doped diamond tool for self-sensing of cutting temperature: Lower thermal capacity and broader applications. Int. J. Adv. Manuf. Technol. 135, 3301–3315. https://doi.org/10.1007/s00170-024-14703-4

Liu, Y.-L., 2016. Effective approaches for the preparation of organo-modified multi-walled carbon nanotubes and the corresponding MWCNT/polymer nanocomposites. Polym. J. 48, 351–358. https://doi.org/10.1038/pj.2015.132

Ľubomír Švorc, Marek Haššo, Olha Sarakhman, Kristína Kianičková, Dalibor M. Stanković, Pavel Otřísal, 2018. A progressive electrochemical sensor for food quality control: Reliable determination of theobromine in chocolate products using a miniaturized boron-doped diamond electrode. Microchem. J. 297–304. https://doi.org/10.1016/j.microc.2018.07.007

Luo, J., Wang, H., Zuo, D., Ji, A., Liu, Y., 2018. Research on the Application of MWCNTs/PLA Composite Material in the Manufacturing of Conductive Composite Products in 3D Printing. Micromachines 9, 635. https://doi.org/10.3390/mi9120635

Ma, Y.J., Jiang, D.Q., Meng, J.X., Li, M.X., Zhao, H.H., Wang, Y., Wang, L.Q., 2016. Theophylline: a review of population pharmacokinetic analyses. J. Clin. Pharm. Ther. 41, 594–601. https://doi.org/10.1111/jcpt.12435

Mahemuti, G., Zhang, H., Li, J., Tieliwaerdi, N., Ren, L., 2018. Efficacy and side effects of intravenous theophylline in acute asthma: a systematic review and meta-analysis. Drug Des. Devel. Ther. 12, 99–120. https://doi.org/10.2147/DDDT.S156509

Manasa, G., Bhakta, A.K., Mascarenhas, R.J., Shetti, N.P., 2023. BaO-MWCNT composite material-based electrocatalytic amperometric sensor for the detection of environmentally hazardous Diuron. Microchem. J. 191, 108778. https://doi.org/10.1016/j.microc.2023.108778

Margay, S.M., Farhat, S., Kaur, S., Teli, H.A., 2015. To Study the Efficacy and Safety of Doxophylline and Theophylline in Bronchial Asthma. J. Clin. Diagn. Res. JCDR 9, FC05–FC08. https://doi.org/10.7860/JCDR/2015/12438.5743

Marton, M., Vojs, M., Michniak, P., Behúl, M., Rehacek, V., Pifko, M., Stehlík, Š., Kromka, A., 2022. New chemical pathway for large-area deposition of doped diamond films by linear antenna microwave plasma chemical vapor deposition. Diam. Relat. Mater. 126, 109111. https://doi.org/10.1016/j.diamond.2022.109111

Merve Yence, Ahmet Cetinkaya, Goksu Ozcelikay, S. Irem Kaya, Sibel A. Ozkan, 2021. Boron-Doped Diamond Electrodes: Recent Developments and Advances in View of Electrochemical Drug Sensors. Crit. Rev. Anal. Chem. 52, 1122–1138. https://doi.org/10.1080/10408347.2020.1863769

Meškinis, Š., Gudaitis, R., Vasiliauskas, A., Guobienė, A., Jankauskas, Š., Stankevič, V., Keršulis, S., Stirkė, A., Andriukonis, E., Melo, W., Vertelis, V., Žurauskienė, N., 2023. Biosensor Based on Graphene Directly Grown by MW-PECVD for Detection of COVID-19 Spike (S) Protein and Its Entry Receptor ACE2. Nanomaterials 13, 2373. https://doi.org/10.3390/nano13162373

Metrohm "COOH functionalized multi-walled carbon nanotubes" [WWW Document], n.d. . Metrohm. URL https://metrohm-dropsens.com/products/nanomaterials-and-reagents/carbon-materials/cooh-functionalized-multi-walled-carbon-nanotubes/ (accessed 9.3.25).

Mijajlović, A., Stanković, V., Mutić, T., Djurdjić, S., Vlahović, F., Stanković, D., 2025. Boron-Doped Diamond Electrodes for Toxins Sensing in Environmental Samples—A Review. Sensors 25, 2339. https://doi.org/10.3390/s25072339

Mikkelsen, Ø., Schrøder, K.H., 2003. Amalgam Electrodes for Electroanalysis. Electroanalysis 15, 679–687. https://doi.org/10.1002/elan.200390085

Mirceski, V., Skrzypek, S., Stojanov, L., 2018. Square-wave voltammetry. ChemTexts 4, 17. https://doi.org/10.1007/s40828-018-0073-0

Mitchell, D.C., Knight, C.A., Hockenberry, J., Teplansky, R., Hartman, T.J., 2014. Beverage caffeine intakes in the U.S. Food Chem. Toxicol. 63, 136–142. https://doi.org/10.1016/j.fct.2013.10.042

Mitsugu Yoneda, Naotoshi Sugimoto, Masanori Katakura, Kentaro Matsuzaki, Hayate Tanigami, Akihiro Yachie, Takako Ohno-Shosaku, Osamu Shido, 2017. Theobromine up-regulates cerebral brain-derived neurotrophic factor and facilitates motor learning in mice. J. Nutr. Biochem. https://doi.org/10.1016/j.jnutbio.2016.10.002

Mohajeri, M., Behnam, B., Sahebkar, A., 2019. Biomedical applications of carbon nanomaterials: Drug and gene delivery potentials. J. Cell. Physiol. 234, 298–319. https://doi.org/10.1002/jcp.26899

Mohd Nurazzi, N., Asyraf, M.R.M., Khalina, A., Abdullah, N., Sabaruddin, F.A., Kamarudin, S.H., Ahmad, S., Mahat, A.M., Lee, C.L., Aisyah, H.A., Norrrahim, M.N.F., Ilyas, R.A., Harussani, M.M., Ishak, M.R., Sapuan, S.M., 2021. Fabrication, Functionalization, and Application of Carbon Nanotube-Reinforced Polymer Composite: An Overview. Polymers 13, 1047. https://doi.org/10.3390/polym13071047

Molina, Á., González, J., 2016. Pulse Voltammetry in Physical Electrochemistry and Electroanalysis: Theory and Applications, Monographs in Electrochemistry. Springer International Publishing, Cham. https://doi.org/10.1007/978-3-319-21251-7

Mora, A.S., McBeath, S.T., Cid, C.A., Hoffmann, M.R., Graham, N.J.D., 2022. Diamond electrode facilitated electrosynthesis of water and wastewater treatment oxidants. Curr. Opin. Electrochem. 32, 100899. https://doi.org/10.1016/j.coelec.2021.100899

Mordačíková, E., Vojs, M., Grabicová, K., Marton, M., Michniak, P., Řeháček, V., Bořík, A., Grabic, R., Bruncko, J., Mackuľak, T., Vojs Staňová, A., 2020. Influence of boron doped diamond electrodes properties on the elimination of selected pharmaceuticals from wastewater. J. Electroanal. Chem. 862, 114007. https://doi.org/10.1016/j.jelechem.2020.114007

Moriyama, H., Ogata, G., Nashimoto, H., Sawamura, S., Furukawa, Y., Hibino, H., Kusuhara, H., Einaga, Y., 2022. A rapid and simple electrochemical detection of the free drug concentration in human serum using boron-doped diamond electrodes. Analyst 147, 4442–4449. https://doi.org/10.1039/D2AN01037B

Morton, J., Havens, N., Mugweru, A., Wanekaya, A.K., 2009. Detection of Trace Heavy Metal Ions Using Carbon Nanotube- Modified Electrodes. Electroanalysis 21, 1597–1603. https://doi.org/10.1002/elan.200904588

Muller, J., Huaux, F., Moreau, N., Misson, P., Heilier, J.-F., Delos, M., Arras, M., Fonseca, A., Nagy, J.B., Lison, D., 2005. Respiratory toxicity of multi-wall carbon nanotubes. Toxicol. Appl. Pharmacol. 207, 221–231. https://doi.org/10.1016/j.taap.2005.01.008

Nanot, S., Thompson, N.A., Kim, J.-H., Wang, X., Rice, W.D., Hároz, E.H., Ganesan, Y., Pint, C.L., Kono, J., 2013. Single-Walled Carbon Nanotubes, in: Vajtai, R. (Ed.), Springer Handbook of Nanomaterials. Springer, Berlin, Heidelberg, pp. 105–146. https://doi.org/10.1007/978-3-642-20595-8_4

Negri, V., Pacheco-Torres, J., Calle, D., López-Larrubia, P., 2020. Carbon Nanotubes in Biomedicine, in: Puente-Santiago, A.R., Rodríguez-Padrón, D. (Eds.), Surface-Modified Nanobiomaterials for Electrochemical and Biomedicine Applications. Springer International Publishing, Cham, pp. 177–217. https://doi.org/10.1007/978-3-030-55502-3_6

Neralla, S., 2016. Chemical Vapor Deposition: Recent Advances and Applications in Optical, Solar Cells and Solid State Devices. BoD – Books on Demand.

Niyogi, S., Hamon, M.A., Hu, H., Zhao, B., Bhowmik, P., Sen, R., Itkis, M.E., Haddon, R.C., 2002. Chemistry of Single-Walled Carbon Nanotubes. Acc. Chem. Res. 35, 1105–1113. https://doi.org/10.1021/ar010155r

O. Matvieiev, R. Šelešovská, M. Vojs, M. Marton, P. Michniak, V. Hrdlička, M. Hatala, L. Janikova, J. Chýlková, J. Skopalova, P. Cankař, T. Navratil, 2022. Novel Screen-Printed Sensor with Chemically Deposited Boron-Doped Diamond Electrode: Preparation, Characterization, and Application. Biosensors 12, 241. https://doi.org/10.3390/bios12040241

Okpara, E.C., Nde, S.C., Fayemi, O.E., Ebenso, E.E., 2021. Electrochemical Characterization and Detection of Lead in Water Using SPCE Modified with BiONPs/PANI. Nanomaterials 11, 1294. https://doi.org/10.3390/nano11051294

Osteryoung, J.G., Schreiner, M.M., 1988. Recent Advances in Pulse Voltammetry. C R C Crit. Rev. Anal. Chem.

Oturan, M.A., 2021. Outstanding performances of the BDD film anode in electro-Fenton process: Applications and comparative performance. Curr. Opin. Solid State Mater. Sci. 25, 100925. https://doi.org/10.1016/j.cossms.2021.100925

Ouyang, M., Huang, J.-L., Lieber, C.M., 2002. Fundamental Electronic Properties and Applications of Single-Walled Carbon Nanotubes. Acc. Chem. Res. 35, 1018–1025. https://doi.org/10.1021/ar0101685

Ouyang, M., Li, W.J., 2009. Reusable CNTs-based chemical sensors, in: 2009 IEEE 3rd International Conference on Nano/Molecular Medicine and Engineering. Presented at the 2009 IEEE 3rd International Conference on Nano/Molecular Medicine and Engineering, pp. 188–192. https://doi.org/10.1109/NANOMED.2009.5559088

Paimard, G., Ghasali, E., Baeza, M., 2023. Screen-Printed Electrodes: Fabrication, Modification, and Biosensing Applications. Chemosensors 11, 113. https://doi.org/10.3390/chemosensors11020113

Pantarotto, D., Singh, R., McCarthy, D., Erhardt, M., Briand, J.-P., Prato, M., Kostarelos, K., Bianco, A., 2004. Functionalized Carbon Nanotubes for Plasmid DNA Gene Delivery. Angew. Chem. Int. Ed. 43, 5242–5246. https://doi.org/10.1002/anie.200460437

Peng, J., He, Y., Zhou, C., Su, S., Lai, B., 2021. The carbon nanotubes-based materials and their applications for organic pollutant removal: A critical review. Chin. Chem. Lett. 32, 1626–1636. https://doi.org/10.1016/j.cclet.2020.10.026

Peng, L.-M., Zhang, Z., Qiu, C., 2019. Carbon nanotube digital electronics. Nat. Electron. 2, 499–505. https://doi.org/10.1038/s41928-019-0330-2

Peng, Y., Zhang, W., Chang, J., Huang, Y., Chen, L., Deng, H., Huang, Z., Wen, Y., 2017. A Simple and Sensitive Method for the Voltammetric Analysis of Theobromine in Food Samples Using Nanobiocomposite Sensor. Food Anal. Methods 10, 3375–3384. https://doi.org/10.1007/s12161-017-0867-5

Pereira, G.F., Andrade, L.S., Rocha-Filho, R.C., Bocchi, N., Biaggio, S.R., 2012. Electrochemical determination of bisphenol A using a boron-doped diamond electrode. Electrochimica Acta, ELECTROCHEMICAL FRONTIERS IN GLOBAL ENVIRONMENT AND ENERGY 82, 3–8. https://doi.org/10.1016/j.electacta.2012.03.157

Pippione, G., Olivero, P., Fischer, M., Schreck, M., Pasquarelli, A., 2017. Characterization of CVD Heavily B-Doped Diamond Thin Films for Multi Electrode Array Biosensors. Phys. Status Solidi A 214, 1700223. https://doi.org/10.1002/pssa.201700223

Popov, V.N., 2004. Carbon nanotubes: properties and application. Mater. Sci. Eng. R Rep. 43, 61–102. https://doi.org/10.1016/j.mser.2003.10.001

Pratik Joshi, Parand Riley, K.Yugender Goud, Rupesh K. Mishra, Roger Narayan, 2022. Recent advances of boron-doped diamond electrochemical sensors toward

environmental applications. Curr. Opin. Electrochem. 32. https://doi.org/10.1016/j.coelec.2021.100920

Prelas, Mark Antonio, 1998. Handbook of Industrial Diamonds and Diamond Films. CRC Press.

Pulok K. Mukherjee, 2019. Chapter 7 - Bioactive Phytocomponents and Their Analysis. Qual. Control Eval. Herb. Drugs 237–328. https://doi.org/10.1016/B978-0-12-813374-3.00007-7

Raut, S.S., Sankapal, B.R., 2016. Comparative studies on MWCNTs, Fe2O3 and Fe2O3/MWCNTs thin films towards supercapacitor application. New J. Chem. 40, 2619–2627. https://doi.org/10.1039/C5NJ03628C

Redkin, A.N., Mitina, A.A., Yakimov, E.E., Kabachkov, E.N., 2021. Electrochemical Improvement of the MWCNT/Al Electrodes for Supercapacitors. Materials 14, 7612. https://doi.org/10.3390/ma14247612

Reimer, L., 1998. Scanning Electron Microscopy: Physics of Image Formation and Microanalysis, Springer Series in Optical Sciences. Springer, Berlin, Heidelberg. https://doi.org/10.1007/978-3-540-38967-5

Rejithamol, R., Beena, S., 2022. Carbon Paste Electrochemical Sensors for the Detection of Neurotransmitters. Front. Sens. 3. https://doi.org/10.3389/fsens.2022.901628

Robin Poole, Oliver J Kennedy, Paul Roderick, Jonathan A Fallowfield, Peter C Hayes, Julie Parkes, 2017. Coffee consumption and health: umbrella review of meta-analyses of multiple health outcomes. BMJ J. 360, k194. https://doi.org/10.1136/bmj.j5024

Roy, A., Ray, A., Saha, S., Das, S., 2018. Investigation on energy storage and conversion properties of multifunctional PANI-MWCNT composite. Int. J. Hydrog. Energy 43, 7128–7139. https://doi.org/10.1016/j.ijhydene.2018.02.153

R.P. Heaney, 2002. Effects of caffeine on bone and the calcium economy. Food Chem. Toxicol. 40, 1263–1270. https://doi.org/10.1016/S0278-6915(02)00094-7

Sagar, P., Sahrawat, A., Srivastava, M., Priyanka, Agarwal, P., Srivastava, S.K., 2025. WS2 nanoparticle integrated MWCNT as an efficient electrode material for electrochemical sensing of chloramphenicol in pharmaceutical samples. Microchem. J. 210, 112922. https://doi.org/10.1016/j.microc.2025.112922

Scheindlin, S., 2007. A new look at the xanthine alkaloids. Mol. Interv. 7, 236. https://doi.org/10.1124/mi.7.5.1

Scurek, M., Brat, K., 2024. A narrative review of theophylline: is there still a place for an old friend? J. Thorac. Dis. 16, 3450–3460. https://doi.org/10.21037/jtd-23-1781

Šelešovská, R., Navrátil, T., Hrdlička, V., Michniak, P., Hatala, M., Vojs, M., Marton, M., Matvieiev, O., Janíková, L., Chýlková, J., 2022. Novel screen-printed sensors with chemically deposited boron-doped diamond and their use for voltammetric determination of attention deficit hyperactivity disorder medication atomoxetine. Electrochimica Acta 403, 139642. https://doi.org/10.1016/j.electacta.2021.139642

Serrano, N., Díaz-Cruz, J.M., Ariño, C., Esteban, M., 2016. Antimony- based electrodes for analytical determinations. TrAC Trends Anal. Chem. 77, 203–213. https://doi.org/10.1016/j.trac.2016.01.011

Shi, K., Shiu, K.-K., 2001. Determination of Uric Acid at Electrochemically Activated Glassy Carbon Electrode. Electroanalysis 13, 1319–1325. https://doi.org/10.1002/1521-4109(200111)13:16%253C1319::AID-ELAN1319%253E3.0.CO;2-C

Silva, Á.R.L. da, Araújo, D.M. de, Silva, E.B.S. da, Vieira, D.S., Monteiro, N. de K.V., Martínez-Huitle, C.A., 2017. Understanding the behavior of caffeine on a boron-doped diamond surface: voltammetric, DFT, QTAIM and ELF studies. New J. Chem. 41, 7766–7774. https://doi.org/10.1039/C7NJ00386B

Singh, D.K., Kumar Mishra, A., Materny, A. (Eds.), 2024. Raman Spectroscopy: Advances and Applications, Springer Series in Optical Sciences. Springer Nature, Singapore. https://doi.org/10.1007/978-981-97-1703-3

Singh, N., Shreshtha, A.K., Thakur, M.S., Patra, S., 2018. Xanthine scaffold: scope and potential in drug development. Heliyon 4. https://doi.org/10.1016/j.heliyon.2018.e00829

Singh, S., Wang, J., Cinti, S., 2022. Review—An Overview on Recent Progress in Screen-Printed Electroanalytical (Bio)Sensors. ECS Sens. Plus 1, 023401. https://doi.org/10.1149/2754-2726/ac70e2

Sobaszek, M., Skowroński, Ł., Bogdanowicz, R., Siuzdak, K., Cirocka, A., Zięba, P., Gnyba, M., Naparty, M., Gołuński, Ł., Płotka, P., 2015. Optical and electrical properties of ultrathin transparent nanocrystalline boron-doped diamond electrodes. Opt. Mater. 42, 24–34. https://doi.org/10.1016/j.optmat.2014.12.014

Sobhan, A., Oh, J.-H., Park, M.-K., Lee, J., 2020. Reusability of a single-walled carbon nanotube-based biosensor for detecting peanut allergens and *Y. enterocolitica*. Microelectron. Eng. 225, 111281. https://doi.org/10.1016/j.mee.2020.111281

Soffietti, M.G., Nebbia, C., Valenza, F., Amedeo, S., Re, G., 1989. Toxic effects of theobromine on mature and immature male rabbits. J. Comp. Pathol. 100, 47–58. https://doi.org/10.1016/0021-9975(89)90089-3

Sohn, J.A., Kim, H.-S., Oh, J., Cho, J.-Y., Yu, K.-S., Lee, J., Shin, S.H., Lee, J.A., Choi, C.W., Kim, E.-K., Kim, B.I., Park, E.A., 2017. Prediction of serum theophylline concentrations and cytochrome P450 1A2 activity by analyzing urinary metabolites in preterm infants. Br. J. Clin. Pharmacol. 83, 1279–1286. https://doi.org/10.1111/bcp.13211

Soloman, S., 2010. Sensors handbook. New York : McGraw-Hill.

Song, C.W., Cho, D.S., Lee, J.M., Song, P.K., 2020. Effect of Boron Doping on Diamond Film and Electrochemical Properties of BDD According to Thickness and Morphology. Coatings 10, 331. https://doi.org/10.3390/coatings10040331

Sousa, C.P., Ribeiro, F.W.P., Oliveira, T.M.B.F., Salazar-Banda, G.R., de Lima-Neto, P., Morais, S., Correia, A.N., 2019. Electroanalysis of Pharmaceuticals on Boron-

Doped Diamond Electrodes: A Review. ChemElectroChem 6, 2350–2378. https://doi.org/10.1002/celc.201801742

Spătaru, N., Sarada, B.V., Tryk, D.A., Fujishima, A., 2002. Anodic Voltammetry of Xanthine, Theophylline, Theobromine and Caffeine at Conductive Diamond Electrodes and Its Analytical Application. Electroanalysis 14, 721–728. https://doi.org/10.1002/1521-4109(200206)14:11%253C721::AID-ELAN721%253E3.0.CO;2-1

Spiro, M., Grandoso, D.M., Price, W.E., 1989. Protonation constant of caffeine in aqueous solution. J. Chem. Soc. Faraday Trans. 1 Phys. Chem. Condens. Phases 85, 4259. https://doi.org/10.1039/f19898504259

Srikanth, V.V.S.S., Sampath Kumar, P., Kumar, V.B., 2012. A Brief Review on the In Situ Synthesis of Boron-Doped Diamond Thin Films. Int. J. Electrochem. 2012, 218393. https://doi.org/10.1155/2012/218393

Stanković, D.M., 2015. Sensitive voltammetric determination of thymol in essential oil of *Carum copticum* seeds using boron-doped diamond electrode. Anal. Biochem. 486, 1–4. https://doi.org/10.1016/j.ab.2015.06.026

Stanković, D.M., Mehmeti, E., Svorc, L., Kalcher, K., 2015a. Simple, Rapid and Sensitive Electrochemical Method for the Determination of the Triketone Herbicide Sulcotrione in River Water Using a Glassy Carbon Electrode. Electroanalysis 27, 1587–1593. https://doi.org/10.1002/elan.201400729

Stanković, D.M., Samphao, A., Kuzmanović, D., Kalcher, K., 2015b. Novel electroanalyical method for the determination of andrographolide from *Andrographis paniculata* extract and urine samples. Microchem. J. 122, 16–19. https://doi.org/10.1016/j.microc.2015.04.005

Supraja, P., Tripathy, S., Govind Singh, S., 2023. Smartphone-powered, ultrasensitive, and selective, portable and stable multi-analyte chemiresistive immunosensing platform with PPY/COOH-MWCNT as bioelectrical transducer: Towards point-of-care TBI diagnosis. Bioelectrochemistry 151, 108391. https://doi.org/10.1016/j.bioelechem.2023.108391

Suresh, R.R., Lakshmanakumar, M., Arockia Jayalatha, J.B.B., Rajan, K.S., Sethuraman, S., Krishnan, U.M., Rayappan, J.B.B., 2021. Fabrication of screen-printed electrodes: opportunities and challenges. J. Mater. Sci. 56, 8951–9006. https://doi.org/10.1007/s10853-020-05499-1

Suzuki, A., Ivandini, T.A., Yoshimi, K., Fujishima, A., Oyama, G., Nakazato, T., Hattori, N., Kitazawa, S., Einaga, Y., 2007. Fabrication, Characterization, and Application of Boron-Doped Diamond Microelectrodes for in Vivo Dopamine Detection. Anal. Chem. 79, 8608–8615. https://doi.org/10.1021/ac071519h

Švancara, I., Prior, C., Hočevar, S.B., Wang, J., 2010. A Decade with Bismuth-Based Electrodes in Electroanalysis. Electroanalysis 22, 1405–1420. https://doi.org/10.1002/elan.200970017

Svítková, J., Ignat, T., Švorc, Ľ., Labuda, J., Barek, J., 2016. Chemical Modification of Boron-Doped Diamond Electrodes for Applications to Biosensors and Biosensing. Crit. Rev. Anal. Chem. 46, 248–256. https://doi.org/10.1080/10408347.2015.1082125

Švorc, Ľ., Kalcher, K., 2014. Modification-free electrochemical approach for sensitive monitoring of purine DNA bases: Simultaneous determination of guanine and adenine in biological samples using boron-doped diamond electrode. Sens. Actuators B Chem. 194, 332–342. https://doi.org/10.1016/j.snb.2013.12.104

Szunerits, S., Boukherroub, R., 2018. Graphene-based nanomaterials in innovative electrochemistry. Curr. Opin. Electrochem. 10, 24–30. https://doi.org/10.1016/j.coelec.2018.03.016

Tan, X., Lin, C., Fugetsu, B., 2009. Studies on toxicity of multi-walled carbon nanotubes on suspension rice cells. Carbon 47, 3479–3487. https://doi.org/10.1016/j.carbon.2009.08.018

Taylor, A., Baluchová, S., Fekete, L., Klimša, L., Kopeček, J., Šimek, D., Vondráček, M., Míka, L., Fischer, J., Schwarzová-Pecková, K., Mortet, V., 2022. Growth and comparison of high-quality MW PECVD grown B doped diamond layers on {118}, {115} and {113} single crystal diamond substrates. Diam. Relat. Mater. 123, 108815. https://doi.org/10.1016/j.diamond.2021.108815

T. Luong, J.H., B. Male, K., D. Glennon, J., 2009. Boron -doped diamond electrode : synthesis, characterization, functionalization and analytical applications. Analyst 134, 1965–1979. https://doi.org/10.1039/B910206J

Tomas Brodin, Susanna Piovano, Jerker Fick, Jonatan Klaminder, Martina Heynen, Micael Jonsson, 2014. Ecological effects of pharmaceuticals in aquatic systems-impacts through behavioural alterations. Philos. Trans. R. Soc. B Biol. Sci. 369, 20130580. https://doi.org/10.1098/rstb.2013.0580

Tully, J.J., Houghton, D., Breeze, B.G., Mollart, T.P., Macpherson, J.V., 2024. Quantitative Measurement Technique for Anodic Corrosion of BDD Advanced Oxidation Electrodes. ACS Meas. Sci. Au 4, 267–276. https://doi.org/10.1021/acsmeasuresciau.3c00069

Umadevi, D., Panigrahi, S., Sastry, G.N., 2014. Noncovalent Interaction of Carbon Nanostructures. Acc. Chem. Res. 47, 2574–2581. https://doi.org/10.1021/ar500168b

Uslu, B., Ozkan, S.A., 2007. Electroanalytical Application of Carbon Based Electrodes to the Pharmaceuticals. Anal. Lett. 40, 817–853. https://doi.org/10.1080/00032710701242121

Valenzuela-Muñiz, A.M., Alonso-Nuñez, G., Miki-Yoshida, M., Botte, G.G., Verde-Gómez, Y., 2013. High electroactivity performance in Pt/MWCNT and PtNi/MWCNT electrocatalysts. Int. J. Hydrog. Energy 38, 12640–12647. https://doi.org/10.1016/j.ijhydene.2012.11.134

Vardharajula, S., Ali, S.Z., Tiwari, P.M., Eroğlu, E., Vig, K., Dennis, V.A., Singh, S.R., 2012. Functionalized carbon nanotubes: biomedical applications. Int. J. Nanomedicine 7, 5361–5374. https://doi.org/10.2147/IJN.S35832

Vinoth, S., Wang, S.-F., 2024. Interspersed of Scheelite-Type BaWO4 Nanoparticles Decorated on CNF for the Electrocatalytic Sensing of Theobromine in Food Products. ACS Appl. Nano Mater. 7, 25388–25399. https://doi.org/10.1021/acsanm.4c04331

Viswanathan, S., Rani, C., Ho, J.A., 2012. Electrochemical immunosensor for multiplexed detection of food-borne pathogens using nanocrystal bioconjugates and MWCNT screen-printed electrode. Talanta 94, 315–319. https://doi.org/10.1016/j.talanta.2012.03.049

Viswanathan, S., Rani, C., Vijay Anand, A., Ho, J.A., 2009. Disposable electrochemical immunosensor for carcinoembryonic antigen using ferrocene liposomes and MWCNT screen-printed electrode. Biosens. Bioelectron. 24, 1984–1989. https://doi.org/10.1016/j.bios.2008.10.006

Wang, T., Randviir, E.P., Banks, C.E., 2014. Detection of theophylline utilising portable electrochemical sensors. Analyst 139, 2000–2003. https://doi.org/10.1039/C4AN00065J

Wang, W., Serp, P., Kalck, P., Silva, C.G., Faria, J.L., 2008. Preparation and characterization of nanostructured MWCNT-TiO2 composite materials for photocatalytic water treatment applications. Mater. Res. Bull. 43, 958–967. https://doi.org/10.1016/j.materresbull.2007.04.032

Wang, Y., Hu, S., 2016. Applications of Carbon Nanotubes and Graphene for Electrochemical Sensing of Environmental Pollutants. J. Nanosci. Nanotechnol. 16, 7852–7872. https://doi.org/10.1166/jnn.2016.12762

Wang, Zhiwen, Wang, Ziqi, Liu, Y., Zhao, H., Li, B., Guo, Q., Xu, A., Ma, H., Chen, L., Jia, X., 2024. Study on boron distribution in boron-doped diamond synthesized at HPHT conditions. Int. J. Refract. Met. Hard Mater. 120, 106608. https://doi.org/10.1016/j.ijrmhm.2024.106608

Watanabe, T., Yoshioka, S., Yamamoto, T., Sepehri-Amin, H., Ohkubo, T., Matsumura, S., Einaga, Y., 2018. The local structure in heavily boron-doped diamond and the effect this has on its electrochemical properties. Carbon 137, 333–342. https://doi.org/10.1016/j.carbon.2018.05.026

Wildgoose, G.G., Banks, C.E., Compton, R.G., 2006. Metal Nanoparticles and Related Materials Supported on Carbon Nanotubes: Methods and Applications. Small 2, 182–193. https://doi.org/10.1002/smll.200500324

Williams, J.S., 1998. Ion implantation of semiconductors. Mater. Sci. Eng. A 253, 8–15. https://doi.org/10.1016/S0921-5093(98)00705-9

Wu, Y., Wang, J., Jiang, K., Fan, S., 2014. Applications of carbon nanotubes in high performance lithium ion batteries. Front. Phys. 9, 351–369. https://doi.org/10.1007/s11467-013-0308-x

Xu, T., Yang, J., 2012. Effects of Surface Modification of MWCNT on the Mechanical and Electrical Properties of Fluoro Elastomer/MWCNT Nanocomposites. J. Nanomater. 2012, 275637. https://doi.org/10.1155/2012/275637

Y Wang, D P Waller, 1994. Theobromine toxicity on Sertoli cells and comparison with cocoa extract in male rats. Toxicol. Lett. 70, 155–164. https://doi.org/10.1016/0378-4274(94)90159-7

Yang, S., Li, X., Zhu, W., Wang, J., Descorme, C., 2008. Catalytic activity, stability and structure of multi-walled carbon nanotubes in the wet air oxidation of phenol. Carbon 46, 445–452. https://doi.org/10.1016/j.carbon.2007.12.006

Yasuaki Einaga, 2022. Boron-Doped Diamond Electrodes: Fundamentals for Electrochemical Applications. Acc. Chem. Res. 55, 3605–3615. https://doi.org/10.1021/acs.accounts.2c00597

Ye, J.-S., Wen, Y., De Zhang, W., Ming Gan, L., Xu, G.Q., Sheu, F.-S., 2004. Nonenzymatic glucose detection using multi-walled carbon nanotube electrodes. Electrochem. Commun. 6, 66–70. https://doi.org/10.1016/j.elecom.2003.10.013

Ying Wang, L D Russell, A P Hikim, D P Waller, 1992. Reproductive toxicity of theobromine and cocoa extracts in male rats. Reprod. Toxicol. 347–53. https://doi.org/10.1016/0890-6238(92)90198-3

Yumura, M., 1999. Chapter 2 - Synthesis and Purification of Multi-Walled and Single-Walled Carbon Nanotubes, in: Tanaka, K., Yamabe, T., Fukui, K. (Eds.), The Science and Technology of Carbon Nanotubes. Elsevier Science Ltd, Oxford, pp. 2–13. https://doi.org/10.1016/B978-008042696-9/50002-1

Zare, H., Ahmadi, S., Ghasemi, A., Ghanbari, M., Rabiee, N., Bagherzadeh, M., Karimi, M., Webster, T.J., Hamblin, M.R., Mostafavi, E., 2021. Carbon Nanotubes: Smart Drug/Gene Delivery Carriers. Int. J. Nanomedicine 16, 1681–1706. https://doi.org/10.2147/IJN.S299448

Zhang, M., Su, L., Mao, L., 2006. Surfactant functionalization of carbon nanotubes (CNTs) for layer-by-layer assembling of CNT multi-layer films and fabrication of gold nanoparticle/CNT nanohybrid. Carbon 44, 276–283. https://doi.org/10.1016/j.carbon.2005.07.021

Zhang, Zhiqiang, Xiang, D., Zhang, Zhipeng, Zhang, Y., Zhao, B., 2023. Study on tribology and cutting performance of boron doped diamond composite coated tool. Int. J. Refract. Met. Hard Mater. 117, 106385. https://doi.org/10.1016/j.ijrmhm.2023.106385

Zhao, G., Li, P., Nong, F., Li, M., Gao, J., Li, D., 2010. Construction and High Performance of a Novel Modified Boron-Doped Diamond Film Electrode Endowed with Superior Electrocatalysis. J. Phys. Chem. C 114, 5906–5913. https://doi.org/10.1021/jp909248w

Zhao, X., Liu, Y., Liu, L., Song, H., Hu, T., Lan, J., Zhai, Z., Li, D., Wang, C., Chen, B., Jiang, X., Huang, N., 2024. Thermal stabilization enhancement of diamond films via boron doping and its antioxidant mechanism. Ceram. Int. 50, 33868–33878. https://doi.org/10.1016/j.ceramint.2024.06.205

Zhou, W., Bai, X., Wang, E., Xie, S., 2009. Synthesis, Structure, and Properties of Single-Walled Carbon Nanotubes. Adv. Mater. 21, 4565–4583. https://doi.org/10.1002/adma.200901071

Zhou, X., 2024. Electrochemical detection of heavy metal ions in water using MWCNT/ZnO nanocomposite. Int. J. Electrochem. Sci. 19, 100559. https://doi.org/10.1016/j.ijoes.2024.100559

Ziegler, J., 1992. Handbook of ion implantation technology.

Zima, J., Švancara, I., Barek, J., Vytřas, K., 2009. Recent Advances in Electroanalysis of Organic Compounds at Carbon Paste Electrodes. Crit. Rev. Anal. Chem. 39, 204–227. https://doi.org/10.1080/10408340903011853

Биографија

Јелена Остојић је рођена 22.01.1997. у Суботици.

Основну школу „Јован Јовановић Змај" и Нижу музичку школу у Суботици на гудачком одсеку, завршила је са одличним успехом 2012. Године. Гимназију „Светозар Марковић", природно-математички смер, завршила је са одличним успехом 2016. године.

Студије хемије на Хемијском факултету Универзитета у Београду уписала је 2016. године. Дипломирала је на Катедри за аналитичку хемију Хемијског факултета Универзитета у Београду 30. Септембра 2021. године под менторством др Далибора Станковића са темом „Волтаметријско одређивање иргасана штампаним електродама модификованим лантан гвожђе оксидом и карбон нитридом". Завршни рад је оцењен највишом оценом (10), а студије је завршила са просечном оценом 7,43.

Мастер академске студије уписала је 2021. године на Катедри за аналитичку хемију Хемијског факулета Универзитета у Београду под менторством др Далибора Станковића, а завршила их 30. Септембра 2022. године. Њен мастер рад, под називом „Развој електроаналитичких метода за квантитативно одређивање кофеина и никотина бором допованим дијамантским електродама и штампаним електродама модификованим угљеничним наноцевима", оцењен је највишом оценом (10), а студије је завршила са просечном оценом 10,00.

Докторске академске студије уписала је 2022. године на Катедри за аналитичку хемију Хемијског факултета Универзитета у Београду, такође под менторством др Далибора Станковића.

Током мастер и докторских студија, у оквиру *CEEPUS (Central European Exchange Programme for University Studies)* програма, остварила је сарадњу са више европских универзитета и истраживачких института. Боравила је на Хемијском институту (Катедра за аналитичку хемију) Универзитета у Грацу (Аустрија), Хемијско-технолошком факултету (Катедра за аналитичку хемију) Универзитета у Пардубицама (Чешка) и Институту за електронику и фотонику Факултета електротехнике и информационих технологија на словачком технолошком Универзиту у Братислави (Словачка).

Чланица је Српског хемијског друштва од 2021. године и Клуба младих хемичара Србије од 2022. године. Током студија учествовала је на Конференцији младих хемичара Србије и на „YISAC" (*The 30th Young Investigators' Seminar on Analytical Chemistry*) конференцији.

2022. године основала је своју фирму и од тада послује као самостална предузетница у области развоја брендова, са фокусом на сарадњи са компанијама из струке, комерцијалним лабораторијама и сродним секторима, промовишући кроз своје пословање науку и иновације.

У слободно време бави се стрељаштвом и свирањем виолине.

Течно говори енглески језик и поседује основно знање италијанског језика.

Библиографија

Као резултат ове дисертације проистекла су три научна рада, од којих је један публикован у часописима категорије М21 и два публикована у категорији М22.

М21:

Ostojić, J., Savić, S., Manojlović, D., Metelka, R., Stanković, V., & Stanković, D. (2025). A rapid, reusable, and portable electrochemical assay for caffeine monitoring in beverage samples based on boron doped diamond and multi walled carbon nanotubes. *Diamond and Related Materials*, *156*, 112450. https://doi.org/10.1016/j.diamond.2025.112450

М22:

Ostojić, J., Stanković, V., Miljković, M., Ortner, A., Metelka, R., & Stanković, D.M. (2025). Fast, Accurate, and Point-of-Care Electrochemical Sensing Platform for Theobromine Determination in Food Samples Based on Boron-Doped Diamond Printed Electrode. *Journal of The Electrochemical Society*, 172, 037523 https://doi.org/10.1149/1945-7111/adc341

Ostojić, J., Stanković, D., Manojlović, D., Metelka, R., & Stanković, V. (2025). Theophylline electrochemical sensing in pharmaceutical drugs using disposable boron-doped diamond thin film electrodes. *Functional Diamond*, *5*(1). https://doi.org/10.1080/26941112.2025.2579320

Радови који нису део дисертације:

Научни рад у међународном часопису категорије М21+

Knežević, S., Ostojić, J., Ognjanović, M., Savić, S., Kovačević, A., Manojlović, D., Stanković, V., & Stanković, D. (2023). *The environmentally friendly approaches based on the heterojunction interface of the LaFeO3/Fe2O3@g-C3N4 composite for the disposable and laboratory sensing of triclosan*. Science of The Total Environment, 857, 159250. https://doi.org/10.1016/j.scitotenv.2022.159250

Конференције

Jelena Ostojić, Kurt Kalcher, Astrid Ortner, Dalibor Stanković (2023, November 4th) *Determination of Theobromine in Chocolate with Screen-Printed Boron-Doped Diamond Electrode*, IX Conference of the Young Chemists of Serbia, Novi Sad, Serbia

Jelena Ostojić, Radovan Metelka, Kurt Kalcher, Astrid Ortner, Dalibor Stanković (2023, June 25-27) *Detection and Quantification of Caffeine and Theobromine with Screen-Printed Boron-Doped Diamond Electrode*, 28th Young Investigators' Seminar on Analytical Chemistry (YISAC 2023), Belgrade, Serbia

Изјава о ауторству

Име и презиме аутора: Јелена Б. Остојић

Број индекса: ДХ36/2022

Изјављујем

да је докторска дисертација под насловом

“Development of voltammetric methods for the detection and quantification of xanthine alkaloids using disposable printed sensors“

„Развој волтаметријских метода за детекцију и квантификацију ксантинских алкалоида применом једнократних штампаних сензора“

•резултат сопственог истраживачког рада;

•да дисертација у целини ни у деловима није била предложена за стицање друге дипломе

према студијским програмима других високошколских установа;

•да су резултати коректно наведени и

•да нисам кршио/ла ауторска права и користио/ла интелектуалну својину других лица.

У Београду, Потпис аутора

21.11.2025 _____

Изјава о истоветности штампане и електронске верзије докторског рада

Име и презиме аутора: Јелена Б. Остојић

Број индекса: ДХ36/2022

Студијски програм: Хемија

Наслов рада: Development of voltammetric methods for the detection and quantification of xanthine alkaloids using disposable printed sensors

Наслов на српском језику: Развој волтаметријских метода за детекцију и квантификацију ксантинских алкалоида применом једнократних штампаних сензора

Ментори: др Далибор Станковић, др Радован Метелка

Изјављујем да је штампана верзија мог докторског рада истоветна електронској верзији коју сам предао/ла ради похрањивања у Дигиталном репозиторијуму Универзитета у Београду.

Дозвољавам да се објаве моји лични подаци везани за добијање академског назива доктора наука, као што су име и презиме, година и место рођења и датум одбране рада.

Ови лични подаци могу се објавити на мрежним страницама дигиталне библиотеке, у електронском каталогу и у публикацијама Универзитета у Београду.

У Београду, Потпис аутора

21.11.2025 _____

Изјава о коришћењу

Овлашћујем Универзитетску библиотеку „Светозар Марковић“ да у Дигитални репозиторијум Универзитета у Београду унесе моју докторску дисертацију под насловом:

Development of voltammetric methods for the detection and quantification of xanthine alkaloids using disposable printed sensors

која је моје ауторско дело.

Дисертацију са свим прилозима предала сам у електронском формату погодном за трајно архивирање.

Моју докторску дисертацију похрањену у Дигиталном репозиторијуму Универзитета у Београду и доступну у отвореном приступу могу да користе сви који поштују одредбе садржане у одабраном типу лиценце Креативне заједнице (Creative Commons) за коју сам се одлучила.

1. Ауторство (CC BY)

2. Ауторство – некомерцијално (CC BY-NC)

3. Ауторство – некомерцијално – без прерада (CC BY-NC-ND)

4. Ауторство – некомерцијално – делити под истим условима (CC BY-NC-SA)

5. Ауторство – без прерада (CC BY-ND)

6. Ауторство – делити под истим условима (CC BY-SA)

(Молимо да заокружите само једну од шест понуђених лиценци. Кратак опис лиценци је саставни део ове изјаве).

У Београду, Потпис аутора

21.11.2025 _____

1. Ауторство. Дозвољавате умножавање, дистрибуцију и јавно саопштавање дела, и прераде, ако се наведе име аутора на начин одређен од стране аутора или даваоца лиценце, чак и у комерцијалне сврхе. Ово је најслободнија од свих лиценци.

2. Ауторство – некомерцијално. Дозвољавате умножавање, дистрибуцију и јавно саопштавање дела, и прераде, ако се наведе име аутора на начин одређен од стране аутора или даваоца лиценце. Ова лиценца не дозвољава комерцијалну употребу дела.

3. Ауторство – некомерцијално – без прерада. Дозвољавате умножавање, дистрибуцију и јавно саопштавање дела, без промена, преобликовања или употребе дела у свом делу, ако се наведе име аутора на начин одређен од стране аутора или даваоца лиценце. Ова лиценца не дозвољава комерцијалну употребу дела. У односу на све остале лиценце, овом лиценцом се ограничава највећи обим права коришћења дела.

4. Ауторство – некомерцијално – делити под истим условима. Дозвољавате умножавање, дистрибуцију и јавно саопштавање дела, и прераде, ако се наведе име аутора на начин одређен од стране аутора или даваоца лиценце и ако се прерада дистрибуира под истом или сличном лиценцом. Ова лиценца не дозвољава комерцијалну употребу дела и прерада.

5. Ауторство – без прерада. Дозвољавате умножавање, дистрибуцију и јавно саопштавање дела, без промена, преобликовања или употребе дела у свом делу, ако се наведе име аутора на начин одређен од стране аутора или даваоца лиценце. Ова лиценца дозвољава комерцијалну употребу дела.

6. Ауторство – делити под истим условима. Дозвољавате умножавање, дистрибуцију и јавно саопштавање дела, и прераде, ако се наведе име аутора на начин одређен од стране аутора или даваоца лиценце и ако се прерада дистрибуира под истом или сличном лиценцом. Ова лиценца дозвољава комерцијалну употребу дела и прерада. Слична је софтверским лиценцама, односно лиценцама отвореног кода.